THE CELESCOPE EXPERIMENT

R. J. DAVIS

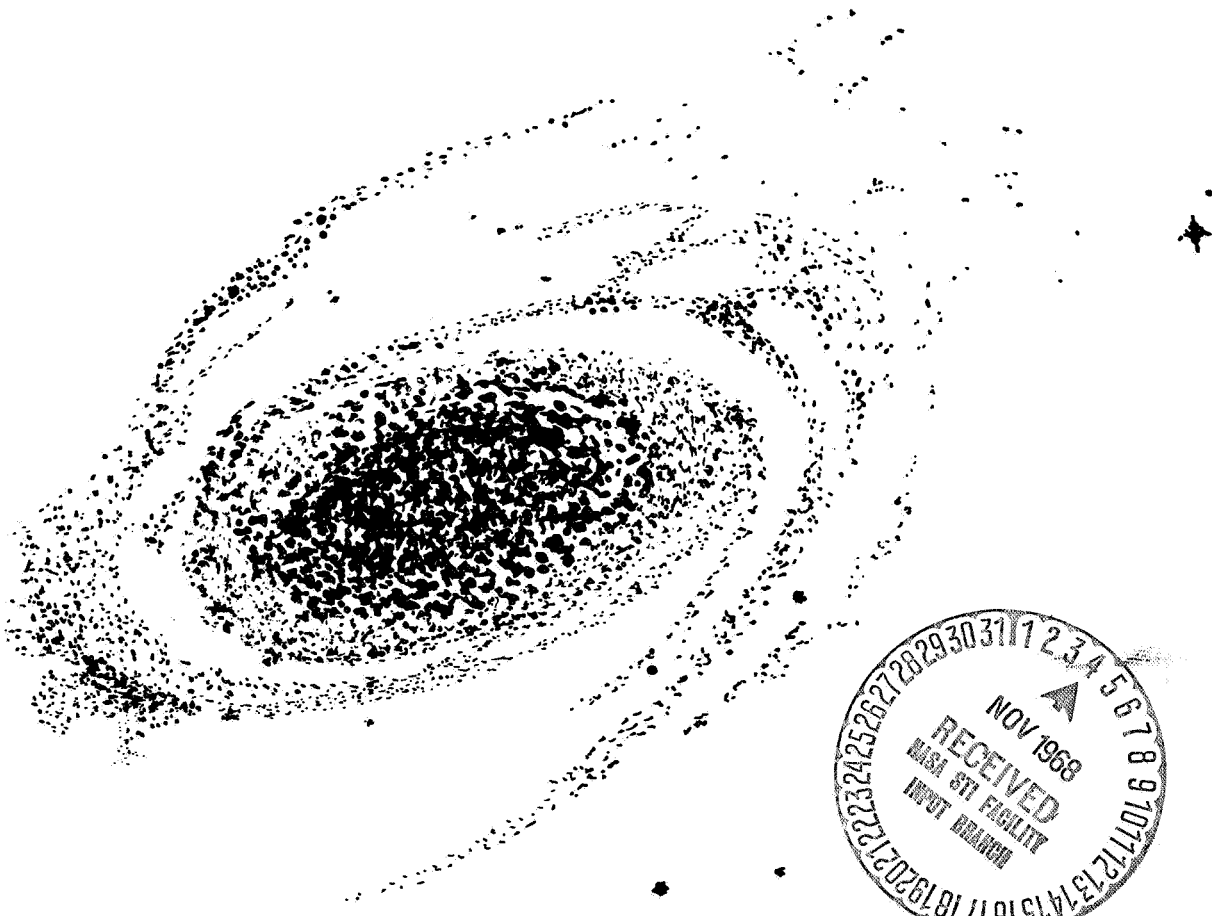

Smithsonian Astrophysical Observatory
SPECIAL REPORT 282

Research in Space Science
SAO Special Report No. 282

THE CELESCOPE EXPERIMENT

Edited

by

Robert J. Davis

July 18, 1968

Smithsonian Institution
Astrophysical Observatory
Cambridge, Massachusetts 02138

804-84

THE CELESCOPE EXPERIMENT

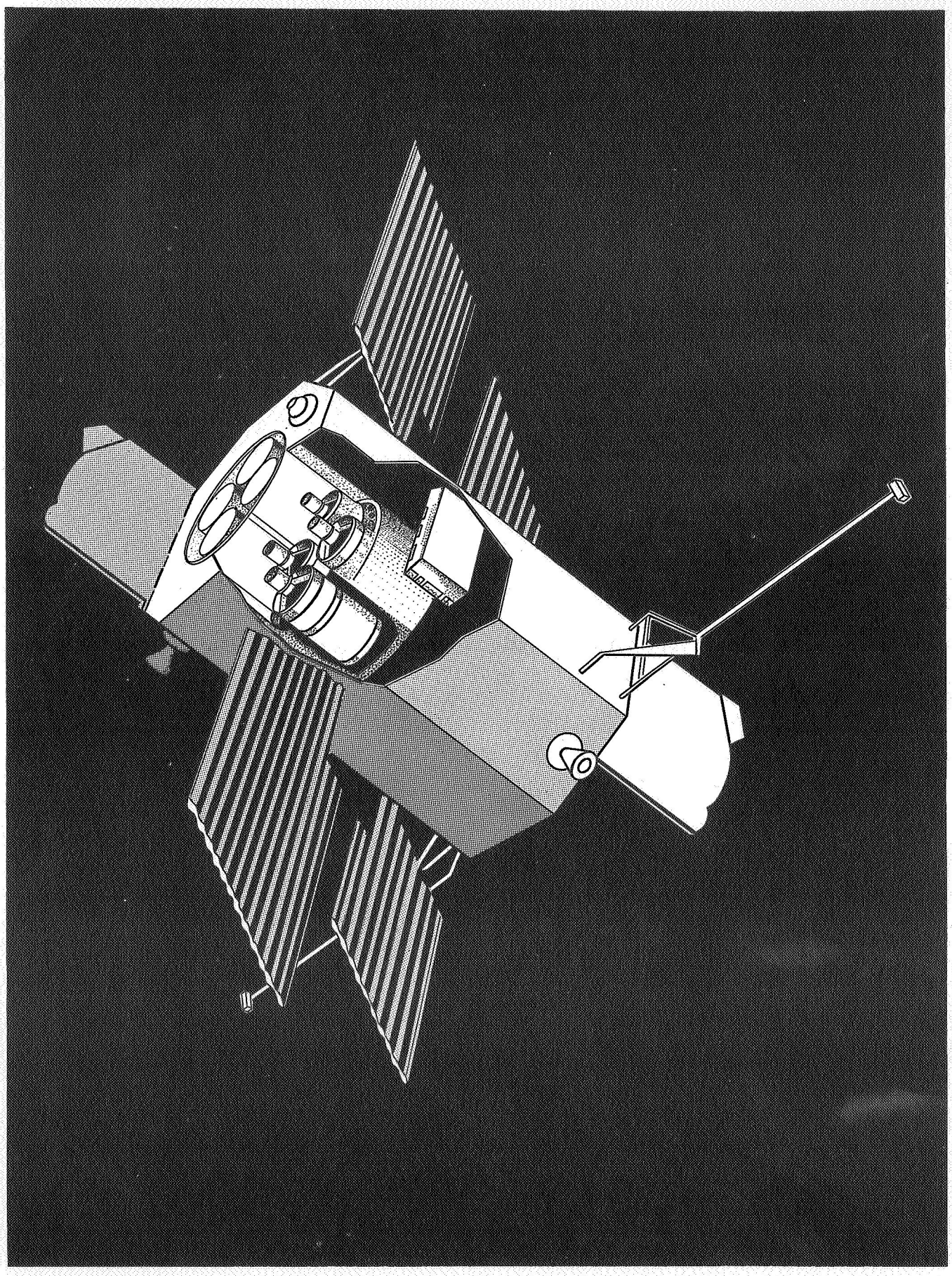

PREFACE

The primary purpose of this Special Report is to inform interested scientists of the capabilities and limitations of the Celescope experiment. Testing of the Celescope experiment as an independent subsystem has been completed; the experiment has now been installed in Orbiting Astronomical Observatory (OAO) Spacecraft No. A-2, in preparation for launch in October of 1968. This report may therefore be considered as final regarding all aspects of the Celescope experiment except those related directly to its deployment in the OAO system.

It is the policy of the Smithsonian Astrophysical Observatory (SAO) to receive from guest investigators requests for observations suitable to this instrumentation and to inform the requesting agency promptly of our recommendation regarding the request. Our ability to conduct observing programs accepted from guest investigators will, of course, depend upon the status of the equipment and can never be guaranteed in advance. No guest observing will be conducted during the first 3 months of OAO operation.

In addition to SAO's policy of honoring suitable requests from guest investigators, the National Aeronautics and Space Administration (NASA) has, as a condition of accepting SAO as an OAO experimenter, reserved a portion of the Celescope observing time for guest investigators.

This report supersedes Special Report No. 110, published December 1962. Since this new report is addressed to a different group of readers than was No. 110, it does not provide so much detail as did the earlier one. Detailed information can be obtained from the various Project Celescope reports listed in Appendix A.

Portions of this Special Report have been extracted from materials prepared under contract to the Smithsonian Institution by Electro-Mechanical Research, Inc., of Sarasota, Florida (Contract SI-522) and by Arthur D. Little, Inc., of Cambridge, Massachusetts (Contracts SI-638, SI-660, and SI-752), and, with permission, from an article (Davis, 1966a) in Advances in Electronics and Electron Physics.

I wish to thank the various members of the Celescope staff who contributed much of the material contained in this Special Report; detailed comments by Dr. W. A. Deutschman and Dr. Y. Nozawa were especially helpful. I also wish to thank Dr. D. Malaise, of the Institut d'Astrophysique, Université de Liège, who during his tenure as NASA COPERS Fellow at Harvard College Observatory made important contributions to our calibration techniques and to some of the descriptive material used in this report; Mr. E. Gerard, of the Observatoire de Paris, who as a graduate student at Harvard College Observatory studied the effects of the space radiation environment on the Celescope experiment and prepared a report on that subject that has been partially incorporated into this special report; and Dr. C. A. Lundquist, who has reviewed this report and provided many useful comments.

Robert J. Davis
Smithsonian Astrophysical Observatory

INTRODUCTION

Until very recently, astronomers have been forced to conduct their observations from the bottom of the earth's atmosphere, which significantly limits the accuracy, sensitivity, and scope of their observations. Important classes of objects, such as the x-ray stars, lay undiscovered pending man's ability to place the necessary instruments above the absorbing layers of the atmosphere. Important physical processes, such as those occurring in the atmospheres of the hotter stars, required observations in that part of the ultraviolet spectrum that is totally absorbed by the atmosphere in order to confirm and refine the relevant theoretical concepts. Studies of remote galaxies, required for refining our theories of the universe, have been hampered by the blurring effects of the atmosphere. Studies of faint objects are hindered by the brightness of the surrounding sky. Our understanding of the sun required that it be studied in the ultraviolet and x-ray regions of the spectrum, and that it be studied with higher resolution than any available from the ground. Even from the highest mountains, not even the sun is bright enough to provide detectable radiation below a wavelength of 2850 Å.

The Celescope experiment is addressed primarily to the study of the atmospheres of the hotter stars by means of photometric measurements in those regions of the ultraviolet that are accessible only from above the earth's atmosphere. Named for its pioneering as a truly celestial telescope, the Celescope concept originated from a series of meetings in February 1958 involving the scientific staffs of Harvard College Observatory (HCO) and Smithsonian Astrophysical Observatory (SAO). Project Celescope has been supported by the National Aeronautics and Space Administration (NASA) as part of their Orbiting Astronomical Observatory (OAO) program. Other experimenters in the program are the University of Wisconsin, Goddard Space Flight Center (GSFC), Princeton University, and University College (London). The OAO program is described by Ziemer (1961) and by Rogerson (1963). The second OAO satellite, which will be launched in 1968, will contain SAO's Celescope experiment and the University of Wisconsin's ultraviolet photometry experiment.

The manner chosen for accomplishing the primary mission of the Celescope project is to conduct a sky survey, with reasonable photometric accuracy, in four ultraviolet bands centered at 2600, 2300, 1600, and 1500 Å. The 1500 Å band includes the hydrogen Lyman-alpha resonance line at 1216 Å, whereas the other bands are insensitive to that wavelength. One of the most important aspects of this survey is the generation of a catalog containing ultraviolet photometric data for all stars observed.

The Celescope is a set of four 12-inch f/2 telescopes, each equipped with a television camera. The field of view of each is approximately 2° square. The instrument is designed to operate primarily as a television stellar photometer.

Project Celescope now functions under NASA contract No. NAS 5-1535. The instrumentation was procured through a subcontract to Electro-Mechanical Research, Incorporated, of Sarasota, Florida. The Uvicon television camera tubes were procured through a subcontract to Westinghouse Electric Co., of Pittsburgh, Pennsylvania, and Elmira, New York.

TABLE OF CONTENTS

LIST OF ILLUSTRATIONS

LIST OF ILLUSTRATIONS (Cont.)

LIST OF ILLUSTRATIONS (Cont.)

THE CELESCOPE EXPERIMENT

Edited by

Robert J. Davis

1. ASTROPHYSICAL BACKGROUND

Short-wave electromagnetic radiation reacts strongly with matter. At wavelengths longer than 3200 Å, the effects of the earth's atmosphere can be rather well eliminated from observational data by proper reduction procedure. For wavelengths shorter than 2800 Å, no appreciable amount of radiation can penetrate the atmosphere below an altitude of approximately 30 km. Altitudes of 40 km are necessary for making reasonably good observations between 2000 and 3000 Å, and altitudes of 100 km are necessary for making reasonably good observations below 2000 Å.

Since the OAO will have an orbit of 800-km altitude, the earth's atmosphere will not affect observations conducted with the Celescope experiment. The short-wavelength limit for our survey is set primarily by an engineering constraint requiring that the television camera tube be provided with a faceplate transparent to the radiation being measured. We use lithium fluoride for this faceplate material in order to obtain the greatest possible wavelength coverage; the transparency of this material limits us to observations above 1050 Å.

1.1 Absorption by the Earth's Atmosphere

Tousey (1961) gives a chart showing the depth of penetration of incident ultraviolet radiation into the atmosphere. With the exception of a small, dusky "window" near 2100 Å, the level to which 37% of the incident radiation penetrates is above 30 km for all wavelengths shorter than 3000 Å. Between

2000 and 3000 Å, the absorption is caused primarily by ozone (O_3). Although the maximum ozone density occurs near 20 km (Griggs, 1966), appreciable amounts extending to 40 km effectively block the radiation between 2200 and 2800 Å.

Between 1000 and 2000 Å, the absorption is produced primarily by molecular oxygen (O_2). Throughout most of this region, 37% of the incident radiation penetrates to a level near 100 km. The vertical distribution of molecular oxygen is discussed by Kamiyama (1959).

1.2 Stellar Atmospheres

One of Celescope's goals is the measurement of the brightnesses of at least 25,000 main-sequence early-type stars in four spectral bands between 1000 and 3000 Å. The datum of interest is the shape of the spectral-energy distribution curves of the different types of stars. Only for the atmospheres of main-sequence early-type stars do we now have a reasonably clear picture of what to expect. As was the case with the great sky surveys of the past — e.g., the Henry Draper Catalog and the Palomar Sky Atlas — we plan to acquire our data by a survey of the entire available portion of the celestial sphere and thus increase our chances of making important unexpected discoveries. We have planned our instrumentation and observational program so as to balance the payload limitations of the Celescope with these scientific objectives.

Experiments from rockets and satellites have already given astronomers a limited amount of observational information concerning ultraviolet stellar spectra. Stecher and Milligan (1962) obtained spectra of seven stars between 1600 and 4100 Å. This program is continuing and has been extended to a short-wavelength limit of 1100 Å (Stecher, 1967). Heddle (1964) observed 22 stars at an effective wavelength near 1950 Å. Byram, Chubb, and Friedman (1961) observed 42 stars at effective wavelengths near 1250 and

and 1450 Å. Chubb and Byram (1963) and Byram, Chubb, and Werner (1965) later observed about the same number of stars at 1115, 1314, and 1427 Å. Henize and Wackerling (1966) and Heinze, Wackerling, and O'Callaghan (1967) obtained photographs of a large number of stars and of about 50 stellar spectra in the 2300 to 4000 Å range. Morton and Spitzer (1966) and Morton (1967) obtained spectra of six stars in Orion and two in Scorpio, between 1200 and 2000 Å. Smith (1967) measured the brightnesses of 96 stars at an effective wavelength near 1376 Å.

These observations indicate ultraviolet fluxes that are a factor of 3 to 10 lower than had been indicated by the model stellar atmospheres most widely used in predicting the spectra for the hotter stars. Part of this discrepancy is due to the omission of line blanketing in these model atmospheres (Morton, 1965); part is due to interstellar absorption (Boggess and Borgman, 1964; Smith, 1967); and part may be due to calibration errors. Of the 21 stars observed both by Smith (1967) and by Chubb and Byram (1963), Smith's observations at 1376 Å gave fluxes averaging 2.6 times higher than Chubb and Byram's observations at 1427 Å (7 stars), and 1.9 times higher than Chubb and Byram's observations at 1314 Å (16 stars). Of the five stars observed both by Heddle (1964) and by Stecher and Milligan (1962), Heddle's broad-band observations at 1950 Å gave fluxes averaging 2.7 times higher than Stecher and Milligan's spectrophotometric observations at the same wavelength. All the above comparisons show considerable scatter about these mean values, increasing from a factor of 3 at the shorter wavelengths to a factor of 10 at the longer wavelengths. Bless, Code, and Houck (1968) have reviewed the available data and concluded that the best observational data are accurate to about ± 0.25 mag, and that the best blanketed model atmospheres are consistent with them.

This problem of the ultraviolet fluxes from hot stars is of great importance to theoretical astrophysics. One goal of Celescope is to strengthen the observational foundation, and to chart the path for observing programs and instrumentation for future, more specialized satellites that are being planned.

Figures 1 through 5 compare the theoretical spectral distributions of stars of various spectral types with the conservative provisional spectral distributions we used during the design of the Celescope experiment. Figure 2 also includes a comparison of these spectral distributions with the available observational material. (It should be noted that Smith's (1967) observations at 1376 Å include a correction for interstellar absorption, whereas the other observations do not.)

Figures 6 through 9 indicate the relationship between spectral type and limiting V magnitude for each of the four Celescope spectral ranges. Each figure shows, for one of these spectral ranges, the bright and faint limits for routine Celescope observations. The bright limit is set by the danger of damaging our most sensitive detector; it is based upon the theoretical unblanketed spectral distribution curves and is the same for all four figures. The faint limit is set 2.5 mag above the noise level of the instrumentation, where the system is capable of measuring to an accuracy of 0.1 mag rms. Curves based on both the theoretical and the provisional spectral distributions are shown in the figures. The observational capabilities of the Celescope instrumentation are discussed in more detail in Section 2 of this report.

The scientific objective on which we based the Celescope design was an ultraviolet sky survey to the limiting magnitudes shown in Figures 6 through 9. Since the Celescope experiment can observe about 1.5% of the sky in a week and since Celescope has control of the OAO only every other week, it will take 2 years to complete a survey of the entire sky — longer than the expected lifetime of either the spacecraft or the experiment. Therefore our plan is to concentrate our observations in a set of selected areas (described more fully in Section 3), and obtain a reasonably accurate statistical sampling of stars throughout the celestial sphere, filling in between them when we are not able to observe a selected area. Because we cannot observe within 45° of either the sun or the antisolar direction, we will need 6 months to obtain really uniform coverage.

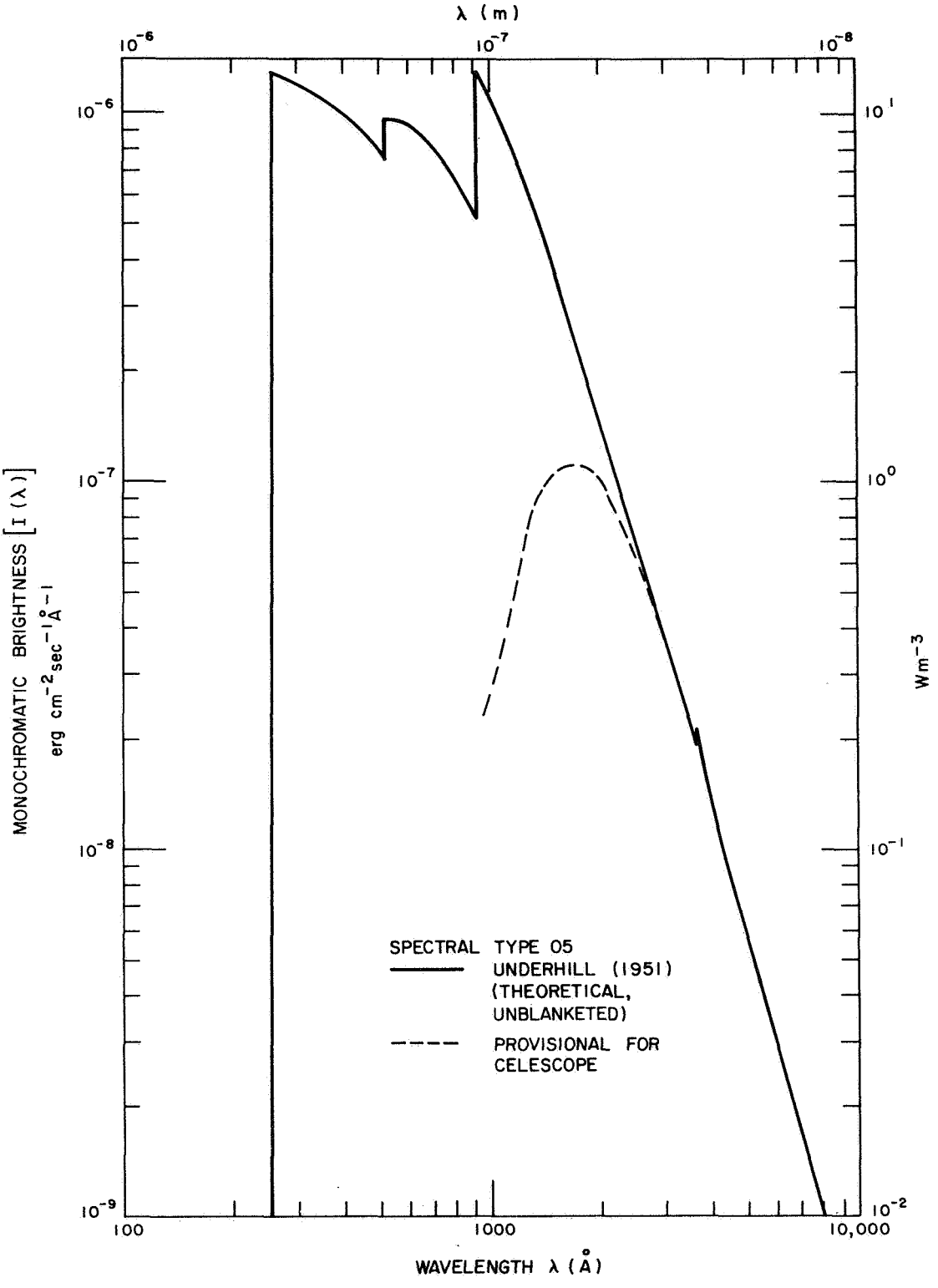

Figure 1. Spectral distribution for an O5 star.

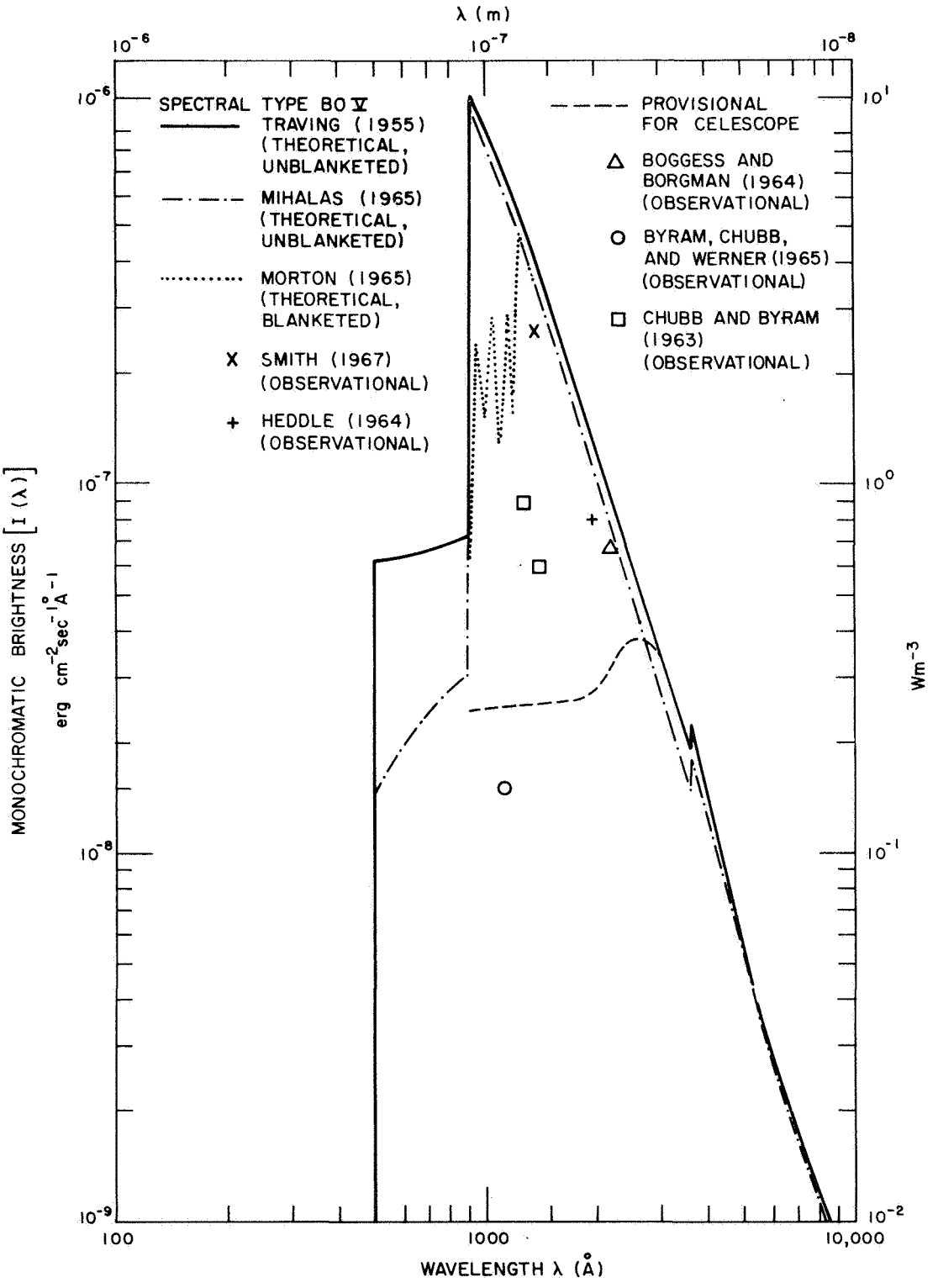

Figure 2. Spectral distribution for a B0 star.

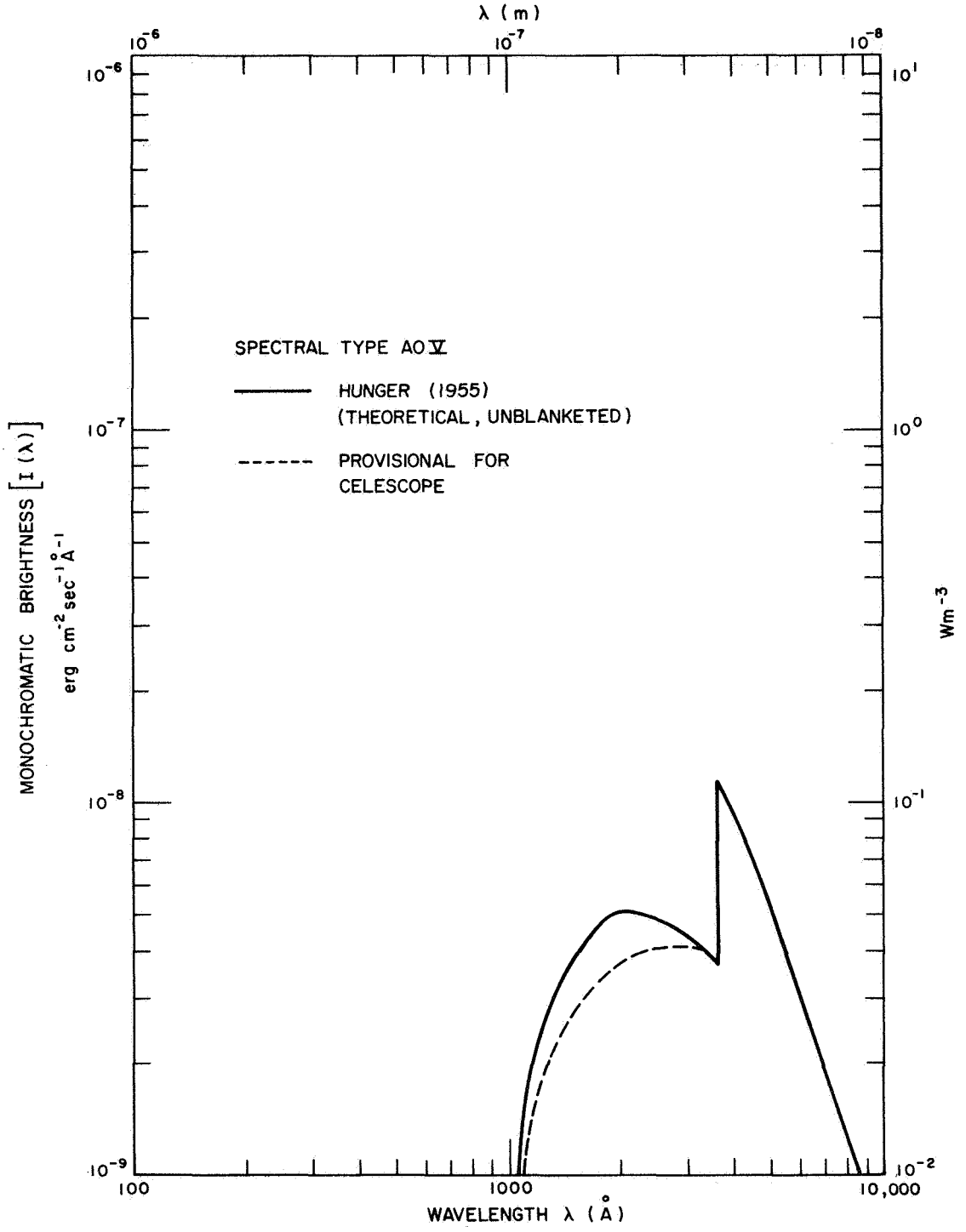

Figure 3. Spectral distribution for an A0 star.

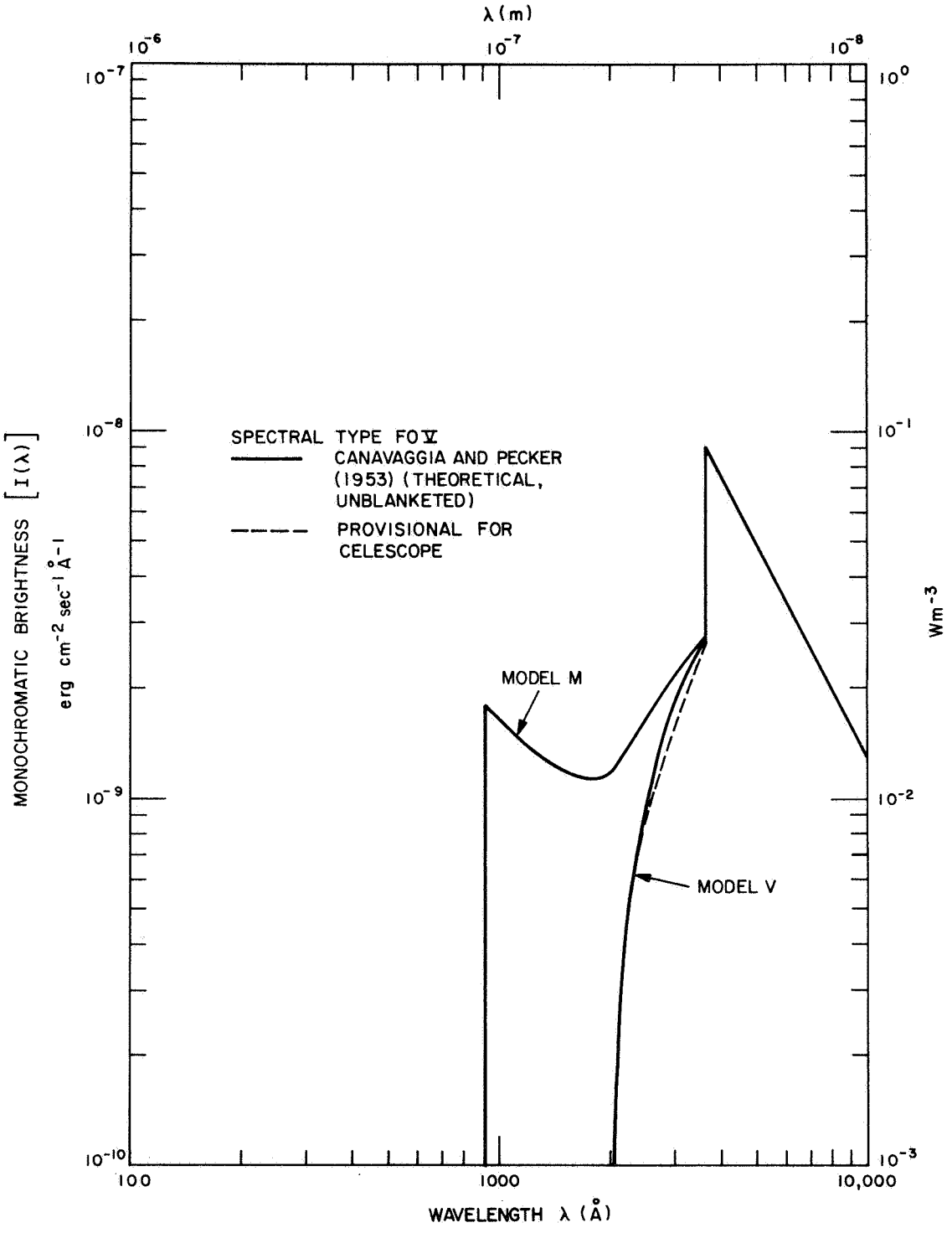

Figure 4. Spectral distribution for an F0 star.

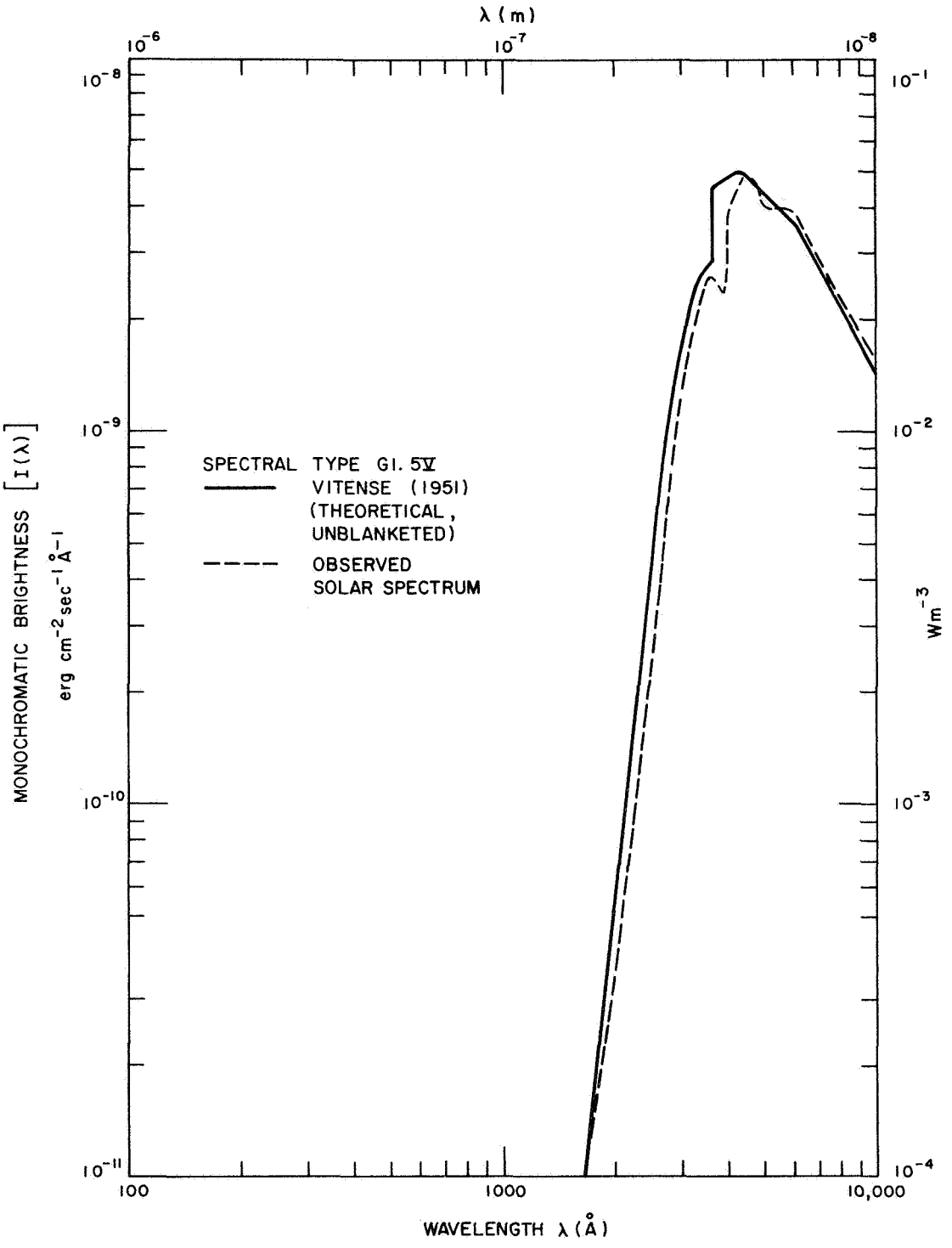

Figure 5. Spectral distribution for a G1.5 star.

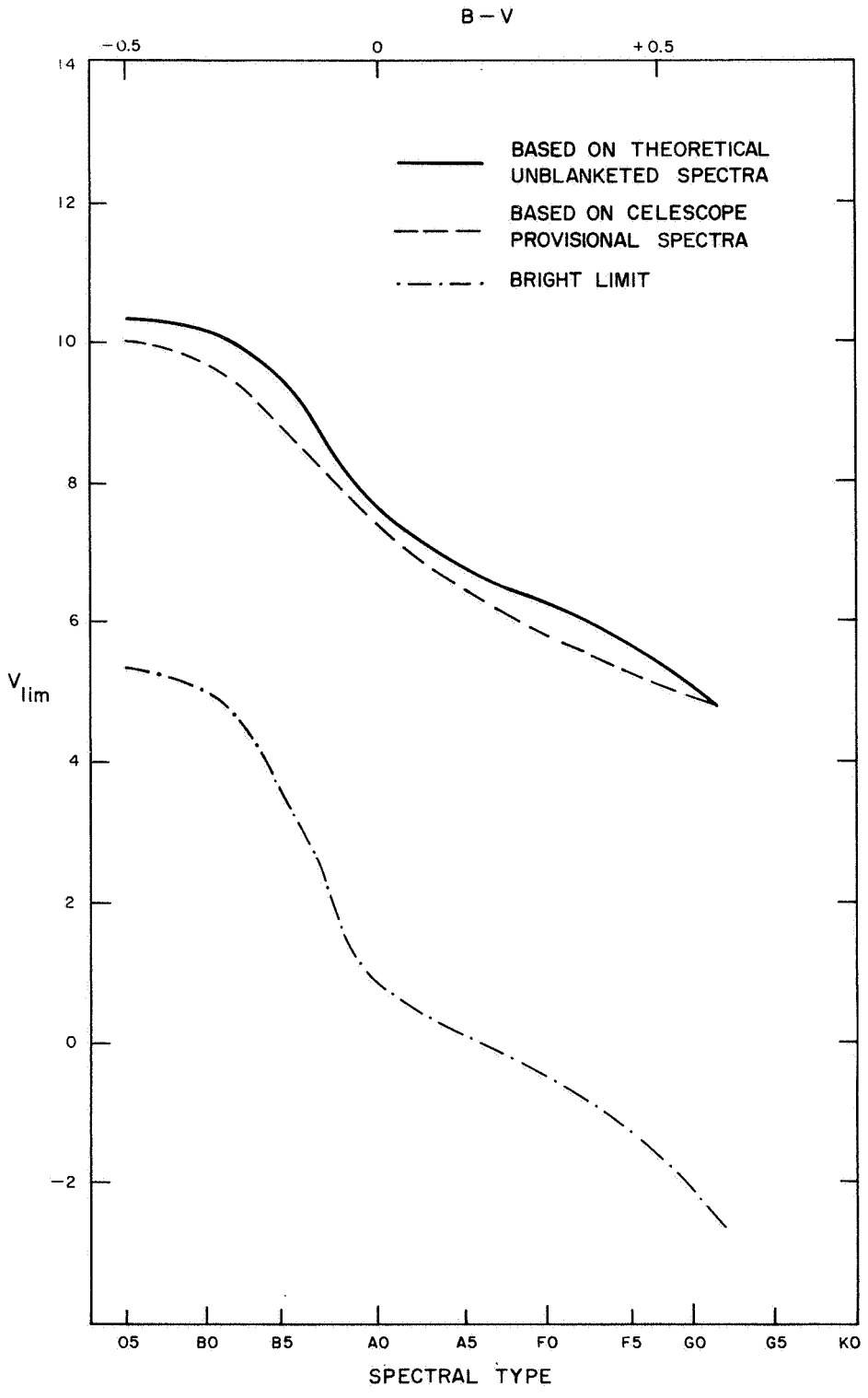

Figure 6. Limiting magnitude for U_1 spectral region (2100 to 3200 Å), as a function of spectral type.

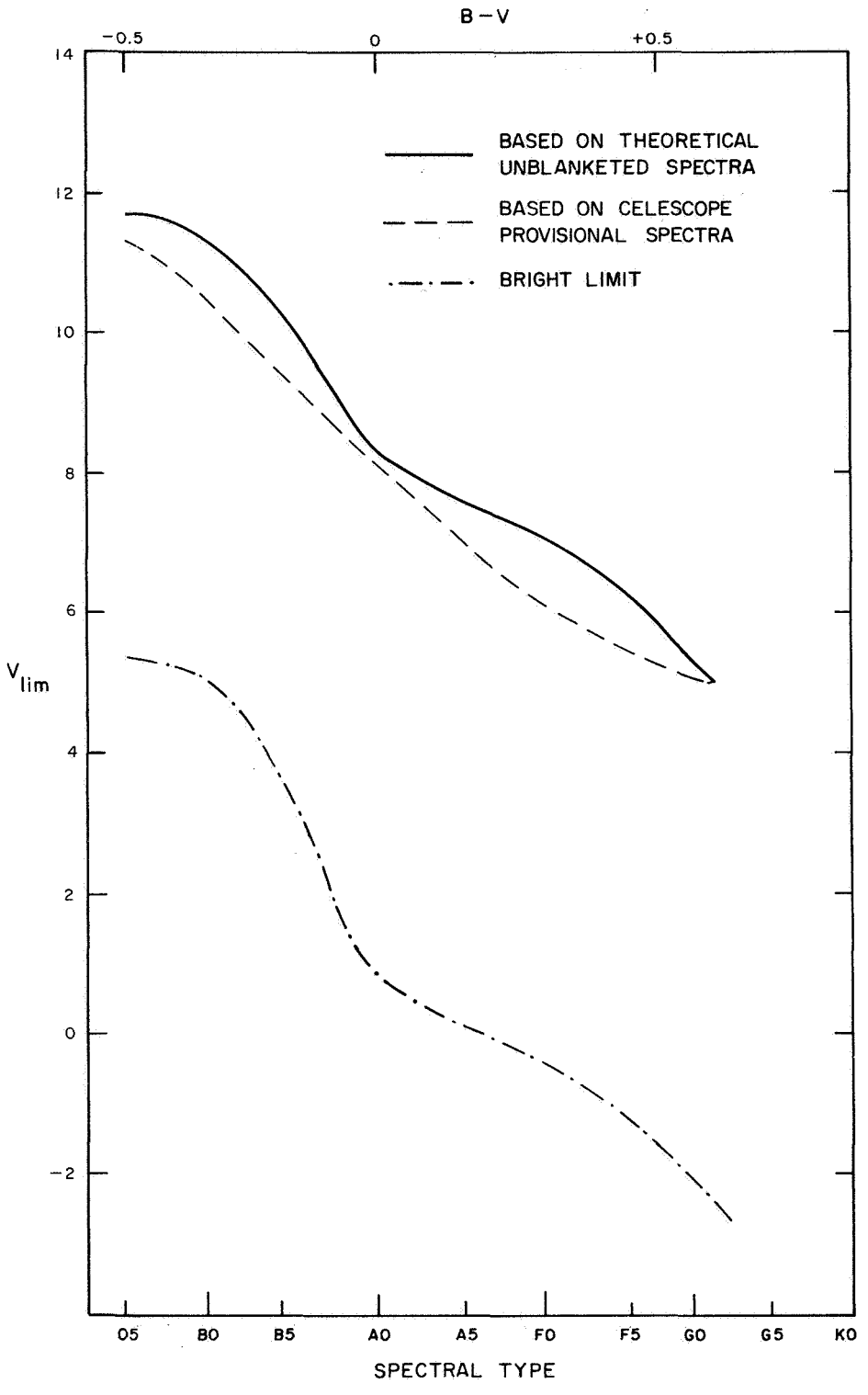

Figure 7. Limiting magnitude for U_2 spectral region (1550 to 3200 Å), as a function of spectral type.

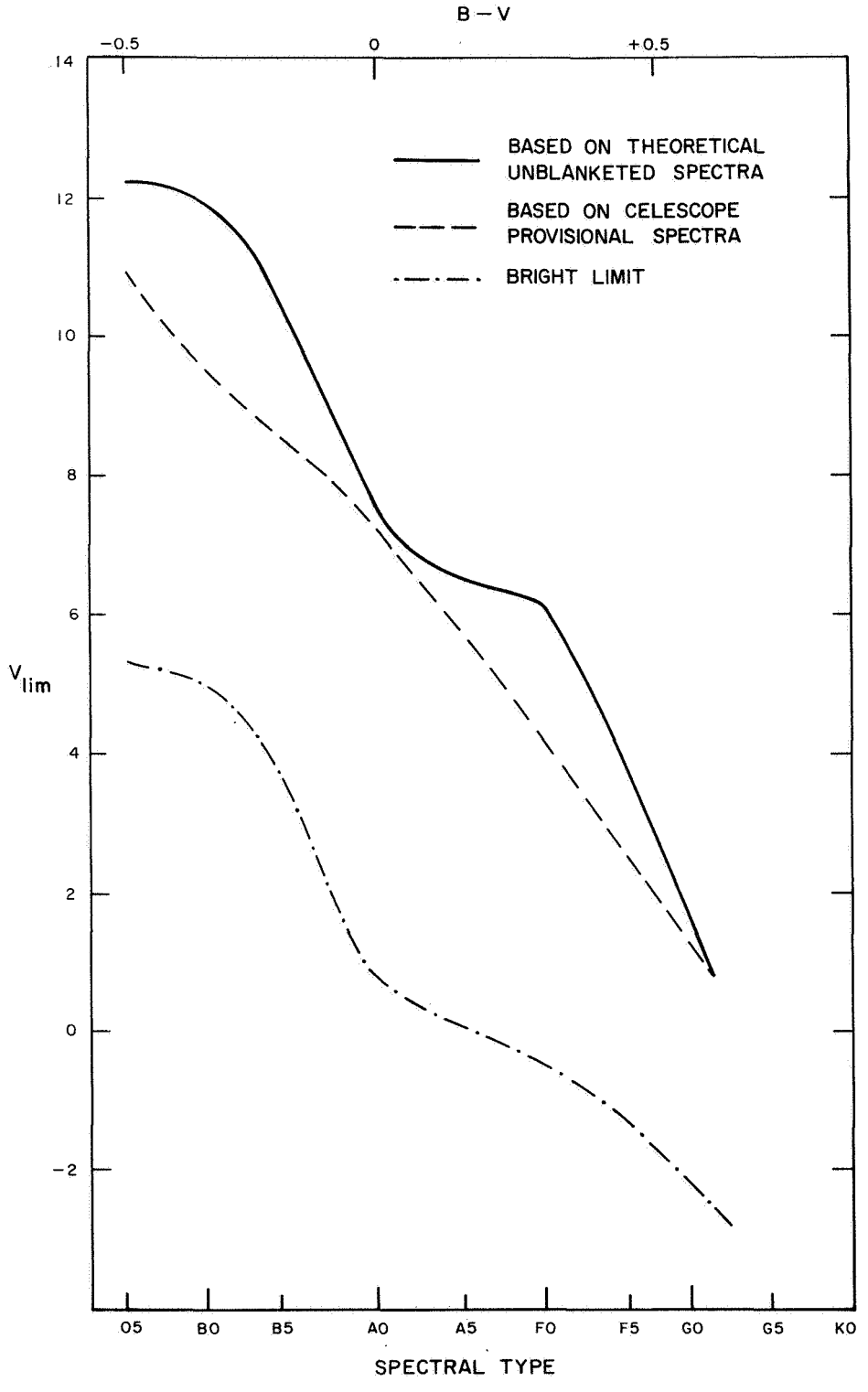

Figure 8. Limiting magnitude for U_3 spectral region (1350 to 2150 Å), as a function of spectral type.

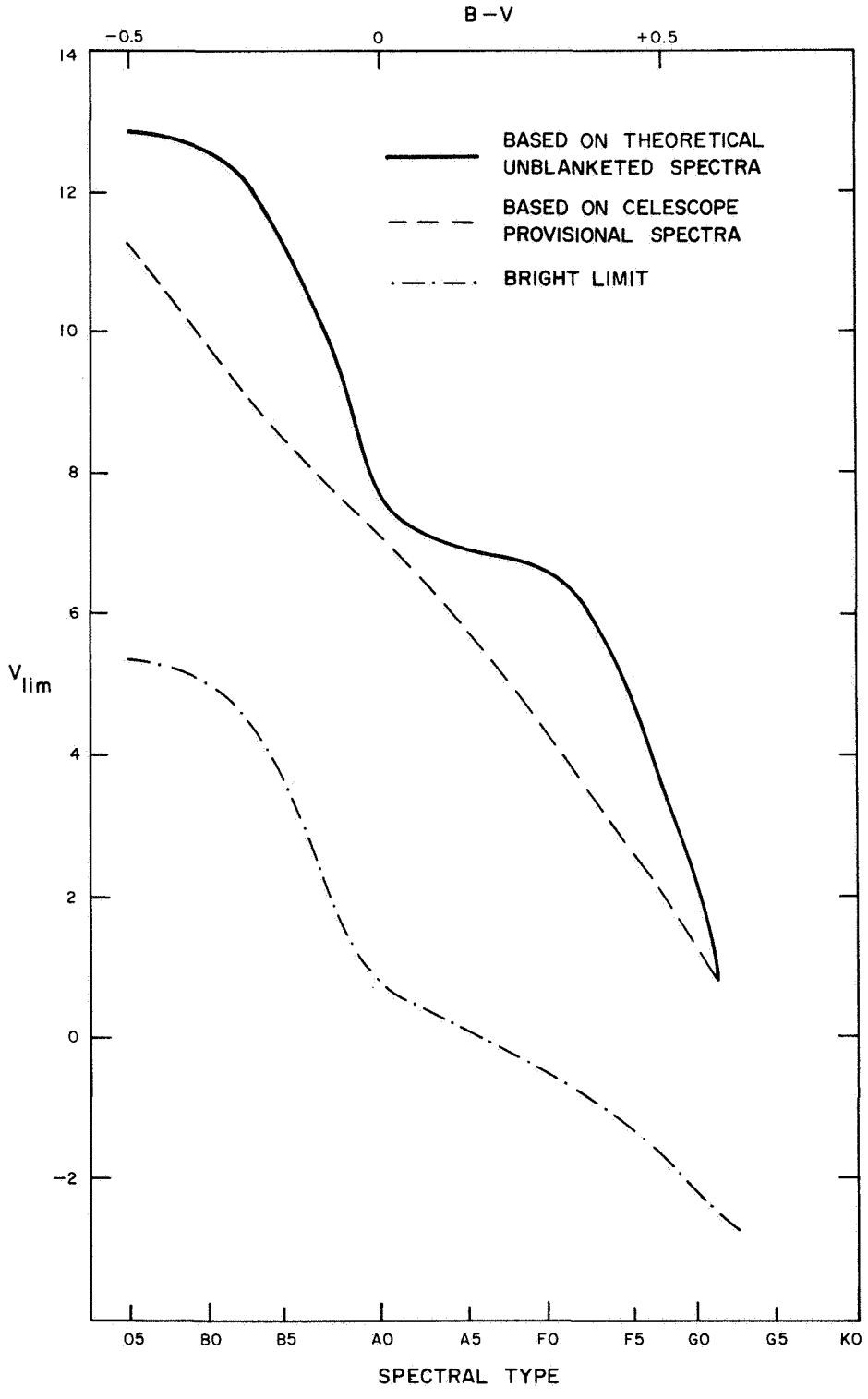

Figure 9. Limiting magnitude for U_4 spectral region (1050 to 2150 Å), as a function of spectral type.

Figure 10 indicates the distribution of stars of various spectral types that we expect to observe. The visual region is included for reference. As we shorten the effective wavelength of our photometric system, we get a smaller and smaller proportion of the later-type stars.

The significance of our survey depends both upon the number of stars of each spectral type we observe, and upon the distribution of our observations around the celestial sphere. In the first week we will try to observe several hundred O and B stars in one region of the sky. In the first month we will observe over 1000 O and B stars, about 100 A stars, and over 50 F and G stars, distributed somewhat unevenly over the sky.

1.3 Interstellar Absorption

The interstellar medium consists of two components — gas and dust — which are recognized and studied by their absorption of light from distant stars. The gaseous component absorbs only in narrow spectral lines and has no measurable effect in terms of a broad-band photometric system such as Celescope, with the possible exception of the effects of the hydrogen Lyman-alpha line on our U_4 magnitude. Morton's (1967) observations indicate, however, that even that line is probably too narrow to affect the broad-band magnitudes of stars bright enough to be observed by Celescope.

The effects of interstellar dust are of significant importance to the Celescope experiment, and the evaluation of these effects is another of its scientific goals. Interstellar dust absorbs more strongly at short wavelengths than at long wavelengths, thus reddening the spectra of distant stars. Figure 11 shows a representative selection of published interstellar reddening curves, normalized to a (B - V) color excess of 1 mag. The ultraviolet portion of the interstellar reddening law rests upon a very small amount of observational material, mostly from stars with little reddening.

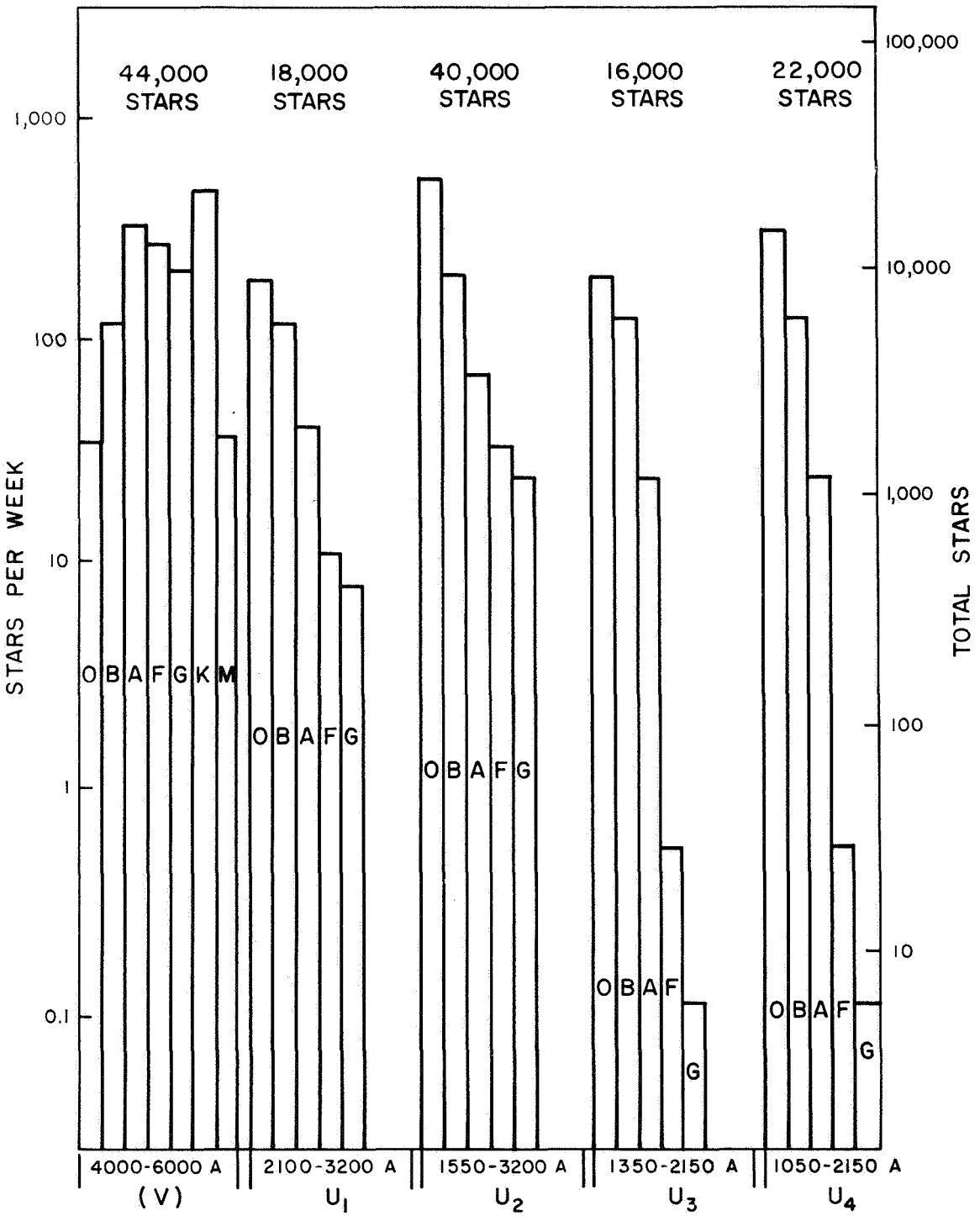

Figure 10. Number of stars of various spectral types expected to be observed with Celescope (V is shown for reference, to a limiting magnitude of +8. 0).

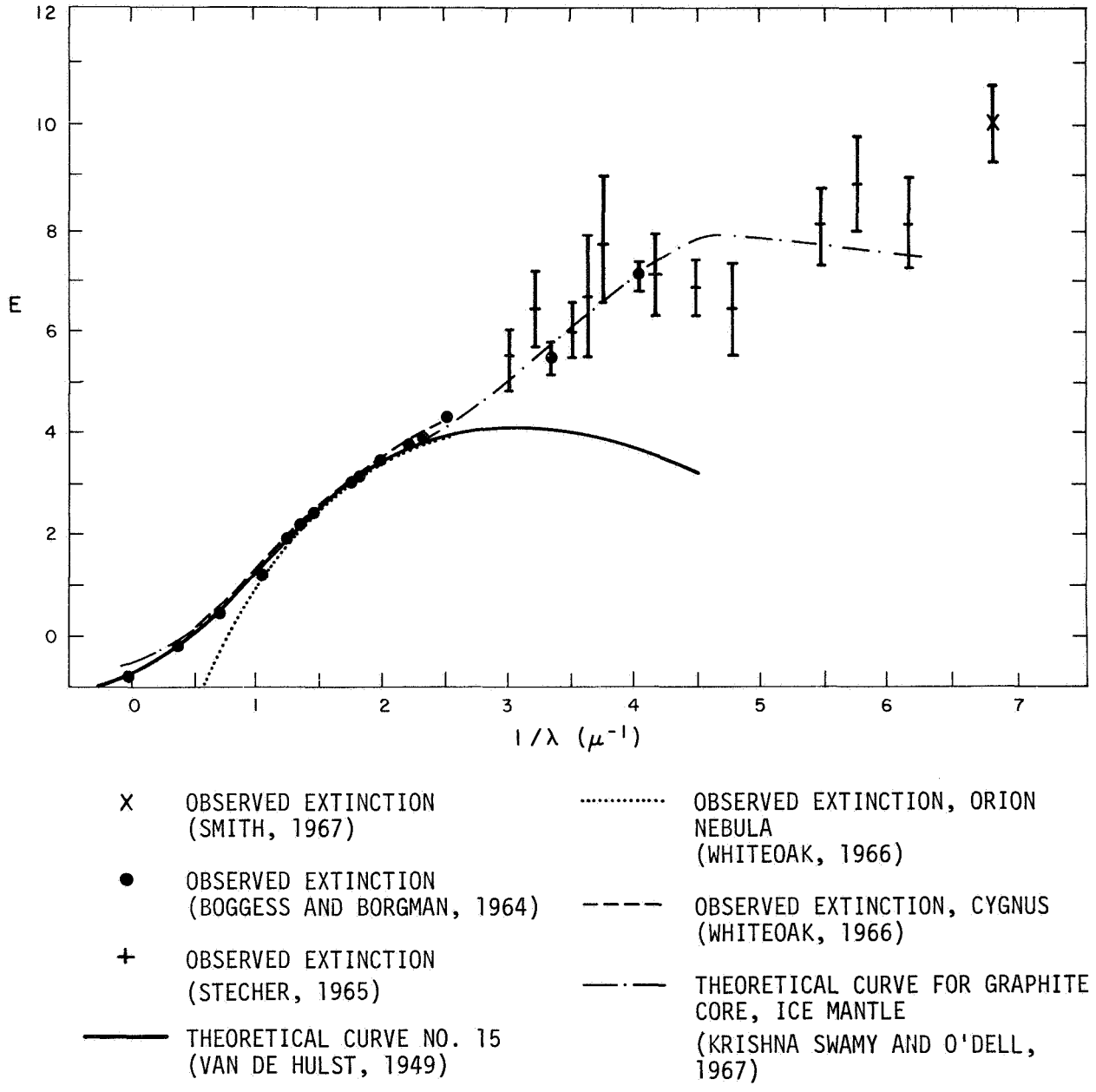

Figure 11. Normalized extinction curves. Error bars indicate probable errors.

2. CAPABILITIES OF THE INSTRUMENTATION

The Celescope experiment has four ultraviolet-sensitive television photometers, each of which consists of a 31-cm f/2 Schwarzschild telescope, two fixed optical filters, and a Uvicon television camera. Power, signal-processing, and electronic control are provided by the separate electronic package. The experiment is rigidly mounted in the spacecraft, with its optical axis pointed in the aft direction. An ultraviolet photometry and spectrophotometry experiment by the University of Wisconsin, pointing in the forward direction, is rigidly attached to the bottom end of the Celescope experiment. The OAO spacecraft furnishes primary power, signal transmission, and stabilization for both experiments. The Celescope instrumentation is described in more detail in Section 5 of this report. (Figure 26 is a cutaway view of one of the telescopes.)

2.1 Field of View

Figure 12 shows the field of view of the four Celescope photometers. For each photometer, the intersection of the optic axis with the celestial sphere is indicated by the intersection of the arrows labelled Y_c and Z_c. The field of view is limited both by the size of the photocathode, shown in Figure 12 as the outer circle, and by the size and position of the scanning raster, shown in Figure 12 as the outer square. Any object in the area common to both photocathode and scanning raster will contribute to the video signal. Shown within this common area are a circle of 2° diameter and a square 2° on a side, centered on the optic axis. This 2° square is the usable field of view for Celescope. The C-1 camera is skewed 15° relative to the primary coordinate system, owing to a misinterpretation of alignment procedures when this camera was manufactured. This skewing does not affect the usable field of view and was therefore retained.

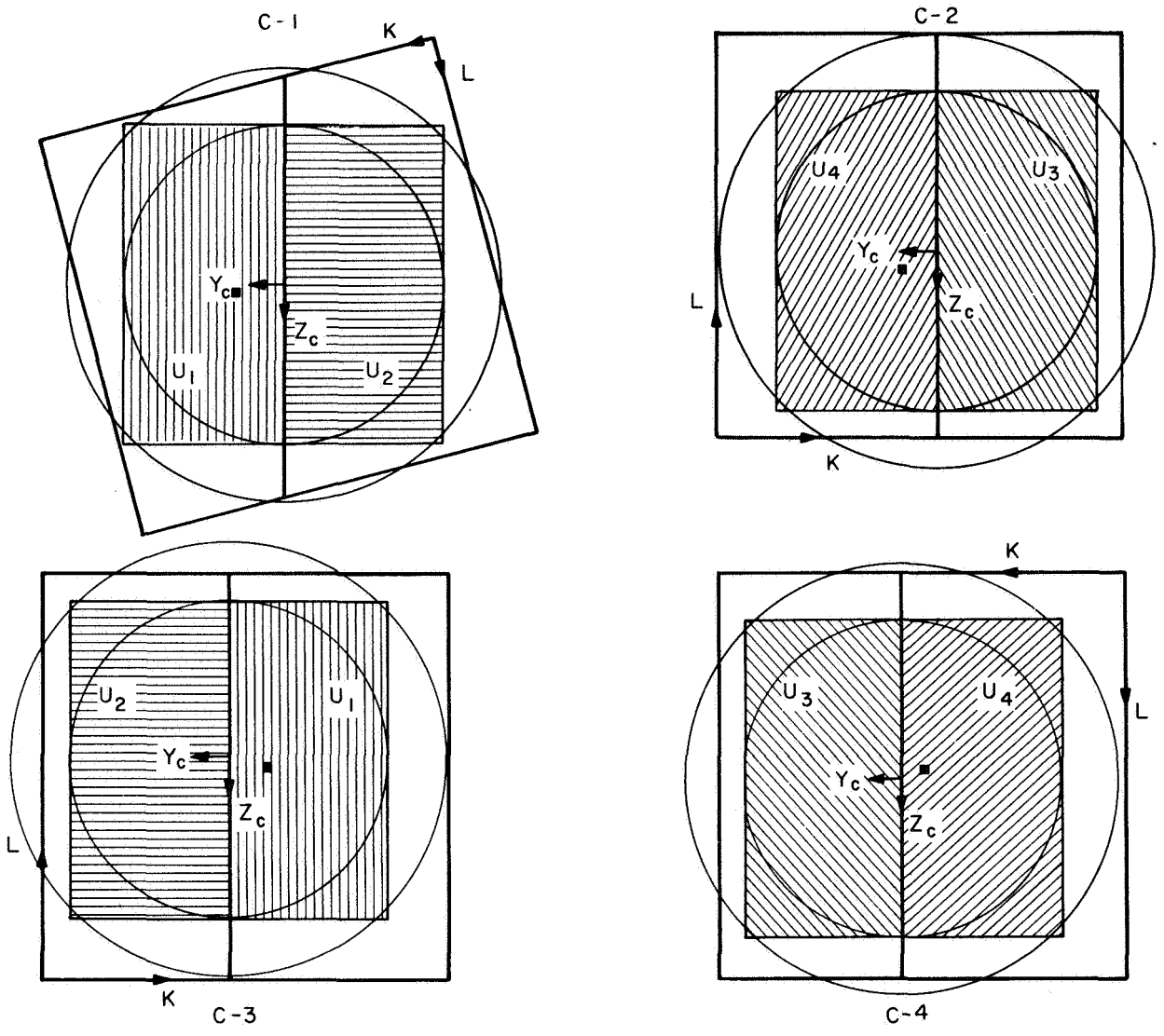

Figure 12. Celescope field of view.

The position of the scanning raster relative to this usable field of view is subject to shifts of up to 10 arcmin, owing primarily to the effects of the earth's magnetic field. To provide both an accurate indication of the position of the optic axis, and an independent means of photometric calibration, each photometer is equipped with a calibrator lamp, which can be turned on or off by command; the position of this calibration image is shown in Figure 12, for each photometer, by a small filled square.

In order to preclude loss of a spectral region in the event of failure of one of the photometers, two optical filters have been mounted in front of each Uvicon to divide the field of view into two portions with different spectral responses designated as U_1, U_2, U_3, or U_4 in Figure 12. The corresponding response curves are shown in Figure 13. The short-wavelength response is a function primarily of the transmittances of the optical filter materials, and does not vary appreciably from one telescope to another for the same type of filter. The long-wavelength response is a function primarily of the quantum efficiencies of the Uvicons, and depends not only upon the photocathode material, but also upon differences in performance from one Uvicon to another. Thus, as is shown in Figure 13, the long-wavelength response of the F-1 telescope is different from that of the F-3 telescope, and that of the F-2 telescope is different from that of the F-4 telescope. (The designation of a telescope as F-1, F-2, F-3, or F-4 refers to the serial number assigned to the hardware as the telescope was built; the designation of a camera as C-1, C-2, C-3, or C-4 refers to the electronic channel in Bay E-4 to which the telescopes are connected. In the flight Celescope payload, telescope F-1 is connected to camera chain C-1; F-2 is connected to C-2; F-3 to C-3; and F-4 to C-4.

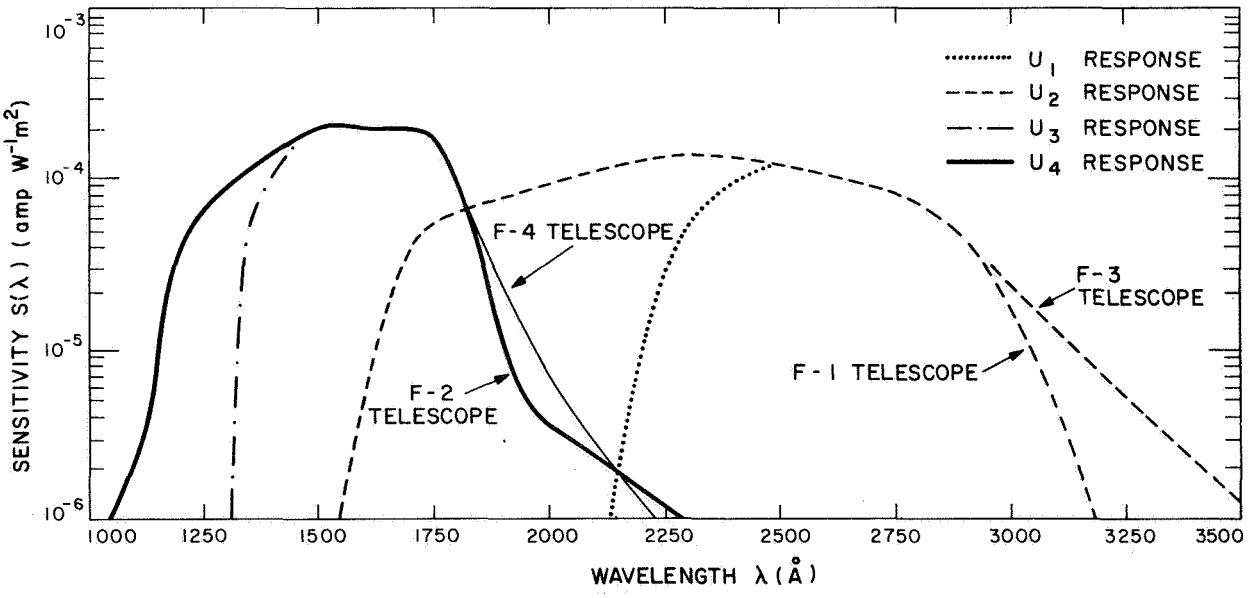

Figure 13. Typical spectral-response curves for Celescope.

2.2 Stabilization and Orientation

Orientation of the Celescope experiment is accomplished by means of appropriate commands to the OAO stabilization subsystem. Orientation is determined by measuring the positions of guide stars relative to the OAO control axes with six two-axis star trackers. Because of the limited allowable gimbal excursion, the limited number of guide stars assigned, and the occultation of guide stars by the earth, not all slew maneuvers are permissible. The permissibility of a desired maneuver is established by NASA's Support Computer Program System (SCPS), which attempts to find a sequence of orientation commands that will maintain favorable gimbal angles for at least two star trackers at all times. If this path causes one star tracker to exceed the allowable gimbal angle, the slew maneuver must hold the OAO at that position while another tracker is commanded to acquire a new guide star. Although no concise set of rules can be formulated to give the user absolute assurance that his desired orientation sequence will be accepted by the SCPS, most maneuvers of less than 5° will be accepted, and most maneuvers of greater than 20° will be rejected.

Additional constraints on allowable orientations are set by the requirement that direct sunlight must not impinge on the outer end of either experiment, and that the orientation relative to the sun be such as to achieve adequate power from the solar paddles. The first constraint requires that the spacecraft must be rolled 180° when the optical axis crosses the great circle 90° from the sun. This complicated maneuver is not allowed in the first 30 days of the flight and must be used as little as possible thereafter. The second constraint implies that the line perpendicular to the solar paddles lie within 10° of the sun.

In order to minimize the possibility of damage to the Celescope experiment, SAO is for the present requiring that it not be operated when pointing at the earth (or at any point in the atmosphere below 200 km altitude), the moon, Venus, Mars, Jupiter, Saturn, or any star brighter than the bright limit shown in Figures 6 through 9.

The position of a star within the Celescope field of view is specified by η, the angular distance from the great circle labelled Z_c (with positive η in the direction indicated by the Y_c arrow), and by ζ, the angular distance from the great circle labelled Y_c (with positive ζ in the direction indicated by the Z_c arrow). The orientation of the OAO is specified by α_0, the right ascension of the $-X_c$ axis (Celescope optic axis) in 1950.0 coordinates; δ_0, the declination of the $-X_c$ axis in 1950.0 coordinates; and ρ, the roll angle measured counterclockwise from the Y_c arrow to the north direction. The relationships among the Celescope coordinate system, the OAO orientation, and the celestial coordinate system are shown in Figure 14.

OAO No. A-2 has only coarse guidance capabilities, no error signals being provided by either experimenter. These capabilities provide pointing control accurate to within 1 arcmin rms, corresponding to about two television lines in our raster and is considerably more accurate than our a priori knowledge of the position of the raster relative to the optic axis.

2.3 Spectral Response

Figure 13 shows typical spectral-response curves for the four Celescope passbands. We have calibrated the spectral response at a minimum of 14 positions within the field of view of each telescope, finding no major variations in the shapes of these curves across the photocathode, but variations in the amplitudes of up to a factor of 2 from the least sensitive position to the most sensitive position. Variations from one photometer to another occur primarily at the long-wavelength end of the response curves and result from variations in the Uvicon's photocathode response. The typical curves shown in Figure 13 apply at the center of the field of view. Calibration is discussed in more detail in Section 6 of this report.

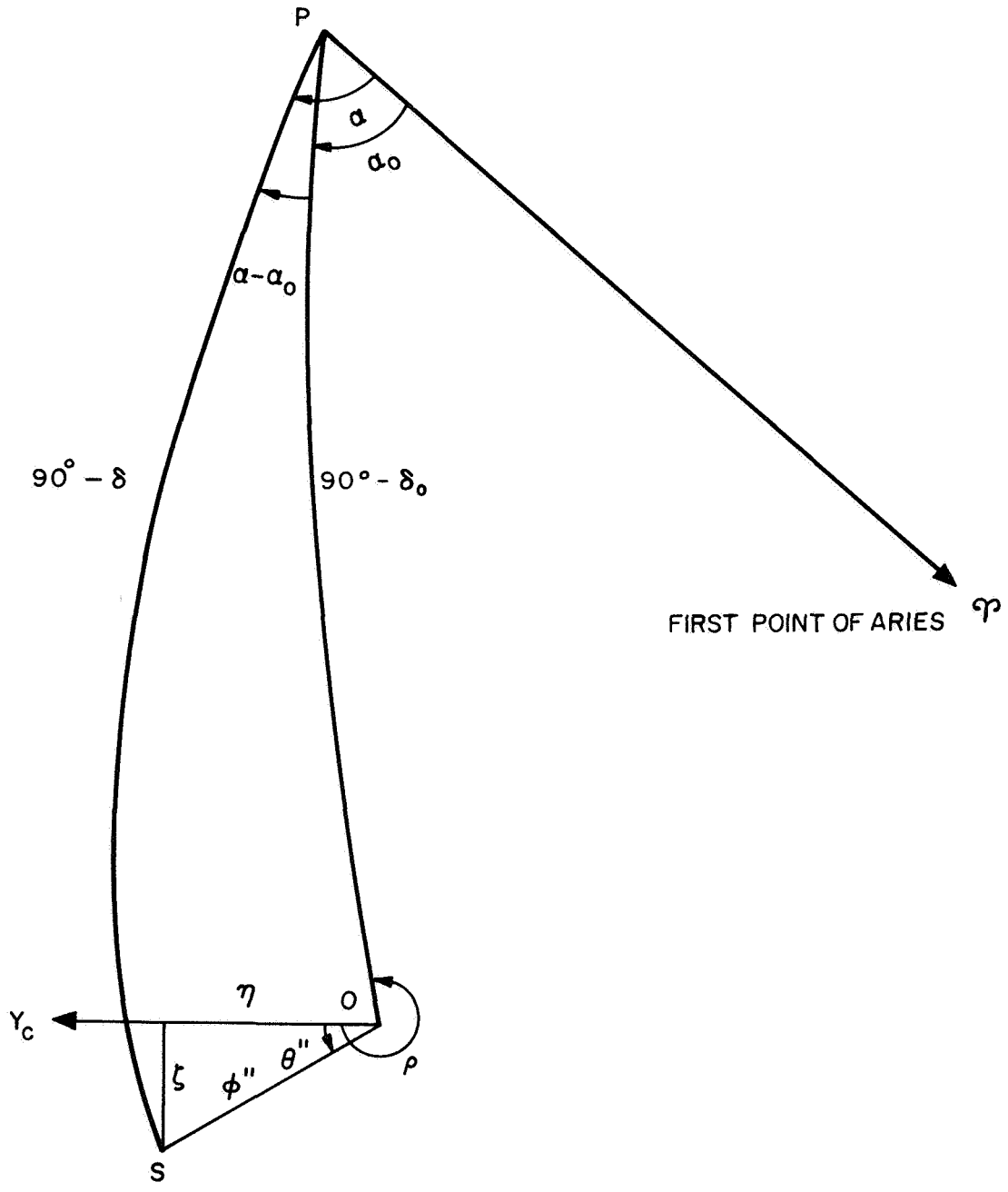

Figure 14. Star position and Celescope coordinate system as seen looking at the celestial sphere from the inside.

2.4 Sensitivity and Photometric Accuracy

If a television signal is to be used for stellar photometry, it must provide a type of information from which the following input variables can be derived: Λ, the effective wavelength; $I(\Lambda)$, the intensity at that wavelength; and (α,δ), the direction to the star in right ascension and declination.

Whether the television picture is transmitted as an analog or as a digital signal, the information can be expressed and analyzed mathematically as a matrix A in which the coefficient $a_{k,\ell}$ represents the signal amplitude for the kth television scanning line and the ℓth television-picture element. If a television system is to function satisfactorily as a stellar photometer, each of the four desired input variables must be derivable from this output matrix. In other words, the following scalar functions of this matrix must be accurately defined over the range of interest to the astronomer: $\Lambda(A)$, the color transfer function; $I(A)$, the intensity transfer function; $\alpha, \delta(A)$, the position transfer function. In this report, we use the term "transfer function" solely in reference to the intensity transfer function, as defined above and as discussed in more detail in the paragraph below. It is important to note that the foregoing requirement is much less stringent than would be the case if it were required that the television signal be used directly to produce a picture displaying this same information to an observer. The functional design of the Celescope experiment, however, is very similar to that of the more usual picture-producing television systems from which the Celescope concept was initially derived.

The manner in which the Uvicon converts the photoelectric signal from the photocathode into a video signal is described in detail by Goetze (1966), Boerio, Beyer, and Goetze (1966), Beyer and Goetze (1966), Beyer, Green, and Goetze (1966), Doughty (1966), and Marshall and Roane (1966). Their studies have shown that as the input signal increases in strength, the output signal increases in both width and amplitude, in such a manner that

$$it_{ex} = f_p(V_\Sigma) \quad ,$$

where V_Σ is the summation of the coefficients of the output matrix, i is the photoelectric current, and t_{ex} is the length of time that high voltage is applied to the imaging section of the Uvicon. The relationship between input intensity and output amplitude is called the transfer function f_p. The form of the transfer function depends strongly on the manner in which the Uvicon is operated and on the circuit parameters of the system in which it is installed. In practice, we must calibrate this transfer function separately for the analog and digital modes, using the actual flight configuration of the electronic system. It is again necessary to make separate calibrations at a number of different positions on the photocathode and to determine the effect of temperature variations on these transfer functions. Figure 15 compares a typical transfer function obtained during calibration of Uvicon No. R19A with those given by the manufacturers (Beyer, Green, and Goetze, 1966) and to that given by Davis (1966a) for an earlier calibration of the same tube. Such a comparison demonstrates the importance of calibrating the camera tube in the actual electronic system with which it will be operated in space.

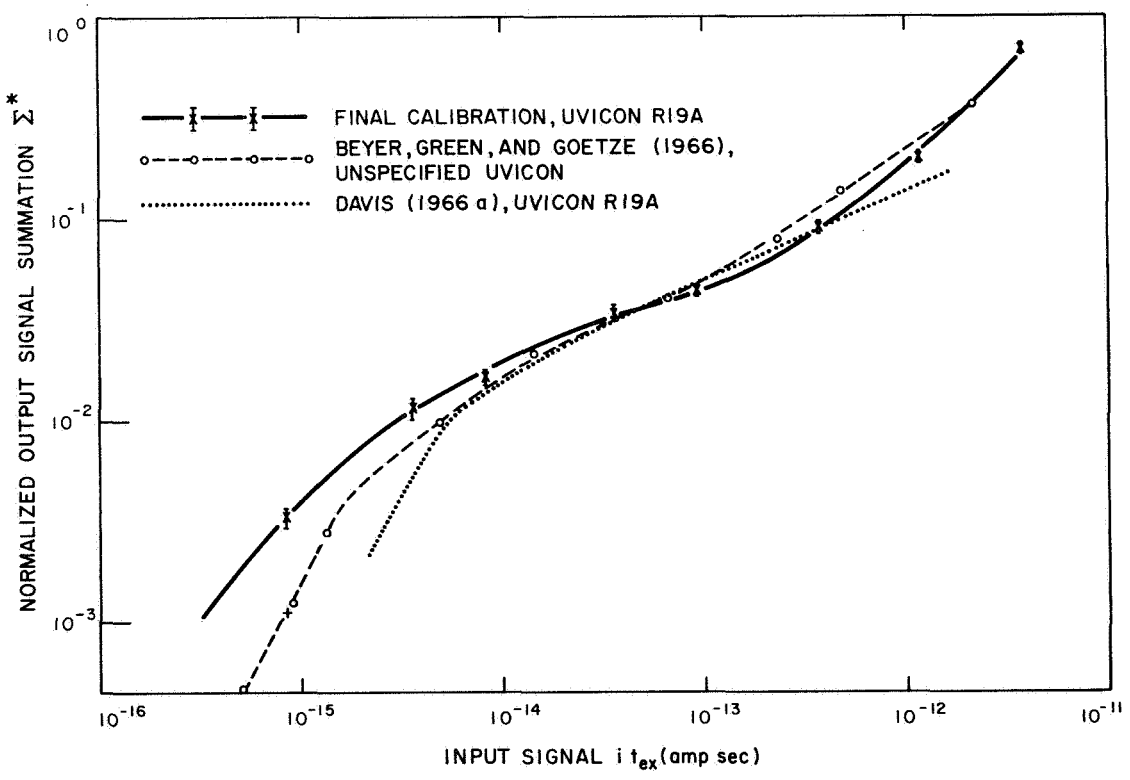

Figure 15. Intensity transfer function for typical Uvicons using three different scanning techniques.

The sensitivity of the Celescope system to faint stars depends upon the exposure time and upon the noise level in the video signal. Our standard exposure time that will be used for all routine observations is 60 sec. When a dangerously bright star is within the field of view, we can reduce our threshold sensitivity 2.5 mag by reducing the exposure time to 6 sec; shorter exposure times are not recommended. If we plan to observe a faint star of special interest, we can increase our threshold sensitivity 1.75 mag by increasing the exposure time to 300 sec; longer exposure times are not recommended.

The rms system noise signal, referred to the Uvicon camera output, is approximately 0.15 mvolt. We have defined threshold sensitivity to correspond to a peak signal of 0.45 mvolt above the average background level; such a signal has less than a 1% probability of being a noise pulse. Experience has shown that a star twice as bright as this threshold level is easily recognized and measured, whereas a star half as bright as this threshold level cannot be seen at all. To illustrate this point, Figure 16 shows the portion of the output signal matrices containing the on-axis calibration signals for three brightness levels for Celescope photometer no. C-1, in units of 5×10^{-5} volt. The elements containing significant signals are circled. The other elements contain noise signals.

Each brightness level is repeated three times during calibration to provide information regarding the photometric accuracy of the system. Figures 15 and 16 indicate representative output variations to be expected when identical inputs are imposed on a Celescope photometer. These fluctuations correspond to an rms accuracy, for brightnesses between 2 and 8000 times threshold, of about ±0.1 mag. They appear to be due primarily to fluctuations in the control voltages and environmental conditions imposed on the Uvicon, and not to the electronic noise that limits threshold sensitivity.

For our standard exposure time of 60 sec, threshold sensitivity corresponds to a photoelectric current, i_N, of 1×10^{-17} amp. If we assume a spectrum $I_0(\lambda)$ for a 0-mag star, we can use the spectral-response curves of Figure 13 to determine the photocurrent,

$$i_0 = \int_0^\infty S(\lambda) I_0(\lambda)\, d\lambda \quad ,$$

that the star will produce in one of the Celescope photometers. The threshold magnitude can then be defined as

$$V_{th} = 2.5 \log \frac{i_0}{i_N} \quad .$$

The limiting magnitudes, V_{lim}, plotted in Figures 6 through 9 are 2.5 mag brighter than V_{th}.

2.5 Resolution

Under ideal conditions, the Celescope television system is just capable of resolving two stars separated by a distance of two television lines (1 arcmin). The optical system has a limiting resolution of about 0.7 arcmin. The resulting ideal system resolution of 1.5 arcmin is valid throughout most of the field of view for stars fainter than 10 times threshold. Figure 17 shows a set of photographs of a resolution test pattern taken during selection of high-voltage divider values for Uvicon 65-40-031A. (The values chosen as optimum were F3 = 16, F2 = 3.8.) Each ring is 0.23 larger than the next; the points in the third ring are separated by about 5 arcmin. For brighter stars, image spread reduces system resolution in accordance with the curve shown in Figure 18.

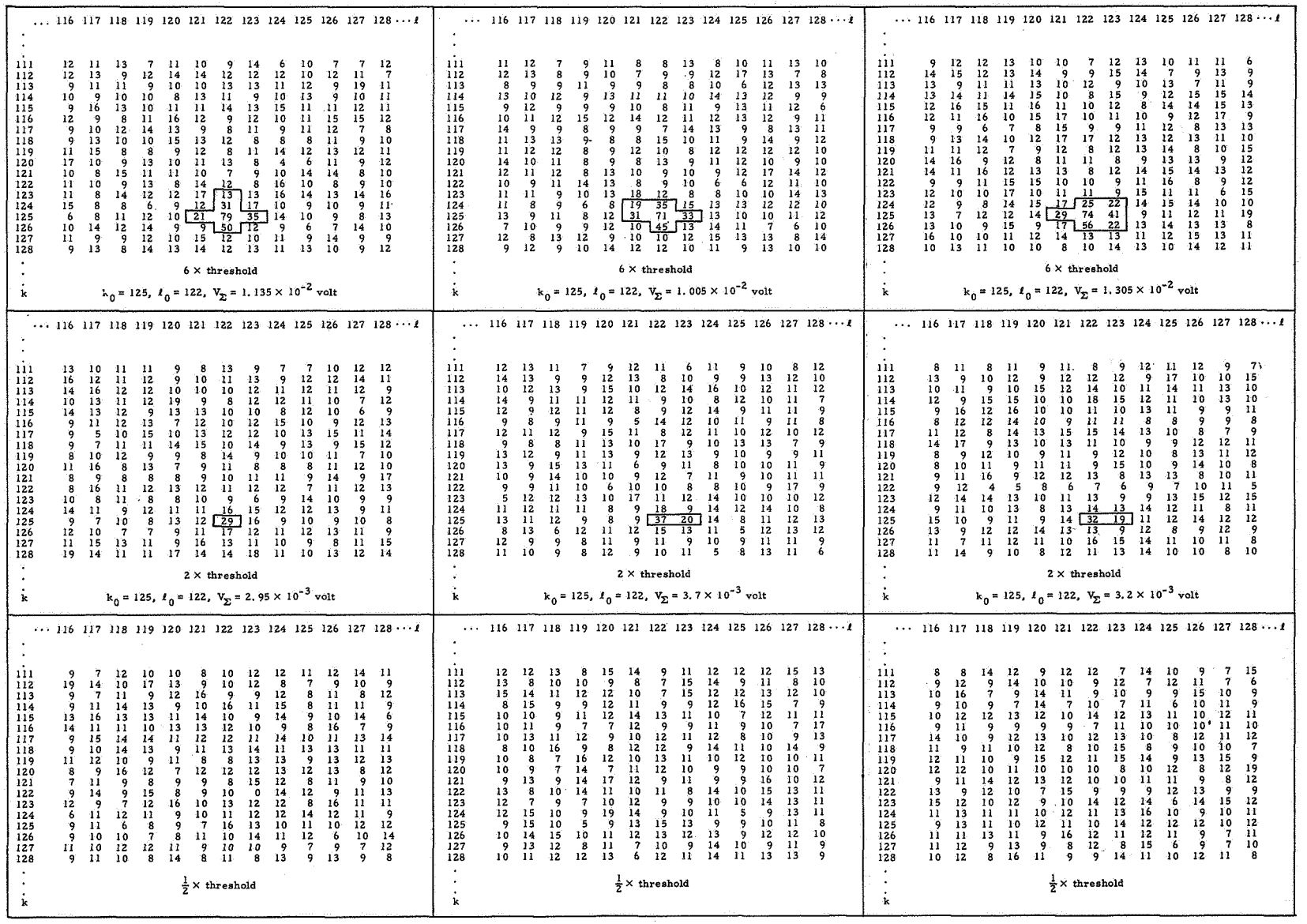

Figure 16. Representative Celescope output signals.

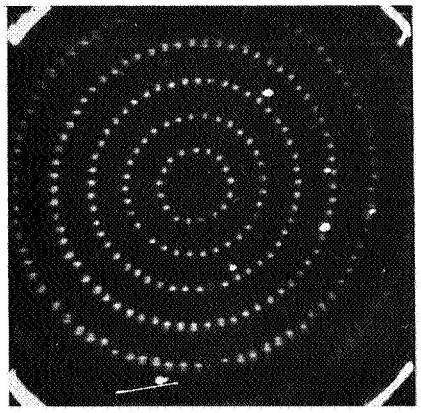

F2 = 3.5

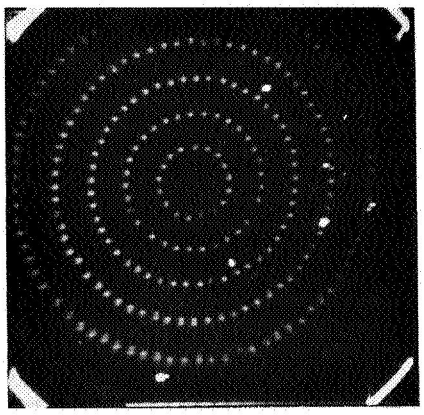

F2 = 3.6

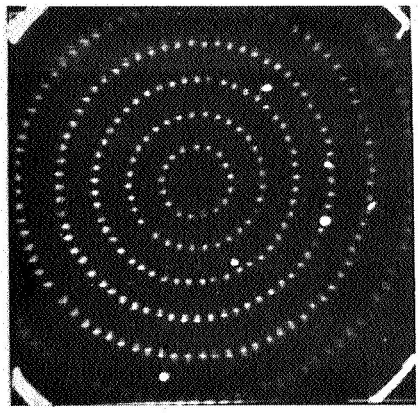

F2 = 3.7

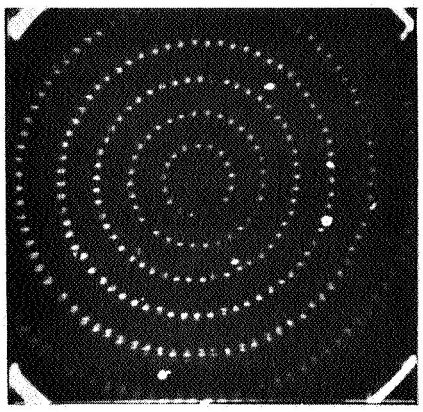

F2 = 3.8

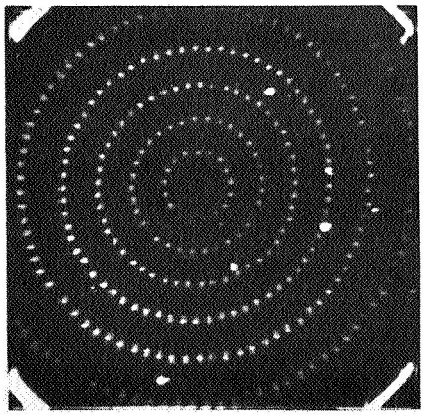

F2 = 3.9

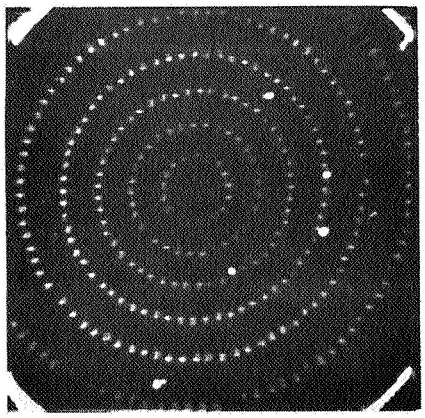

F2 = 4.0

Figure 17. Optimization of F2 voltage for tube no. 65-40-031A.

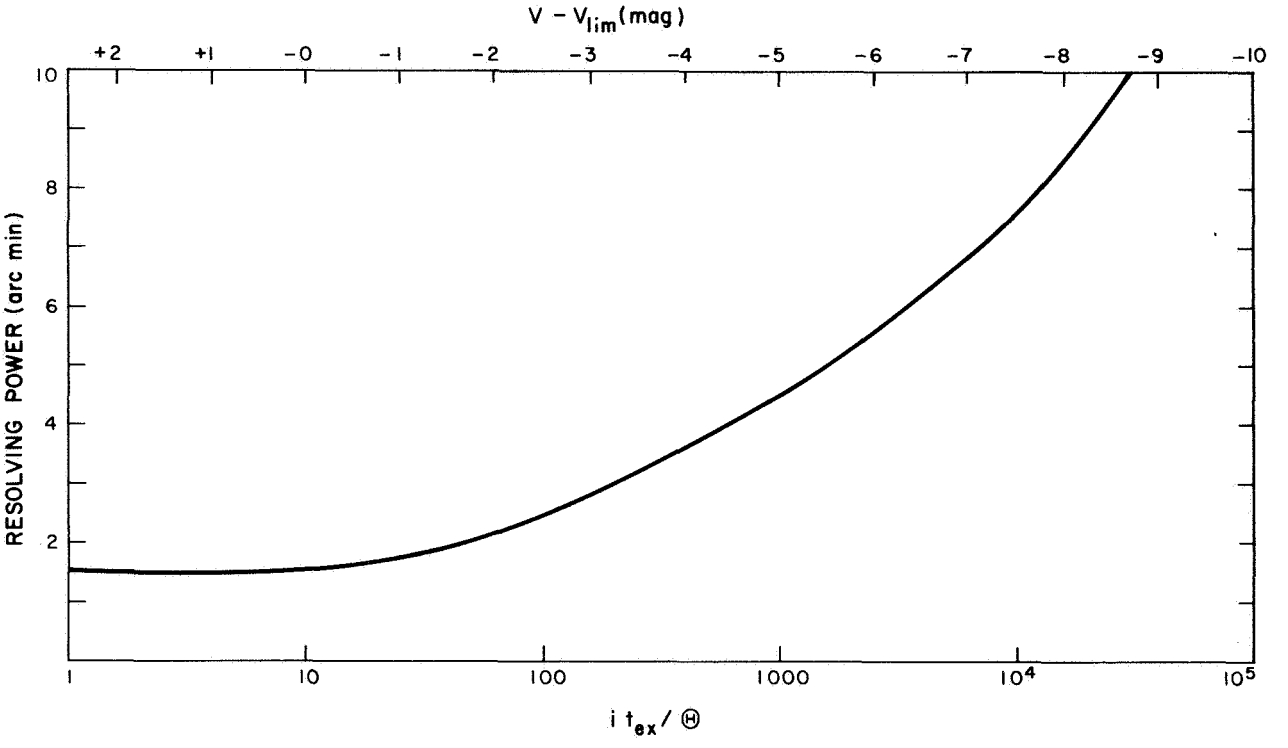

Figure 18. Angular resolution as a function of star brightness.

3. METHOD OF OPERATION

The Celescope instrumentation has been planned and designed to function primarily as a real-time OAO experiment. The complex sequence of voltage switching required to generate each television picture is achieved by transmitting a corresponding sequence of experiment commands via the OAO radio command system. The video signal controlled by these commands is normally coupled directly to the wide-band transmitter of the OAO spacecraft for real-time transmission to the ground. The command storage and data storage of the OAO spacecraft are available to the Celescope experiment for supplementary and emergency use, but are not large enough to allow efficient use of the Celescope instrumentation in other than a real-time mode.

Seven types of command are available for controlling the Celescope experiment:

1. Data-handling commands that control the storage of engineering telemetry data.

2. Redundant subsystem-selection commands that enable us to change from an inoperative subsystem to its replacement.

3. System operating-mode commands that allow a selection among real-time analog, real-time digital, and stored digital modes of video operation.

4. Video-selection commands that select the camera whose video signal is connected to the spacecraft and is controlled by the system operating-mode selection.

5. Television-adjustment commands that independently control the focusing voltages for each of the four cameras.

6. Television-operating commands that independently control the operating voltages for each of the four cameras.

7. Commands that turn the calibration lamps on and off.

In addition to these experiment commands, we have use of the following spacecraft commands:

1. SAO on-off commands that connect our experiment to the spacecraft power system.

2. Data-handling commands that control the storage and real-time transmission of Celescope status data, Celescope video data, and spacecraft status data.

A full description of Celescope commands and of OAO instructions available to Celescope is found in the Celescope Operations Manual.

Both the OAO system and the Celescope experiment were designed primarily for control by digital computer. In general, no command can be sent to the spacecraft or to the Celescope experiment without its effects first being evaluated by the SCPS program on NASA's 360 computer. We input commands to the computer via a set of instructions called the Experimenter's Target List (ETL). The ETL specifies the following information to the SCPS:

1. Ground-station contact.

2. Spacecraft orientation for the first target, relative either to 1950.0 celestial coordinates (right ascension, declination, and roll) or to the previous orientation (amount of slew in pitch, yaw, and roll).

3. Command sequence required for accomplishing the observation desired at the first target.

4. Orientations and command sequences required for second target, etc.

SAO uses two techniques for generating target list: semiautomatic generation by a computer program whose function is to maximize the efficiency with which the sky survey is completed, and manual generation by an astronomer when the computer is not available. A Celescope command sequence will be rejected by SAO's compilation program, in either the semi-automatic or the manual method, if it does not conform to the safety rules

incorporated in that program. After analyzing the reasons for rejection of an ETL, the OAO staff will remove the deficiencies and resubmit the ETL until an acceptable list is achieved. At this point, the output from the SCPS is a contact message in OAO command format. This message is reviewed by NASA and SAO personnel for final accuracy, after which it is transmitted to the ground stations for relay to the OAO. Incorporated into the contact message are not only the Celescope and spacecraft commands necessary for acquiring the data specified by the target list, but also a number of routine housekeeping sequences for determining the status of the OAO, for protecting it in the event of certain types of emergency, etc.

At the OAO ground stations, the contact messages are stored in AD/ECS computers for controlled release during the contact. If the telemetered status data fail to fall within specified limits, appropriate emergency sequences are transmitted by the AD/ECS and the remainder of the normal contact message is aborted. Under special conditions, it is possible for the experimenter to transmit experiment commands directly from a console in his operations area at GSFC, and it is possible for NASA to manually call individual OAO commands and command sequences from a console in the OAO operations area at GSFC if the desired command has previously been stored in the AD/ECS for such use. It is normally not permissible, however, to use manual methods for transmission of orientation commands.

In response to commands received from the ground stations, the OAO generates various types of data and transmits them back to the ground stations. NASA screens, combines, and reformats these data for delivery on magnetic tape to the experimenter. The Celescope digital data tape will contain both the digital video signal and the information necessary for relating it to the operation that produced it. If it ever becomes necessary to change to the analog mode of operation, the analog video signal will be transmitted to SAO on an analog-recorded magnetic tape, with a separate listing required for relating the signal to the operation that produced it.

Five ground stations have been assigned to the OAO: Rosman, North Carolina; Quito, Ecuador; Santiago, Chile; Orroral, Australia; and Madagascar. Only the Rosman station is connected to the control center via a wide-band microwave link; the other stations are connected to GSFC via teletype links.

During normal operations, the target list will be prepared 3 weeks before use, and data tapes will not be received at SAO until 3 weeks after the data were received by the ground station. In order to maintain control of operations, our staff at GSFC will receive quick-look data analyses within 90 min of the start of a Rosman contact. We also maintain television monitors in our operations area at GSFC that provide real-time displays of the televised data received at the Rosman station.

Commands can be addressed either for immediate execution by spacecraft or experiment, or for onboard storage to be executed at a specified future time. Each command consists of two 32-bit words, the first specifying the address and the second specifying the function. Transmission of one command requires 128 msec. A command will be transmitted within 1 sec of the time specified by the ETL, if possible. If previous commands have taken more time than expected, the command will be transmitted relative to the previous command, preserving the interval between each command. Reorientation commands must be executed from command storage; other commands may be either real-time or stored.

The OAO command storage has 256 command locations. However, approximately half of this capacity is permanently occupied with various emergency routines. The remaining capacity is normally devoted to slew commands when the OAO is under Celescope control, because approximately 10 commands are required to specify each axis required for a slew. Operation of the Celescope experiment entirely from command memory will therefore require reloading the memory once for each contact.

The time of execution of a stored command can be specified with 16-sec resolution with a maximum delay of approximately 18 hours. Separate commands specified for execution at the same time will be executed at 5-msec intervals.

After execution of a command, a "settling time" is required for the status of the instrumentation to stabilize in the new configuration. The most important settling times to remember when compiling a command sequence for the Celescope experiment are: 0.2 sec for "expose on" and "expose off" commands; 5 min for "mercury calibration lamp on" commands; 10 sec for "xenon calibration lamp on" commands; 180 sec for single-axis slew commands of 2° or less; at least 5 min for most slew commands greater than 2° and less than 30°; a variable settling time between 0 and 10.5 sec for the "beam on" commands required to produce a digital video signal; a variable settling time between 0 and 0.5 sec for the "beam on" commands required to produce an analog video signal.

A normal observing program with the Celescope instrument entails the following steps, transmitted to the OAO by means of the target list and SCPS:

1. At the last contact before commencement of Celescope operations, the following stored commands required for execution and settling prior to contact for preparing the instrumentation for observing are transmitted:

    a. Reorientation commands for slewing to the first target.

    b. "Mercury calibration lamp on" commands if calibration is desired for either the C-1 or the C-3 camera.

    c. A priming sequence of 9 commands for each camera to be used for the observation. From command storage, this sequence requires 165 sec, independently of the number of cameras to be used.

    d. Additional reorientation commands if more than one target is to be observed during the contact.

2. The first 3 min of the contact is reserved for determining and evaluating the status of the spacecraft and experiments. If a malfunction is detected, the normal contact message is aborted and an automatic emergency sequence is substituted.

3. "Xenon calibration lamp on" commands are required 10 sec before "expose on" commands if calibration is desired for either the C-2 or the C-4 camera.

4. Exposure time is controlled by specifying the interval between an "expose on" command and an "expose off" command for each camera. Selection of exposure time and that of pointing direction are the only options normally available for scientific control of the Celescope experiment. The calibration of the equipment is questionable for exposure times less than 5 sec or more than 120 sec. Exposure times longer than 180 sec become difficult to fit into the OAO observing schedule, and exposure times longer than 300 sec are not allowed. All four cameras can be exposed simultaneously. Calibration lamps should be turned off immediately after the end of exposure.

5. A series of six commands is required to read each camera. Only one camera can be read at a time. In either of the digital modes (real-time PCM mode or store mode), 22 sec is required for transmission of the video signal. The total time required varies from 43 sec for one camera to 109 sec for four cameras. In the analog mode, 1 sec is required for transmission of the video signal. The total time required varies from 22 sec for one camera to 28 sec for four cameras.

6. If more than one target is to be observed during the contact, a slew can be performed simultaneously with readout. The priming sequence can be performed before the completion of the slew maneuver. Real-time priming requires 88 sec, independently of the number of cameras used. Expose and readout must then be repeated as above.

7. The last 30 sec of the contact is reserved for the standard OAO departure sequence.

The length of a contact varies between 7 and 12 min. This and other details of each contact, including ground-station assignment, are provided about 3 weeks in advance by NASA in the NETCON tables, available in both printed and computer-compatible formats.

4. PLAN OF OPERATION

As discussed in Section 1 of this report, the Celescope experiment was not designed for the detailed analysis of a small number of objects of special interest, but for the intercomparison of general properties of a large number of objects not individually specified. Reliability analyses indicate that the probability of our observing every object within reach of this instrumentation is considerably less than 1%. Our goal is therefore to find the sequence of slew maneuvers that will maximize the number of objects we expect to observe, while introducing a minimum of bias into the results as a consequence of incomplete sky coverage.

Special observing requests may be introduced into this scheme in a variety of ways, depending upon the urgency of the request, the number of targets involved, and the relative importance of the special observing program.

Our sky-mapping operation will be performed in three stages: First, we will observe an initial region about $15° \times 15°$ that is near both the galactic plane and the pole of the orbit and that conforms to all of the spacecraft constraints; second, we will observe as many as possible of the 50 selected areas that are evenly distributed through the sky; and finally, we will observe the remainder of the sky and the remaining selected areas as they become available. Table 1 specifies the locations of our selected areas.

Orbital operations are planned to proceed through the following stages: (1) rehearsal, including at least 1 month of round-the-clock operation of the OAO by the operations teams to simulate completely the first month in orbit and certain types of emergency situations; (2) launch support, during which time part of the operations team is engaged in prelaunch testing at the Atlantic Missile Range, while the other part of the team is maintaining the

Table 1. Celescope selected areas.

Selected area no.	Galactic coordinates ℓ^{II}	Galactic coordinates b^{II}	Celestial coordinates Right ascension	Celestial coordinates Declination
1	25.11	1.01	277.70	-6.53
2	70.00	0.00	301.37	32.30
3	115.00	-0.01	355.27	61.53
4	160.96	0.38	72.12	44.67
5	205.03	-0.30	98.30	6.93
6	250.63	0.59	122.37	-32.50
7	295.00	0.01	175.27	-61.53
8	340.00	-0.01	250.85	-45.17
9	5.69	23.77	248.12	-10.80
10	47.51	22.51	267.62	22.43
11	90.42	23.02	283.37	60.28
12	137.50	22.50	85.00	75.98
13	183.84	23.23	112.42	35.38
14	227.50	22.49	128.75	-1.68
15	273.45	22.02	159.25	-32.92
16	317.03	22.15	208.95	-38.63
17	2.83	-21.24	289.75	-35.63
18	47.38	-21.68	308.00	2.00
19	91.94	-21.87	337.75	32.30
20	139.00	-21.97	31.25	38.27
21	182.21	-22.27	67.35	14.25
22	227.32	-22.76	87.30	-22.37
23	272.02	-23.53	103.12	-61.83
24	318.74	-23.79	271.50	-75.37
25	23.86	46.51	236.62	13.70
26	70.17	44.61	245.37	44.83
27	114.39	46.21	209.87	70.00
28	160.54	45.67	144.00	55.20
29	206.52	45.46	142.80	23.47
30	249.44	44.60	157.25	-3.00
31	295.00	45.66	186.42	-16.58
32	340.90	45.94	217.87	-9.00
33	24.99	-45.00	322.00	-24.38
34	71.35	-45.01	338.50	3.67
35	115.21	-45.86	6.60	16.40
36	157.93	-45.67	36.25	10.33
37	204.99	-45.01	58.37	-13.77
38	250.17	-43.76	66.57	-44.88
39	292.36	-46.24	33.50	-69.37
40	338.77	-45.84	325.02	-56.30
41	19.65	66.98	216.15	20.08
42	112.92	67.26	198.25	49.67
43	206.84	68.48	167.95	27.58
44	295.24	66.66	189.17	4.25
45	25.08	-66.47	345.62	-28.08
46	115.62	-67.52	9.42	-5.08
47	204.98	-67.51	36.40	-22.20
48	294.00	-65.45	18.25	-51.53
49	214.85	90.00	192.25	27.40
50	259.46	-87.78	14.00	-29.00

ground-support system at GSFC in a state of readiness for launch; (3) post-launch spacecraft initialization; (4) Wisconsin experiment initialization and experimentation; (5) Celescope initialization and initial observations; (6) routine operation, during which time the Celescope experiment and the Wisconsin experiment will be operated alternately for 7 days each. Under these conditions, the Celescope initial region will be completed about 3 weeks after launch, and 15 selected areas will be completed during the first 2 months of OAO operation. Most of the remaining selected areas will be blocked by the solar, antisolar, and flip-circle constraints, so that after 2 months we will begin the final phase of our sky-mapping operation and continue with the selected areas as they became available. As noted above, it would require more than 2 years to complete an all-sky map with this instrument; the probability of the Celescope experiment lasting that long is less than 1%. Our reliability analysis, discussed more fully in Section 5, indicates approximately 90% probability of the Celescope electronic subsystem operating long enough to complete the mapping of the available selected areas. However, this analysis does not include an assessment of Uvicon reliability, because the number of Uvicons built and tested was not great enough to allow proper statistical analysis. Nor does it include the effects of spacecraft reliability.

Responsibility for safe and efficient operation of the OAO rests with the Project Operations Director (POD), a post that is manned continually by one of the properly qualified senior staff members from NASA's OAO Project Office. The displays and personnel of the OAO operations center at GSFC are organized so as to keep the POD informed of the status and operating schedule of the OAO. Figure 19, a layout drawing of the Project Operations Center, shows most aspects of this organization. The SAO Celescope operations team is part of the OAO operations team. The senior member of the SAO team on duty is termed the Celescope Experiment Director. He is responsible to SAO for operating the Celescope experiment in such a manner as to acquire meaningful scientific data, insofar as the real-time information supplied to him will allow. He is also directly and immediately responsible to the POD for operating the SAO experiment in conformance with the formal OAO operating procedures, and for apprising the POD of the status,

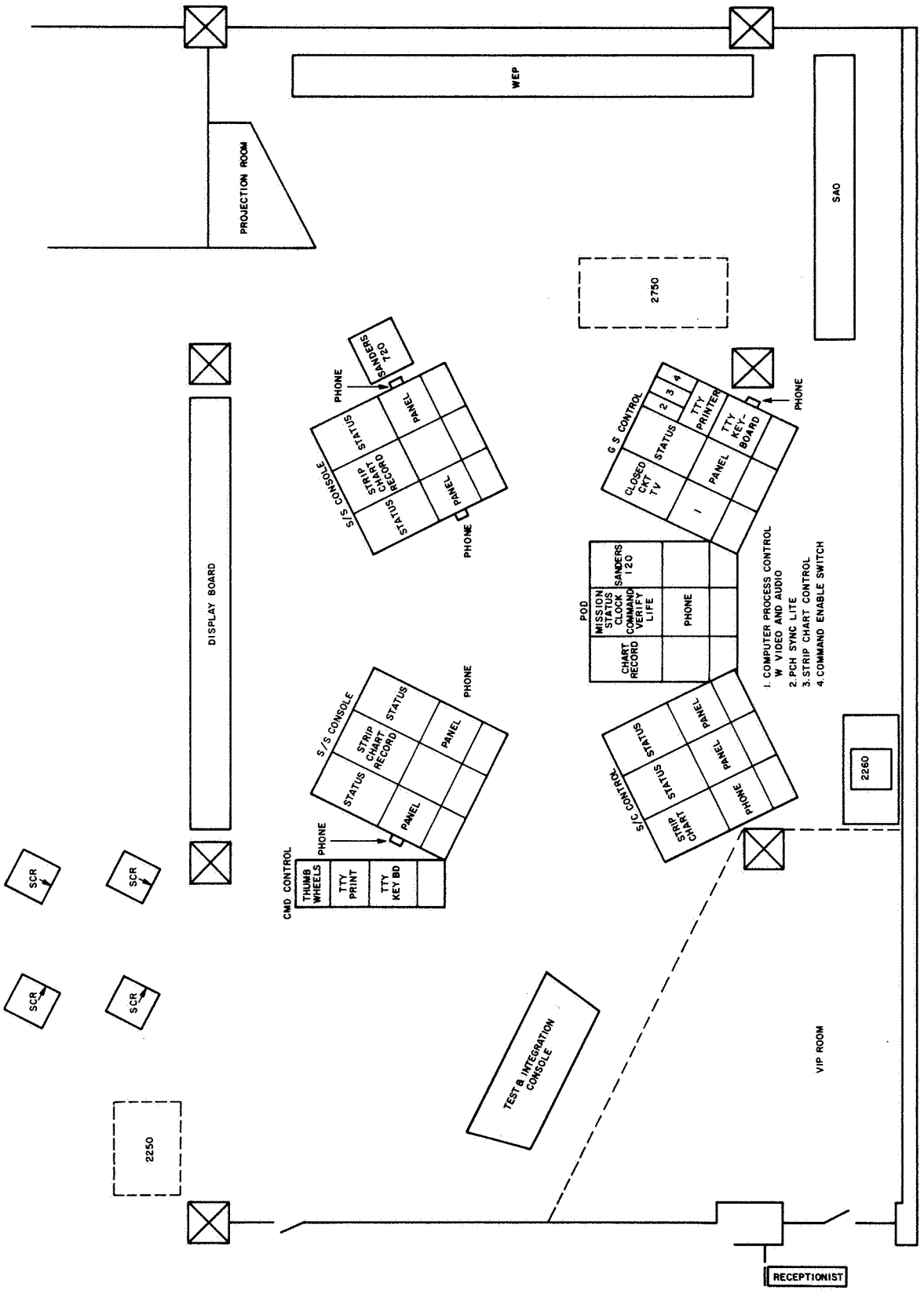

Figure 19. Project Operations Center.

operating schedule, and problems of the Celescope experiment. SAO plans to organize four Celescope operations teams of three members each, to provide full-time coverage under any foreseeable conditions. During SAO's operating week, the duty team will include all three members — the junior members of the team will have responsibility for apprising the Celescope Experiment Director of difficulties encountered in the operation of the experiment, and for operating the Celescope ground-support equipment (GSE). During Wisconsin's operating week, the SAO duty team will be only one member, whose responsibility is to monitor the Celescope status data and in the event of Celescope malfunction during this standby period to alert additional team members and institute emergency procedures.

Responsibility for organizing and supervising the activities of the Celescope operations teams rests with the SAO Operations Director, who is also the Celescope Experiment Director for one of the teams. The SAO Operations Director also supervises the compilation of ETLs at Cambridge with the aid of SAO's computer in Cambridge, Mass., 3 weeks ahead of time. Because of the delays involved in reprocessing in Cambridge, the ETLs rejected by the SCPS, the SAO Operations Director will normally reprocess rejected ETLs, and compile emergency ETLs, through the use of simpler procedures available to him at GSFC.

Although engineering status data will be transmitted, via teletype, from the remote stations to the Operations Center at GSFC immediately after every contact, the video data — which contain all the Celescope scientific data — must normally await shipment of magnetic tape from all stations except Rosman. NASA will process the engineering and the video data for all Rosman contacts in order to provide the Celescope Experiment Director with scientific and engineering quick-look printouts within 90 min of the start of the contact during which they were received. In addition, NASA will process all data relevant to the Celescope experiment and provide SAO with magnetic tapes containing these data in a form acceptable to our computer. During Rosman contacts, ground-support equipment provided by SAO will be furnished with properly formatted real-time signals from the OAO to provide

our operating personnel with real-time displays of equipment status and of the television picture.

Both the quick-look printout, provided by GSFC for the benefit of operating personnel, and the final data reduction, provided by SAO for the benefit of the scientific investigator, present the data as a listing of brightnesses and positions for the stars observed. The principal differences lie in the accuracy with which these data are presented, and the suitability of the presentation for displaying massive quantities of data. The quick-look display presents the experiment director with 2°-square "pictures" of the ultraviolet star field observed and with the orientation of the OAO at the time the picture was taken. The final data reduction at SAO improves the accuracy to about 0.1 stellar mag, determines the position of each star in celestial coordinates to an accuracy of about 1 arcmin, "identifies" the objects observed under certain conditions described more fully below, and organizes these data in a variety of tabular and graphical outputs appropriate to the astrophysical problems under consideration. This final reduction proceeds in a number of steps, the first of which is a catalog listing of the brightnesses and positions of the stars observed.

To serve as an aid in identifying the stars we observe and in associating their ultraviolet properties with information previously known from ground-based observations, we have compiled the Celescope Identification Catalog, a listing of about 100,000 objects theoretically bright enough in the ultraviolet to be detected by the Celescope experiment. To effect an "identification," our data-reduction program requires that the observed star lie within specified limits of a predicted star in both brightness and position. These limits, and the rules by which the brightness of a star in the ultraviolet is predicted from its spectral type, magnitude, and color, will be provided as input to the identification program on the basis of experience and scientific judgment as the analysis proceeds.

5. DESCRIPTION OF THE INSTRUMENTATION

5.1 Flight Equipment

The Celescope experiment consists of two major subassemblies: the Optical Package major subassembly, a cylinder approximately 40 in. in diameter, 57 in. long, and weighing 440 lb; and the Bay E-4 Package major subassembly, a rectangular solid approximately $9 \times 16.5 \times 26$ in., and weighing 87 lb. A 10-ft cable from the Celescope Optical Package (COP) attaches to four connectors on the Bay E-4 Package. Additional connectors are provided on Bay E-4 for connecting the Celescope experiment to the spacecraft or to ground-support equipment. Figures 20 and 21 show these major Celescope subassemblies.

Within the COP are mounted four identical telescopes, each having an aperture of 12.5 in. The secondary mirror obscures the central 6.25 in. of each aperture. This optical system focuses an image of a small region of the sky onto the ultraviolet-sensitive surface of a special television camera tube called the Uvicon. The field of view of the system is limited to a diameter of 2.°8 by the size of the photocathode. It is further limited to a square area about 2° on a side by the limited coverage of the scanning raster. A separate optical system provides a means of focusing a point image from a calibration lamp alongside the star images formed by the main telescope, whenever the lamp is turned on. The focal surface of each telescope is between the primary and secondary mirrors. Direct sky illumination is prevented from reaching this surface by extending the telescope tube about 30 in. beyond the secondary mirror. Figure 22 is a photograph of one of these telescopes. Figure 23 shows the COP with one telescope installed.

The COP is designed to be mounted as the aft experiment in an OAO spacecraft of the type open at both ends. The Bay E-4 Package is designed to be mounted in Bay E-4 of the OAO spacecraft. The Celescope experiment

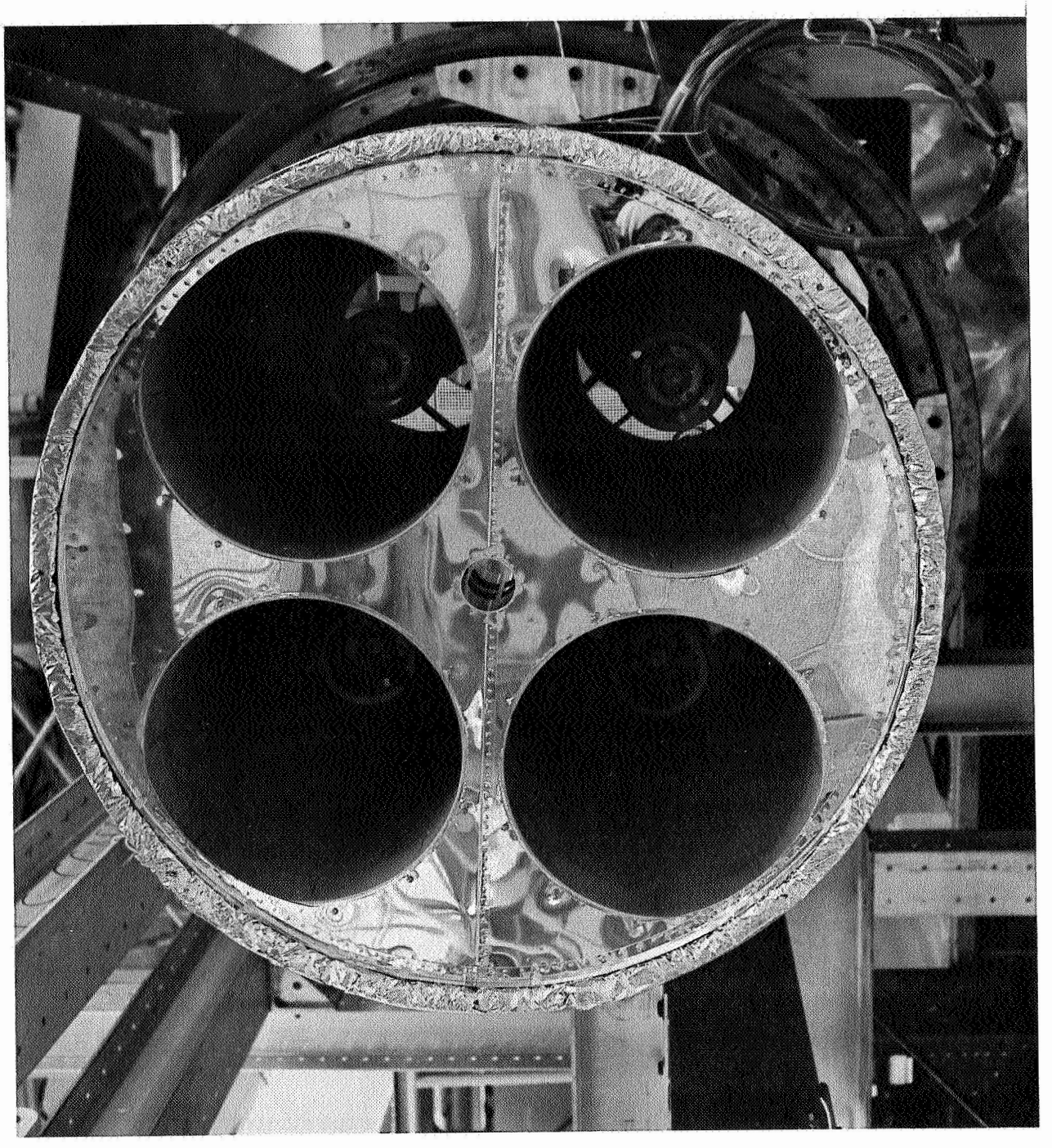

Figure 20. Front view of Celescope Optical Package.

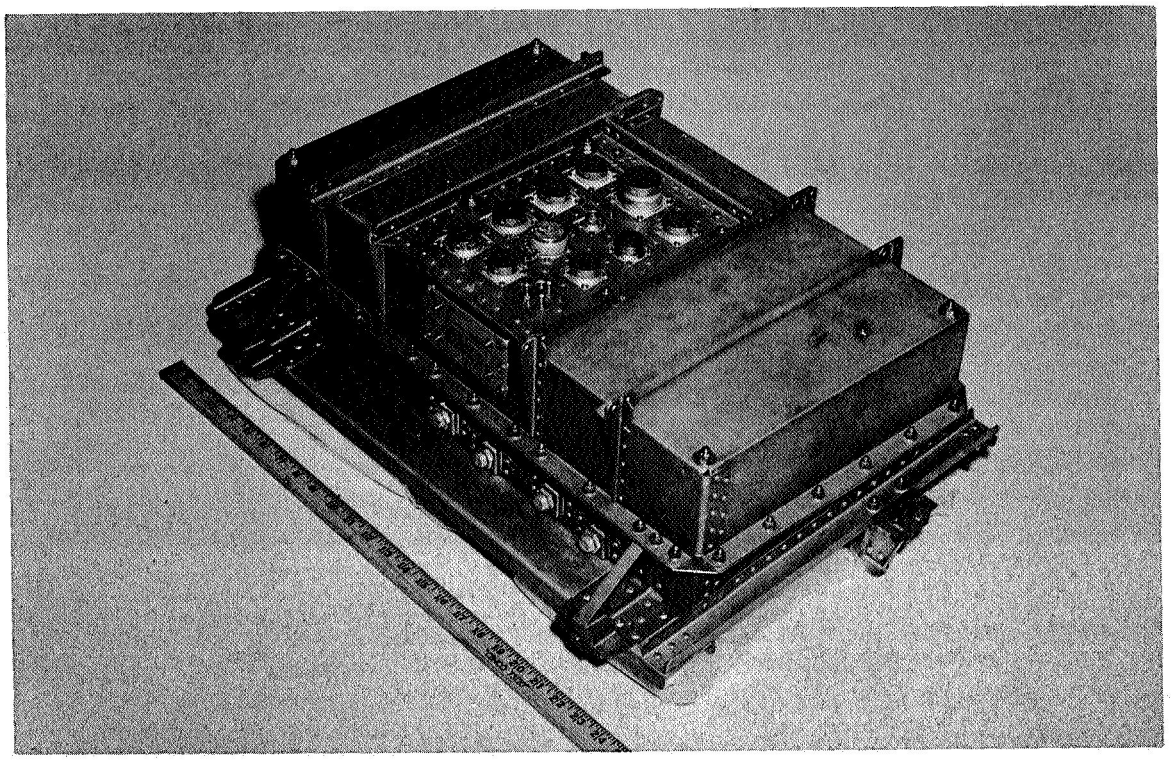

Figure 21. Bay E-4 electronics package.

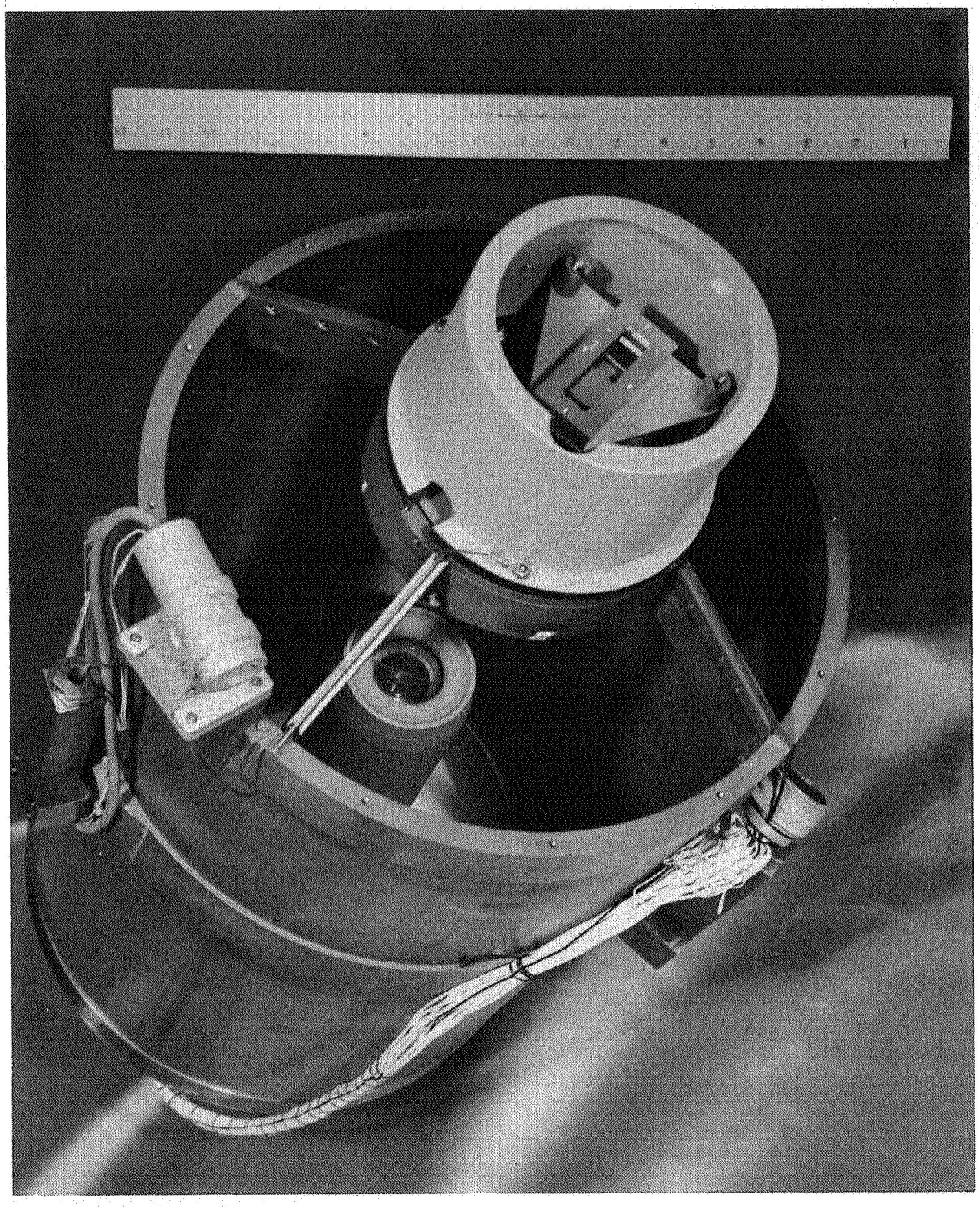

Figure 22. Telescope subassembly.

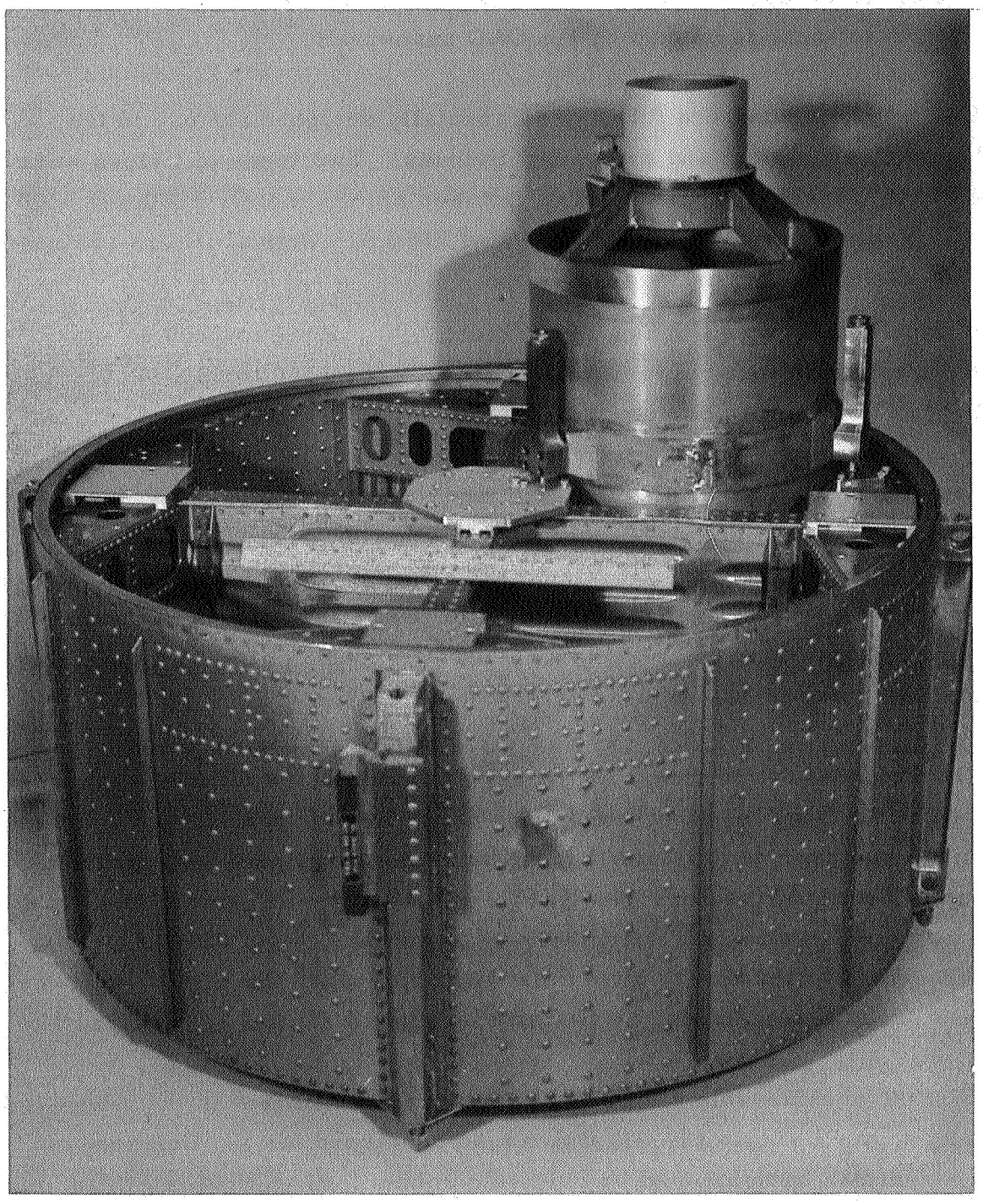

Figure 23. Telescope subassembly mounted in COP before installation of baffling and thermal insulation.

can be operated only when it is supplied with signals and output interfaces equivalent to those furnished by the OAO spacecraft.

The television camera tubes were specially designed for use in the Celescope experiment and are called Uvicons. Two types of Uvicon were developed. The A-type is sensitive between approximately 1050 and 3200 Å. The D-type is sensitive between 1050 and 2150 Å. Optical filters are used to limit further the sensitivity as follows:

A-type Uvicon with Corning 7910 filter:	2100 to 3200 Å
A-type Uvicon with Suprasil quartz filter:	1550 to 3200 Å
D-type Uvicon with barium fluoride filter:	1350 to 2150 Å
D-type Uvicon with lithium fluoride filter:	1050 to 2150 Å .

The field of view of each Uvicon is split into two areas, having different sensitivity characteristics, by mounting two different semicircular optical filters in front of the photocathode. The filter split line is oriented parallel to the direction of the television scanning lines and parallel to the Z_c control axis of the spacecraft.

The Celescope experiment incorporates 54 command functions for adjusting and controlling the electronic operation of the equipment. No command functions are provided for mechanical adjustment or operation, since the design of the equipment ensures that the telescopes will remain in satisfactory focus under all anticipated environmental conditions. The television-camera tube is sensitive to ultraviolet light only when the high voltage is applied to the photocathode, so that no mechanical shutter is provided.

Because considerable electronic complexity is inherent in the television technique, and because the television tube developed for the Celescope experiment can be destroyed by certain combinations of light intensity, tube condition, and operation technique, it is essential that a person familiar with its operation monitor the video signal whenever a Uvicon is being turned on or off, or whenever test data are being gathered. The Celescope is

designed for transmitting pictures one frame at a time, rather than continually as is done in commercial television. In order to produce one such data frame, 17 separate commands must be transmitted to the experiment, with the time intervals between these commands carefully controlled. Prior to issuance of the first such command, the operator must verify, either by status readout or by computer simulation, that the equipment is in a status that will safely allow execution of this command and that all adjustments have been optimized. The rules governing allowable status and command sequences are given in the Celescope Operations Manual.

In the Celescope system, exposure and scanning of the television picture are never performed simultaneously. Exposure is controlled by the high-voltage on and off commands, separately for each telescope. System sensitivity can be adjusted by varying the exposure time — that is, the interval between high-voltage on and high-voltage off. As a result of this exposure, an electronic charge pattern is built up on the Uvicon target, each star image being represented by a point whose charge depends upon the product of exposure time and star brightness. In order to prevent potentially destructive voltage buildup in the thin Uvicon target, the grid nearest the target (G5) is maintained at +9 volts during exposure. Exposure times shorter than 1 sec cannot be accurately controlled. Exposure times longer than 300 sec may damage the equipment.

In order to convert this image into a video signal, the target must be scanned by an electron beam. Correct focusing of this beam on the target requires that G5 be at a voltage near +400 volts. An experiment command must therefore be issued to change the voltage level of G5 prior to scanning. A separate "beam on" command is then sent; the actual execution of "beam on" is automatically inhibited, however, until the deflection voltages complete their cycle and arrive at the "beginning of frame" position. The interval between issuance and execution of the "beam on" command can be as great as 0.48 sec in the analog mode of operation, and as great as 10.5 sec in either of the digital modes of operation, since the sweep generators are continually cycling at the rate appropriate to the selected sweep

mode. After the "expose on" ... "expose off" sequence has been issued, the first "beam on" command causes the next scanning frame to be underscanned, covering a square area corresponding to about 2° × 2° of the sky. This first scan discharges the target to create the video signal, so that subsequent scans contain no information concerning the illumination to which the Uvicon was exposed. At the completion of the first frame, or in the event video is selected for the wrong camera, the beam is automatically turned off and the gain of the deflection amplifiers is automatically increased to overscan the target. As a safety measure, the beam is commanded off, and the target is connected to G5 voltage (high-velocity mode) after completion of the data frame.

As implied above, there are two sweep modes for each camera: analog sweep and digital sweep. The analog mode incorporates a 300-line raster with 1.6-msec sweep duration and 0.48-sec total scan time. The digital mode is internally more complex, but is equivalent to an element-by-element scan of a raster containing 256 lines of 256 elements each. The time spent on each element is 160 μsec; the entire sweep lasts 10.5 sec.

There are three modes of video output, which can be selected by command. The analog mode of operation causes readout to be performed in the analog sweep mode. In this mode, the signal from the Uvicon target is simply amplified and mixed with the synchronization signals for transmission. These sync signals are present whenever the system is in the analog mode. Both the direct PCM mode and the digital store mode of operation cause readout to be performed in the digital sweep mode. Direct PCM is our primary mode of data acquisition, because it has both minimum noise and maximum data content. In this mode, the video signal is sampled at the optimum portion of each 160-μsec picture element and encoded to 7-bit accuracy. As soon as this system operating mode is selected, alternating "1"s and "0"s appear at the video output to provide bit synchronization. Line and picture sync signals appear as soon as the "beam on" is actually executed. These signals replace the intensity data contained in the first five elements of each scanning line, reducing the transmitted raster to 256 lines of 251 elements each.

In store mode operation, 23-bit words are assembled on spacecraft Digital Word 1, indicating position of each picture element and amplitude of its signal. Whenever the amplitude exceeds the threshold level selected by a previously executed command, the experiment generates a "Store Digital Word 1" transfer pulse. The thresholding function is inhibited for the first element of each picture, to provide picture sync information.

Signal characteristics for each mode of operation are more completely defined in the Celescope Operations Manual.

Each telescopic television camera has three numerical designations that can be used to identify it. The first designation refers to the serial numbers of the hardware used in fabrication in the subassembly: F-1, F-2, F-3, and F-4 are installed in the flight payload; S-1 and S-2 are flight spares. The second designation refers to the position of the telescope in the experiment container. This assignment is made in accordance with Figure 24, the telescopes being designated A-1, A-2, D-1, and D-2, respectively. The third designation refers to the manner in which the television camera is connected to Bay E-4 and the manner in which command codes are assigned to Bay E-4, the cameras being designated C-1, C-2, C-3, and C-4, respectively. The importance of making a distinction between these two nomenclature systems was well illustrated during repairs made to the Celescope prototype experiment in late 1964, when it became necessary to change the connection of telescope A-2 from C-2 to C-1, and to change the connection of telescope A-1 from C-1 to C-2. To summarize: a telescope can be recognized as A-1, A-2, D-1, or D-2 from determining its geometrical position in the experiment container; it can be recognized as C-1, C-2, C-3, or C-4 by the command codes required to operate it and by the status data furnished by it. The present assignment is as follows:

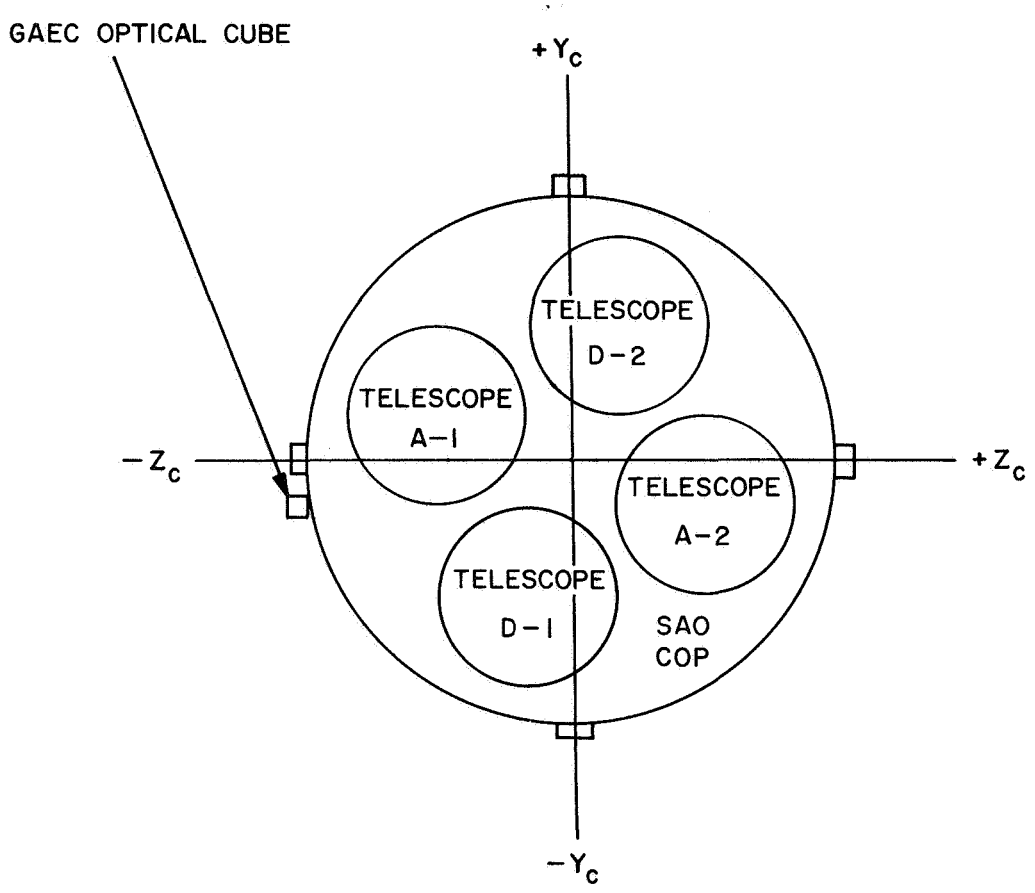

Figure 24. Arrangement of telescope subassemblies in the Celescope experiment.

Telescope subassembly serial number	Experiment container position number	Bay E-4 camera number
F-1	A-1	C-1
F-2	D-1	C-2
F-3	A-2	C-3
F-4	D-2	C-4
S-1	Spare	---
S-2	Spare	---

Celescope utilizes Operation Code Lines (OCL) 13 through 22 from the OAO spacecraft to control its various command functions. Assignment of command functions is specified in the Celescope Operations Manual and in EMR Report CER-93.

Voltages and temperatures at critical locations in the Celescope experiment are monitored by means of analog telemetry signals provided via the spacecraft as Analog Group II. Positions of critical switching functions are monitored by means of digital telemetry signals provided via the spacecraft as Digital Data Words 2 and 3. The coding of these telemetry signals is described in the Celescope Operations Manual.

A detailed description of the flight equipment is given in EMR Project Celescope Technical Manual EMR-SAO-1, Smithsonian OAO Experiment.

5.2 Ground-Support Equipment

Figure 25 is a block diagram of the Celescope OAO system, illustrating the flow of command input and data output. The major blocks on this diagram are: the Celescope payload; the Wisconsin experimental package; the OAO, which contains these and the spacecraft; a remote station; the Celescope display; the Project Operations Center, in which is located the Celescope display; the simulator-command generator; data analysis; and the SAO computer.

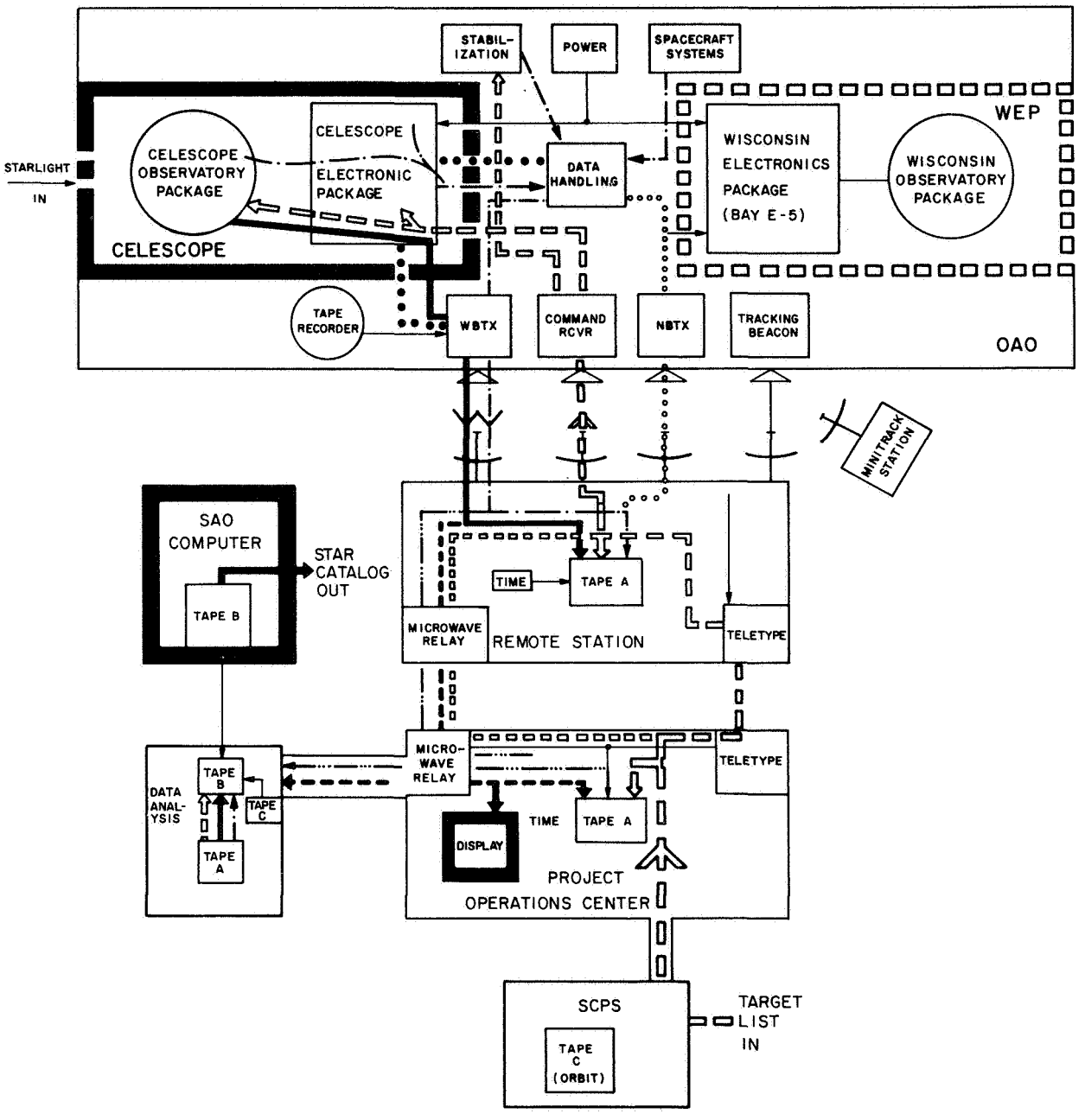

Figure 25. Celescope OAO block diagram.

Figure 25 specifically illustrates the system as planned during orbital operations. Additional ground-support equipment is required during the various testing phases of the program, to replace those portions of the system not involved in such tests. Substitutions can be made as follows:

A. For testing an OAO satellite containing the Celescope experiment: The remote station and Project Operations Center of Figure 25 are replaced by either the Fixed System Test Equipment (FSTE) or the Mobile System Checkout Equipment (MSCE). The only provision for recording Celescope video data is contained in the Celescope GSE Display, for which both the FSTE and the MSCE provide suitable outputs. The system function designated as "data analysis" is performed by the Celescope data-handling equipment.

B. For testing the Celescope experiment when it is not installed in an OAO spacecraft: The spacecraft and the command functions of the ground-based equipment are replaced either by the EMR spacecraft simulator or by the Experiment Test Checkout Unit (ETCU). Recording and processing of video signals is achieved by connecting the Celescope GSE display directly to the Celescope payload. Recording and processing of status data signals are through the ETCU or through the EMR status indicator.

C. For testing the Bay E-4 package major subassembly by itself: The Observatory package major subassembly may be replaced by the EMR Observatory simulator.

D. For testing the Observatory by itself: An EMR camera chain or digital test set is required.

The various units of Celescope ground-support equipment are briefly described below. Complete equipment manuals exist for each unit, describing in detail the equipment, its operation, and detailed interface requirements.

5.2.1 Tonotron storage display

The Tonotron storage display converts any of the three types of Celescope video signals — analog, PCM, or store — into a visible television-monitor picture providing five shades of gray. It can accept these signals from the Celescope payload or from any ground station capable of providing the necessary transfer pulses. It accepts for display one of the first four pictures following receipt of the (manual) enable signal, the desired picture number being selectable by manual switch, and continues to display this picture (for a maximum of 3 min) until manually erased. It provides outputs to which the binary accumulator can be connected.

5.2.2 Spacecraft simulator

The EMR spacecraft simulator supplies electrical power, command signals, and timing signals to Bay E-4 in order to operate the Celescope experiment when NASA equipment is not available for that purpose. Only manual operation is possible with this equipment; no computer interface is provided.

5.2.3 Binary accumulator

The binary accumulator analyzes the video signal from a single point image ("star"), to provide a single numerical output from which the intensity of the star can be immediately determined by referring to a calibration chart. The position of the star must be inserted as a manual input to the binary accumulator. However, any picture that can be repeated (either from a tape recording or by repeating a test procedure) provides information from which to make this adjustment quickly and easily. The binary accumulator must obtain its inputs from the Tonotron display.

5.2.4 X-Y oscilloscope

The X-Y oscilloscope can be adjusted to display continually a monitor picture of the video waveform, when connected to the appropriate output from the Tonotron display. It is equipped with a Polaroid camera attachment that can be used to record selected pictures.

5.2.5 Status indicator

The EMR status indicator can be connected directly to Bay E-4 to provide instantaneous indication of the status data from the Celescope experiment.

5.2.6 Observatory simulator

The EMR Observatory simulator provides dummy loads for the outputs from the Bay E-4 to the Observatory package, and a simulated video signal similar to that from a star. The amplitude and position of this signal can be adjusted manually. In addition, this unit includes display lights to indicate the receipt and execution of Observatory commands from Bay E-4.

5.2.7 Camera chain

The EMR camera chain is not normally used during field activities. It provides for power, control, and handling of video signals directly from the Observatory package or from one of its subassemblies. It does not provide for digital operation of the equipment.

5.2.8 Digital test set

The EMR digital test set is not normally used during field activities. It provides for power, control, and handling of video signals directly from the Observatory package or one of its subassemblies. Operated in conjunction with an ASI computer, it provides the video output in computer-compatible digital format.

5.2.9 Data-acquisition equipment

The data-acquisition equipment includes an Ampex Model FR-1800 system and associated control electronics, and is capable of recording the Celescope video signal in any mode of operation, together with a time base, on magnetic tape.

5.2.10 Data-handling equipment

The data-handling equipment includes an Ampex Model FR-1800 system for playback of recorded video signals, the logic and formatting networks necessary for converting these signals into computer digital format, and a digital tape recorder for recording these signals in correct format for input to the SAO digital computer.

5.3 Reliability of the Flight Equipment

The Celescope experiment must survive the severe launch environment and operate for an extended period of time in the harsh environment of space in order to map the whole sky. This implies severe design requirements for both types of system reliabilities, i. e., survival during launch and in space, and operational reliability in space. To ensure survival of the experiment with high probability, qualification testing has been performed at all levels of assembly to ensure an adequate safety margin in the design of each type of module and subassembly intended for flight. Every type of functional unit of flight hardware had to be tested to prove that the type of functional unit will survive an environment about 50% more severe than the worst case of the expected environment. These environmental conditions include shock, vibration, acceleration, vacuum, high temperature, and low temperature.

In order to ensure that flight hardware was as nearly as possible identical to the units that had been qualified, frequent and rigid quality-control inspection and detailed documentation procedures were established. In addition, all flight units were tested in environments similar to those

expected during launch and orbital operation, to further ensure good quality of workmanship.

High operational reliability of the flight experiment had been achieved by the usual techniques of component selection and redundancy. All components used in flight and qualification units are high-reliability components for which the failure rate is on the order of 10^{-7} failures/hour. Since the Celescope experiment includes about 28,000 electronic components, high-reliability components are essential. To secure high-reliability components, we had to put all components through component-screening tests that consist of lot-acceptance tests, environmental tests, and burn-in tests. All electronic components in the experiment package are solid-state except for the Uvicon camera tubes, the calibration lamps, and the power-switching relays.

Even though high-reliability components had been adopted, the severe reliability design goal made necessary extensive redundancy of functional units. In general, all digital or logical portions of the experiment package were designed to use component redundancy. The basic building block of digital circuits is a quad-redundant pulse inverter whose function is similar to that of a single transistor. The failure rate of the quad-redundant pulse inverter is 4.7×10^{-8} failures/hour. For major portions of analog function units, functional redundancy, rather than component redundancy, was used. All low-voltage power supplies are dual-redundant. The camera-chain electronics are quad-redundant, one chain for each camera. Data-processing electronics (analog-to-digital converter) and digital-sweep generator (digital-to-analog converter) are dual-redundant. All optical (photometric) functions are dual-redundant configurations that allow up to two camera failures without losing any photometric capability.

Special considerations were necessary in the design of the flight experiment, in addition to the normal high-reliability design technique. These special considerations, which are general requirements for all electro-optical experiments in space, are (1) dust control, (2) material and process control, and (3) high-voltage arcing control. All flight hardware was exposed

only to clean-room environment during assembly, testing, storage, and transportation periods. This dust control prevents contamination by dust particles from causing malfunction of the flight experiment. In the high vacuum of space, evaporation and outgassing from the materials used in experiment and spacecraft can lead to equipment failure in a variety of ways. Evaporated or outgassed material can condense on nearby cold surfaces. If the surface is an optical one of the flight experiment, the sensitivity could be reduced to nearly zero. To avoid this optical contamination problem, all materials used in the flight experiment were carefully selected. And all parts and components were processed (for instance, by vacuum bake) to avoid any residual outgassing. Also, any contacts between flight hardware and oily surfaces like human skin had been completely prohibited, to prevent accumulation of organic matter on the surface. If there are high voltages (above 200 volts) in vacuum, there is always a chance to generate arc-over or corona. Even in the high vacuum of space, some outgassed vapor would be sustained near the surface of exposed high voltage. Therefore, all high-voltage power supplies have to be built as arc-proof design, which means that the power supply must be arc-proof in any environment, especially a low-pressure region (about 1 mm Hg or lower). All high-voltage power supplies in the Celescope experiment had been designed, built, and tested as arc-proof.

Based on the various techniques mentioned above, reliability of the Celescope experiment is believed to be very close to the expected value based on analytical prediction. The analytical prediction of system reliability used here is standard technique in which system-failure probability is calculated from failure probability of various functional blocks in the system by topological combination. Failure probability of each functional block was determined by assuming an exponential model of failure probability. The failure rate in each block was obtained by adding the failure rate of every component in the functional block. Since the critical elements in the experiment, the Uvicon tubes, do not have sufficient statistical data to determine failure rate, the calculation excluded Uvicon-tube failure modes. All Uvicon tubes, which were thoroughly tested and inspected, would have a better or at least an equal failure rate of the average image-tube failure rate, 10^{-5} failures/hour.

Figure 26 denotes, as well as is possible in firm mathematical form, our subjective evaluation of the relationship between the value of the experiment and the fraction of the sky mapped. The fraction of the sky mapped before the first telescope module fails is, of course, proportional to the length of time before that failure. After that time the sky is mapped at half this rate until two telescopes of the same type have failed. For mathematical purposes, the experiment is then considered to be terminated.

The two stages of operation as defined above are characterized by two distinct probabilistic survival curves. These two curves are related, and together they determine the expected final value. The basic definition of expected value is

$$\overline{V} = \int_0^\infty V(t)\, dP(t) \quad .$$

Here, $\overline{V}$ is the expected final value of the experiment, V(t) is the value that the program has attained by time t, and P(t) is the reliability of the equipment. Figure 26 shows V(t) and P(t) for both stages of operation.

As is indicated schematically in Figure 26, the V(t) curve has a shape dependent on the time that the first telescope module fails; the dotted line indicates the V(t) curve for such first failure at 30 days after launch.

After extensive manipulation to formulate the exact probabilistic connection between the two stages in mathematical terms, final evaluation of the above integral gives

$$\overline{V} = 87\% \quad .$$

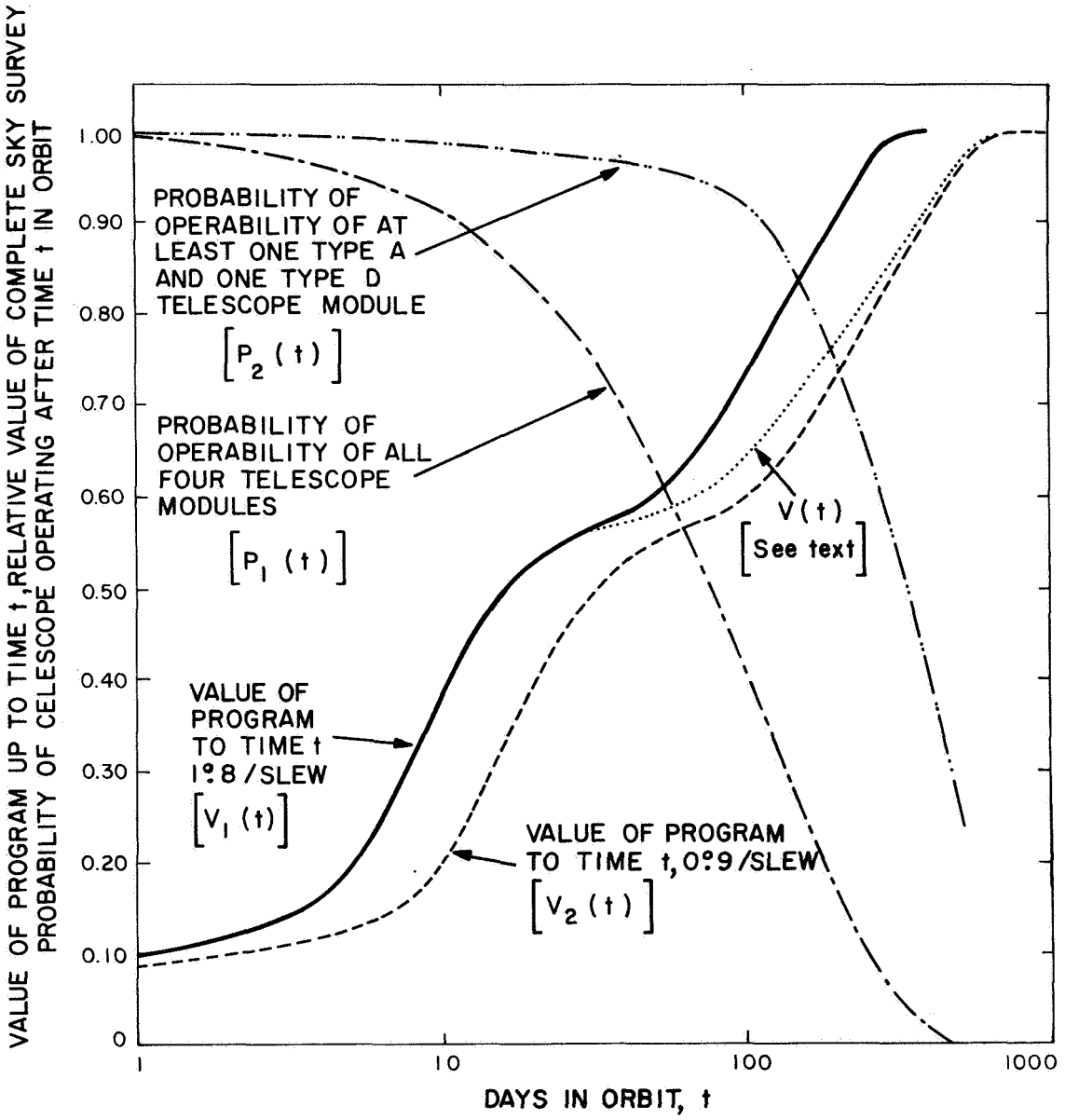

Figure 26. Criteria for success of Celescope.

6. CALIBRATION AND DATA REDUCTION

6.1 Information Processing by the Celescope Equipment

As was stated in Section 2.4 of this report, if a television signal is to be used for stellar photometry, it must provide a type of information from which the following input variables can be derived: Λ, the effective wavelength; $I(\Lambda)$, the intensity at that wavelength; (α, δ), the direction to the star in right ascension and declination. The television signal must also provide the information necessary for determining that a particular signal arises from a star and not from some other type of object.

As was also stated in Section 2.4 of this report, our television signal can be expressed and analyzed mathematically as a matrix A in which the coefficient $a_{k,\ell}$ represents the signal amplitude for the kth television scanning line and the ℓth television-picture element.

Figure 27 and the Frontispiece show cutaway views of the experimental apparatus; photographs of this apparatus appear in Figures 20 through 23. Figure 27 shows the construction of an individual telescopic television camera, and the Frontispiece shows how four such cameras, along with a separate central electronics unit, are mounted into the spacecraft of the OAO. Figure 28 is a block diagram showing the basic design of the Celescope equipment and the various steps by which this equipment transforms the input information into the appropriate output video signal.

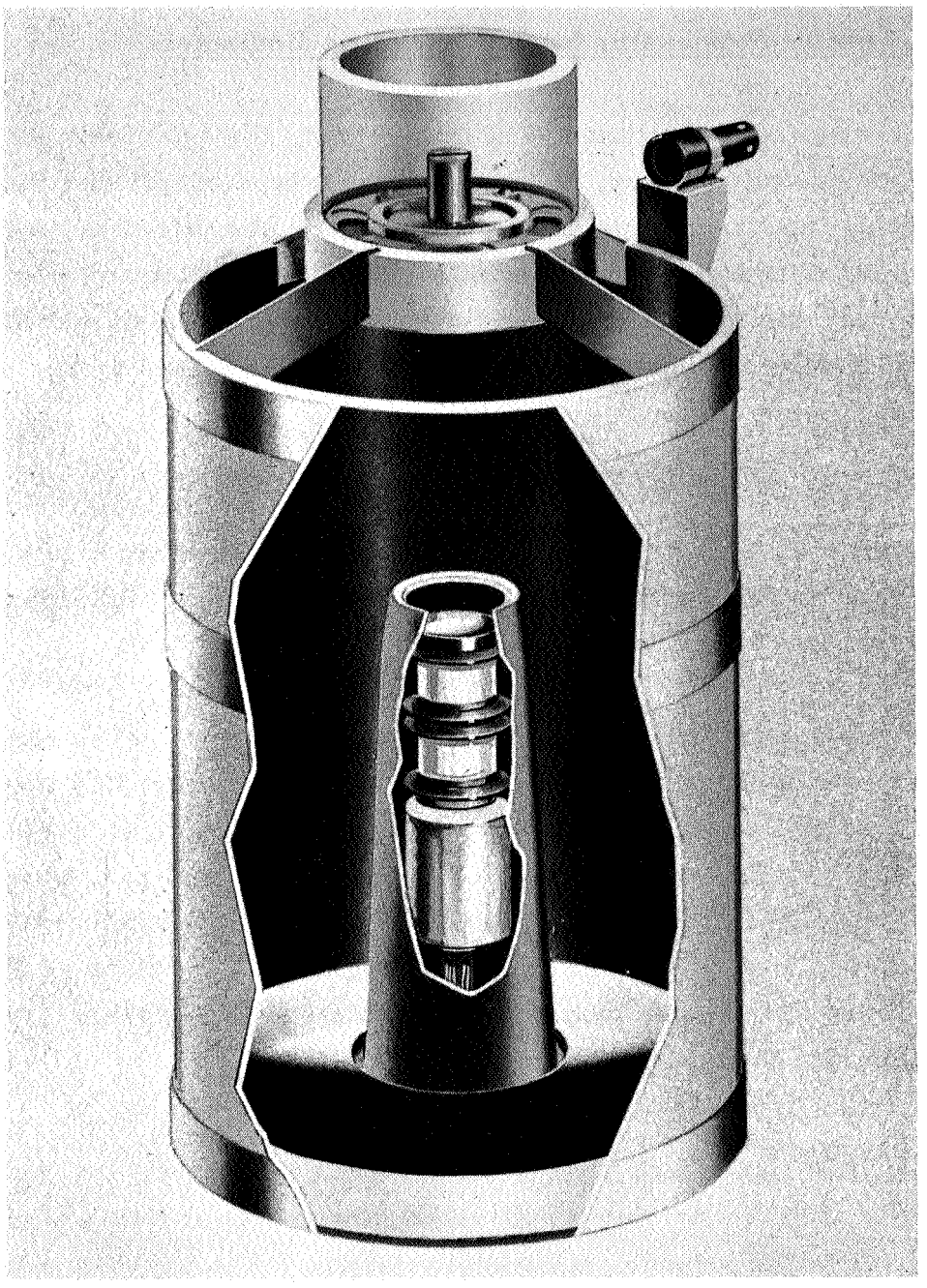

Figure 27. Telescopic television camera.

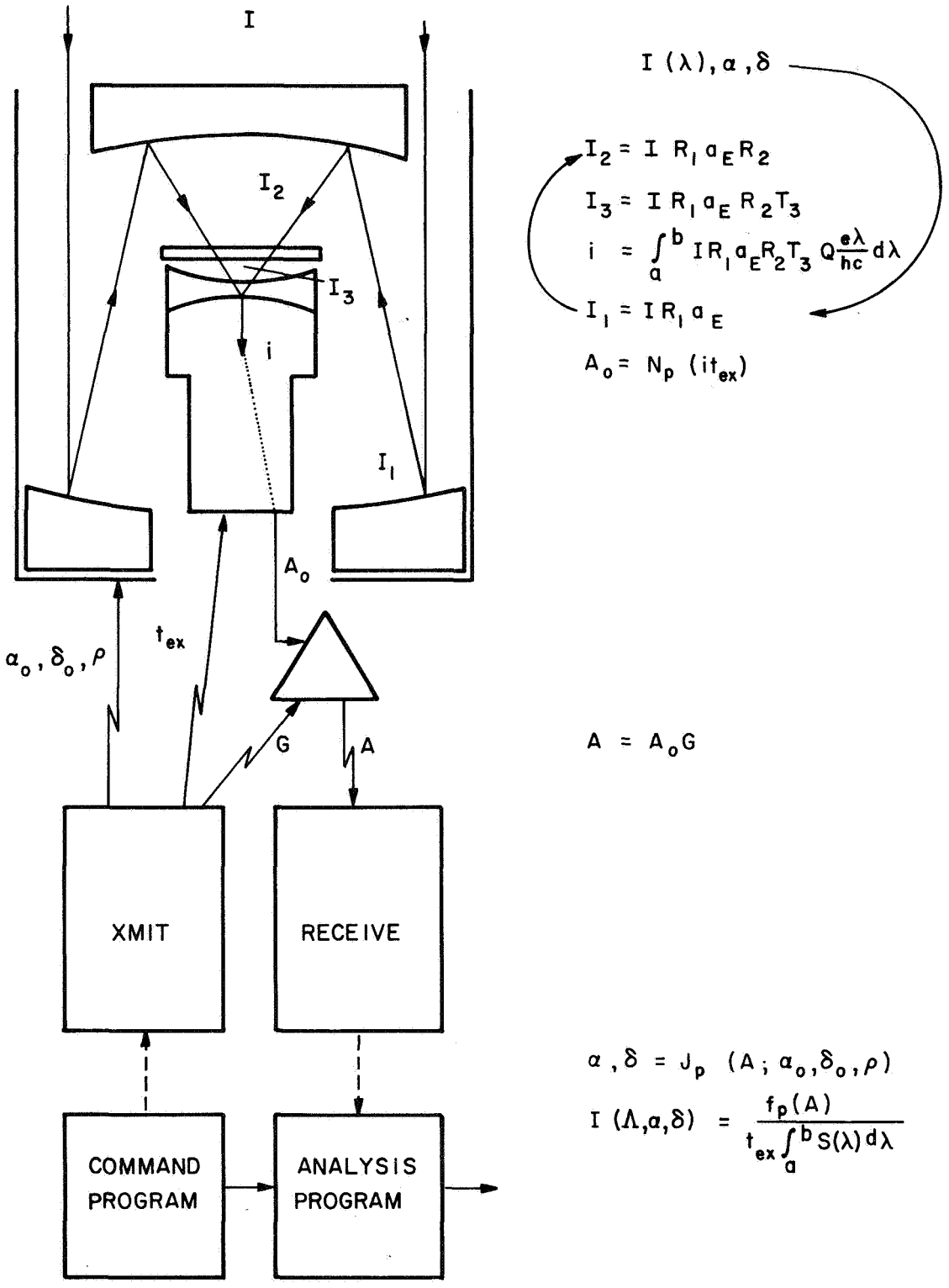

Figure 28. Block diagram and information flow in the Celescope system.

The first transformation, optical focusing, is performed by the optical subsystem in the usual fashion. Light from a star, in direction (α, δ) and of intensity $I(\lambda)$ as a function of wavelength, is collected and reflected by the primary mirror, of collecting area a_E and reflectivity $R_1(\lambda)$. This reflected light from the primary mirror is in turn reflected by the secondary mirror of reflectivity $R_2(\lambda)$, transmitted through the optical filter of transmissivity $T_3(\lambda)$, and imaged at position (x, y) on the photocathode of the Uvicon. The optical subsystem is constructed as a rigid unit, so that this position depends only upon the direction (α, δ) to the observed object, the fixed geometrical design of the optics, and the orientation of the spacecraft. Spacecraft orientation is subject to independent ground-based control and telemetry verification during the lifetime of the satellite. The light intensity received at this point is directly proportional to the incident intensity, the constant of proportionality being the optical sensitivity. Calibration of the positional transfer function of the optical subsystem is a straightforward geometrical problem. Calibration of the intensity transfer function involves simply the measurement of attenuation as a function of wavelength for each of the three optical components of the system. This calibration includes, for each component, a verification that its attenuation is independent of incident intensity, angle of incidence, position on the optical surface, and temperature.

The second transformation is conversion to photoelectric current by the Uvicon photocathode. This process, too, is linear with intensity, the constant of proportionality being the quantum efficiency $Q(\lambda)$. The position (x, y) from which the photoelectric current originates is, of course, the same as the position at which the optical image was focused. In principle, the calibration of quantum efficiency is as simple as that of optical sensitivity. In practice, owing to residual nonuniformities in the photocathodes at the present stage of development of the tube, it is necessary to calibrate $Q(\lambda)$ separately for a number of different positions on the photocathode. And here, again, it is essential to prove that quantum efficiency is independent of temperature.

Taken together, the above calibrations give the optical-position transfer function m and the photoelectric conversion efficiency S in the forms:

$$(\alpha, \delta) = m(x, y; \alpha_0, \delta_0, \rho);$$

$$R_1(\lambda)\ R_2(\lambda)\ T_3(\lambda)\ Q(\lambda; x, y)\ \frac{e\lambda}{hc}\ a_E = S(\lambda; x, y) \quad .$$

In these equations, (α_0, δ_0) is the direction toward which the optic axis is pointed and ρ is the roll orientation of the spacecraft. The photoelectric current is then given simply by the expression

$$i(x, y) = \int_0^\infty I(\lambda)\ S(\lambda; x, y)\ d\lambda \quad .$$

If $S(\lambda)$ is zero outside the interval $a \leq \lambda \leq b$, and if we assume that $I(\lambda)$ is a continuous function, this equation reduces simply to

$$I(\Lambda) = \frac{i(x, y)}{U(x, y)} \quad ,$$

where the sensitivity,

$$U(x, y) = \int_a^b S(\lambda; x, y)\ d\lambda \quad ,$$

is determined by means of the calibration described above, and where Λ is some wavelength in the interval $a \leq \Lambda \leq b$. It is thus possible to exercise some degree of control in the choice of effective wavelength by appropriate selection of materials to be used in the optical filter and in the photocathode. This controls the short-wavelength cutoff a and the long-wavelength cutoff b. Figure 13 shows the sensitivity characteristics that it has been possible to achieve for the Celescope system.

The third transformation is conversion of the photoelectric current into a video signal. The manner in which the Uvicon performs this transformation is described in detail by Goetze (1966); Boerio, Beyer, and Goetze (1966); Beyer and Goetze (1966); Beyer, Green, and Goetze (1966); Doughty (1966); and Marshall and Roane (1966). Their studies have shown that as the input signal increases in strength, the output signal increases in both width and amplitude, in such a manner that

$$it_{ex} = f_p(V_\Sigma) \quad ,$$

where V_Σ is the summation of the coefficients of the output matrix. As was stated in Section 2.4, the form of the transfer function f_p depends strongly on the manner in which the Uvicon is operated and on the circuit parameters of the system in which it is installed.

There is also an easily determined correlation between the position of the image on the photocathode (x, y) and the coordinates of the maximum coefficient in the output matrix (k_0, ℓ_0), and a correlation between the size of the input image w and the width of the output signal. In the case of the Celescope experiment we are interested almost exclusively in point images (stars), for which w = 0.

The fourth transformation is amplification of the video signal and conversion to digital form by the electronic subsystem (described in more detail by Nozawa, 1966). The video gain G is a function only of the amplitude of the matrix coefficient $a_{k,\ell}$ and of the system operating mode. There are three system operating modes: analog, digital-PCM, and digital-store. The calibration of the Celescope electronic subsystem is, therefore, a relatively straightforward matter of determining $G(a_{k,\ell})$ in each of the three operating modes.

With the positional transfer function and the intensity transfer function determined by means of the calibration procedures outlined above and described more fully below, data from the Celescope can be analyzed directly

by a digital computer without any intervening manual operations. This automatic processing concept is one of the most important advantages inherent in the television technique and more than offsets the disadvantages of electronic complexity in the system and in the camera tube. The equations appropriate for this transformation are shown in the lower portion of Figure 28. In actual practice, several additional cross correlations are obtained to verify the calibration during the operating lifetime by use of onboard calibrator lamps and by frequent remeasurement of certain star fields selected for that purpose.

6.2 Calibration Techniques

Our calibration of the Celescope experiment is based on a mathematical model of the manner in which the instrumentation converts starlight into video signals. From the mathematical point of view, this model is complete and consistent. Every step in this mathematical model is supported by a calibration test plan describing in detail the operation required for measuring the quantities involved in performing that mathematical step. This model is completely described in Celescope Technical Bulletin CTB-15, which also designates the test plan supporting each mathematical step.

The accuracy of the model has been estimated by the accuracy with which it has been able to predict the performance of the experiment during system calibration in the Vacuum Optical Bench at GSFC. However, because the conditions under which the instrument will operate in space are considerably different from those under which it was calibrated, we have established procedures for recalibrating the Celescope experiment in orbit. These procedures involve the frequent use of our onboard calibrator lamps during both prelaunch and postlaunch phases of the operation; observations of stars specially measured for that purpose by NASA's rocketborne ultraviolet spectrophotometer (Stecher, 1967); and frequent reobservations of our standard calibration fields.

6.2.1 Optical components

Figure 29 shows the calibration facility we have used for measuring the optical attenuation coefficients for all Celescope optical components. The light source normally used is a windowless hydrogen arc operated at a pressure of 0.7 torr with one stage of differential pumping between the source and the entrance slit to the monochromator. The source is powered by a current-stabilized high-voltage power supply to provide output stability of approximately ±2% during a day's operation. The monochromator is a McPherson 1-m vacuum monochromator, Model 230 S. We normally operate with both entrance and exit slits 1 mm wide, corresponding to a resolution of about 16 Å. Most of our calibrations are performed by scanning the monochromator three times through the relevant spectral range: once for providing a reference signal, once for providing a signal to the device under calibration, and a third time for checking the stability of the reference signal.

When the device under calibration is a mirror surface or an optical filter, the same detector is used for generating both the reference and the calibration signal, the former being generated when the output from the monochromator is caused to fall directly on the detector, and the calibration signal arising when the monochromator output is caused to be reflected by the mirror or transmitted by the filter on its way to that detector. To provide adequate sensitivity throughout the range of interest (900 to 4000 Å), we use as a detector an RCA Type 6199 photomultiplier in combination with a sodium salicylate fluorescent coating as shown in Figure 30. To eliminate second-order effects, we insert a quartz window at the exit slit of the monochromator for wavelengths above 1600 Å, and a plastic window for wavelengths above 3200 Å.

Normally, the item under test is mounted, together with the reference device, in a small vacuum chamber behind the exit slit of the monochromator, as indicated in Figure 29. For testing devices, such as a primary mirror, that are too large for this chamber, we mount the large reflectometer chamber as shown in Figure 31 and introduce our input beam by means of a diagonal mirror.

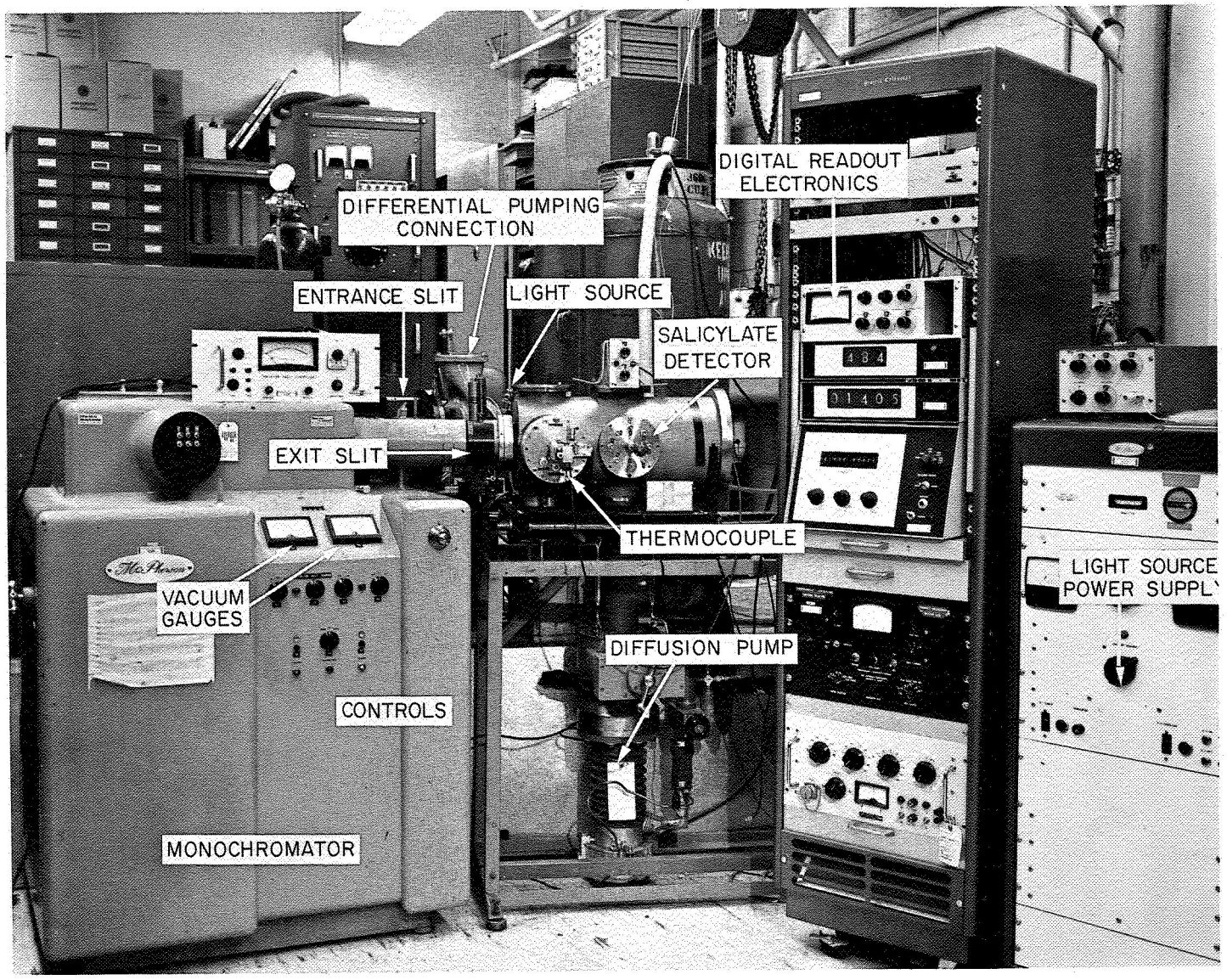

Figure 29. Celescope spectrophotometric calibration equipment.

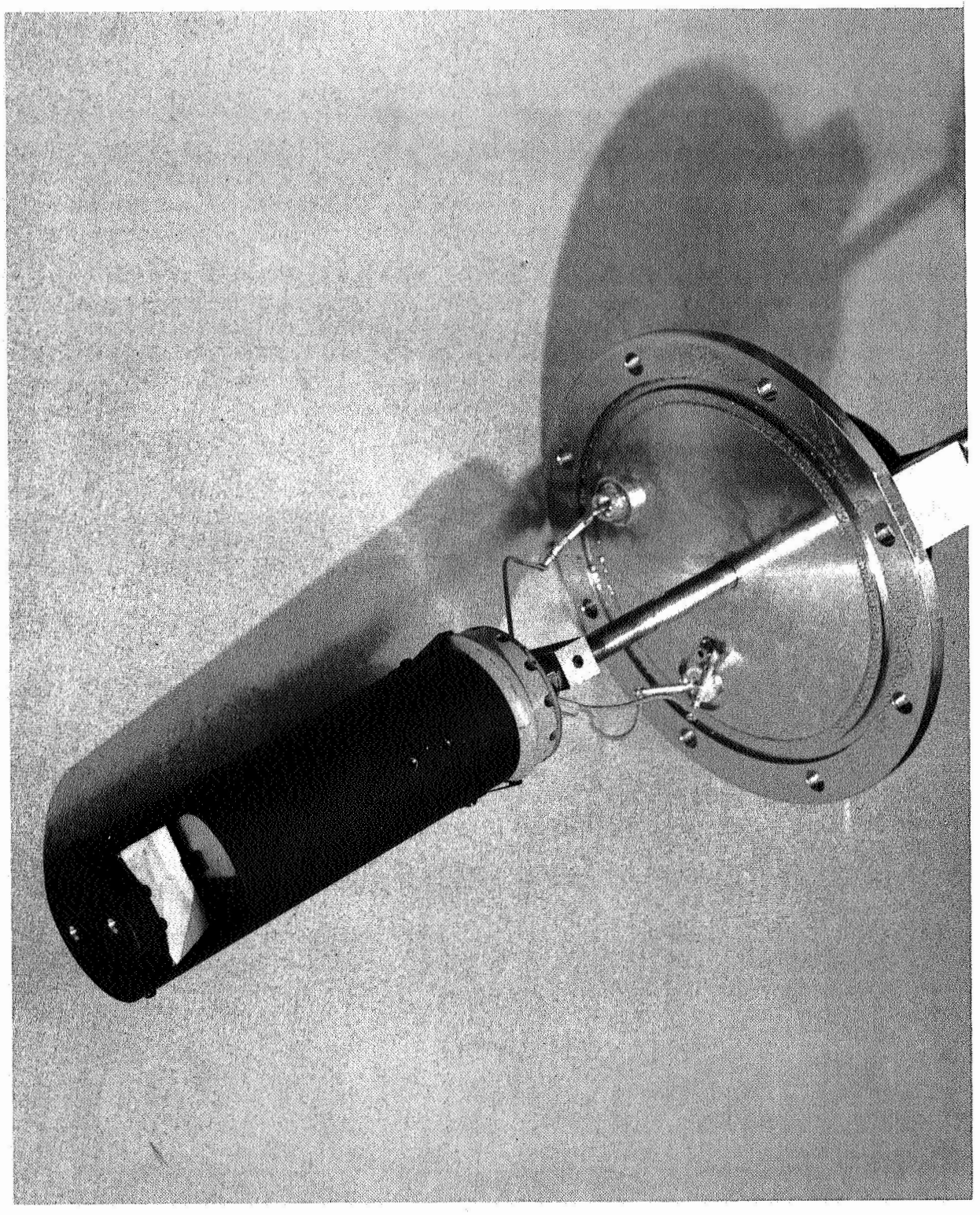

Figure 30. SAO laboratory standard detector no. SSR-1.

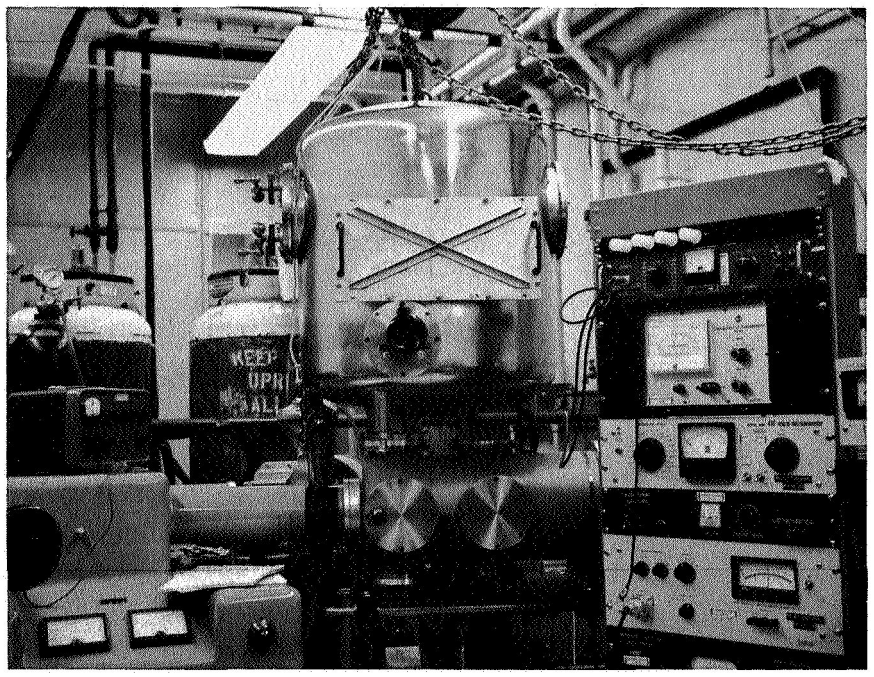

Figure 31. Reflectometer chamber for calibrating Celescope primary optics.

The equation for optical sensitivity given in Section 6.1 above implies that mirror reflectance is a function of wavelength only, and not a function of position on the mirror, time, intensity, temperature, or any other parameters. We have explicitly studied the dependence of mirror reflectance on position and time, finding (as implied) no measurable variations for the type of mirror coatings actually used in the flight experiment. Dependence of reflectance on position, time, intensity, and temperature is also implicitly denied by results of subassembly and system tests.

Figure 32 is a schematic view of the reflectometer, showing a primary mirror mounted in normal testing position. By means of a movable carriage, primary, secondary, and sample mirrors can be suspended upside down in a horizontal plane. Primary and secondary mirrors are mounted with their titanium mounting cells attached; the primary mirror is bolted to a girder ring as well. Utilizing a worm- and pinion-gear drive, with controls external

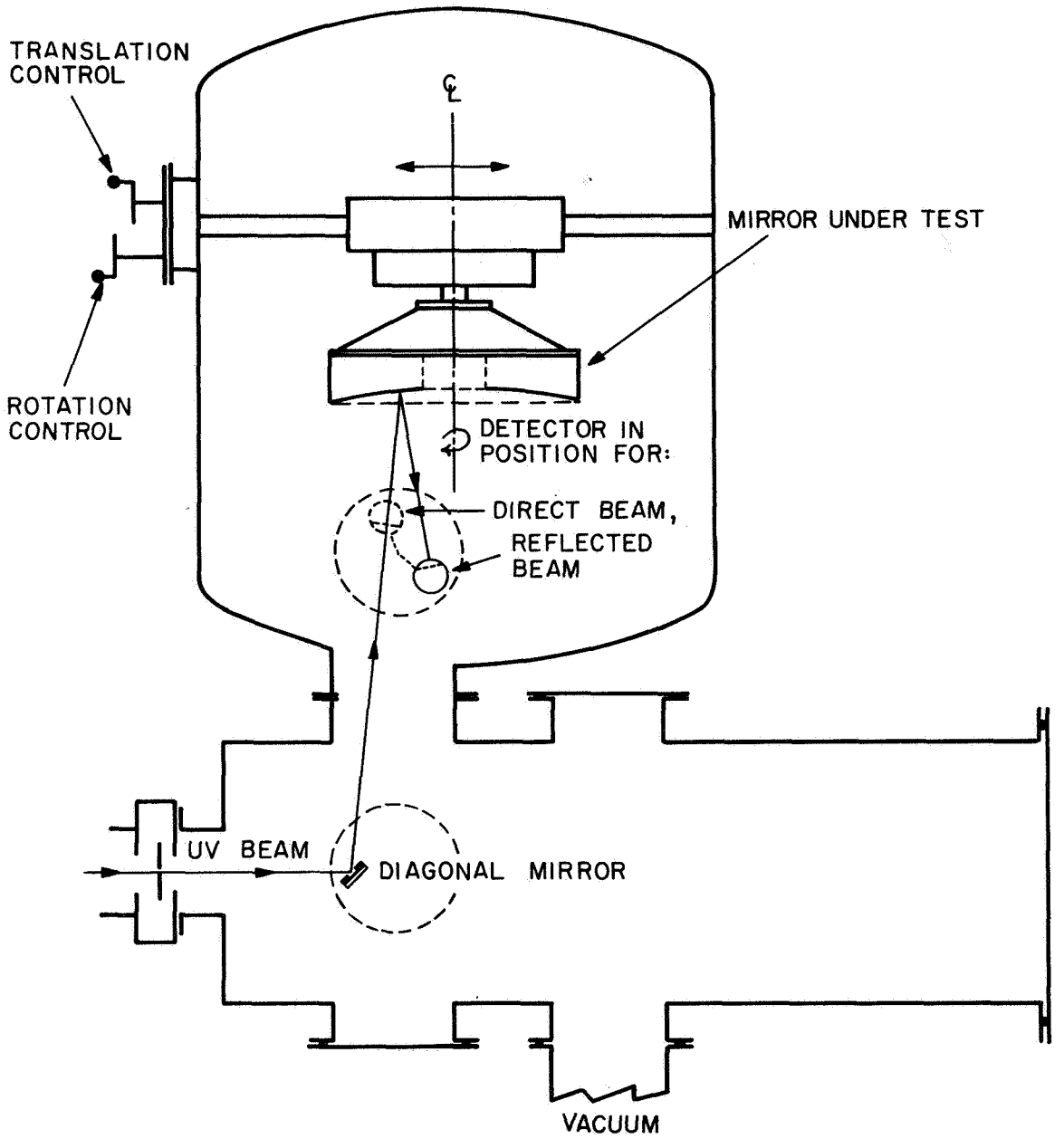

Figure 32. Primary and secondary mirror calibration facility.

to the reflectometer, the mounted flight mirrors can be rotated about their optic axes and translated into a horizontal plane. Each motion is independent of the other. Sample mirrors are mounted, as many as 10 at a time, on a plate that replaces the primary or secondary mounting attachments. Each time a flight mirror is coated, samples are generated on five or more 3/4-inch-square plane mirrors installed, together with the flight mirror, in the aluminizing chamber.

Referring to Figure 32, we can see the optical arrangements during calibration. Radiation from the exit slit is diverted upward into the reflectometer by means of a diagonal mirror mounted in the test chamber below. The beam is limited to an appropriate size by placing an aperture stop adjacent to the diagonal mirror. A sodium salicylate detector is mounted on a front flange plate of the reflectometer with a shaft control that can be rotated or translated. The detector is attached to the shaft with an eccentric arm arrangement so that rotation of the shaft causes the detector to revolve in a circle of approximately 5-inch diameter. In this way, the detector can be positioned in either the incident or the reflected beam as indicated in Figure 32. The incident beam path is fixed, and the mirror under test is moved to determine the position of incidence. Owing to the curvature of primary and secondary mirrors, the reflected beam path varies slightly as the position of incidence is varied; the detector can be adjusted to compensate for this effect.

Reflectance data are obtained by first measuring the response $i_0(\lambda)$ of the detector to the direct (unreflected) beam as the hydrogen spectrum is scanned. The mirror under test is then positioned to bring the beam to the desired point of incidence, the detector is rotated to intercept the reflected beam, and the response $i_R(\lambda)$ is scanned. After the mirror is repositioned, the scan is repeated. Typical procedure for primary or secondary mirror calibration included calibration at nine positions, three points on each of three radii. In addition to full wavelength scans, a limited amount of data was recorded to determine quickly the uniformity of reflectance as a function of position. These measurements were made at one wavelength only, 1216 Å,

and consisted of measuring the reflected beam at 30° increments of polar angle for a fixed radius. Typical data are presented in Figure 33 as reflectance versus position on the mirror. A detailed test plan was always used for reflectance measurements; this plan is designated as SAO Calibration Test Instruction CTI-9. The accuracy with which the beam can be positioned on the mirror surface is probably not better than ±1/8 inch in radius and ±2° in angle. Since the dimensions of the incident beam are about 1/4 × 1/4 inch, this uncertainty in position is not considered to be important.

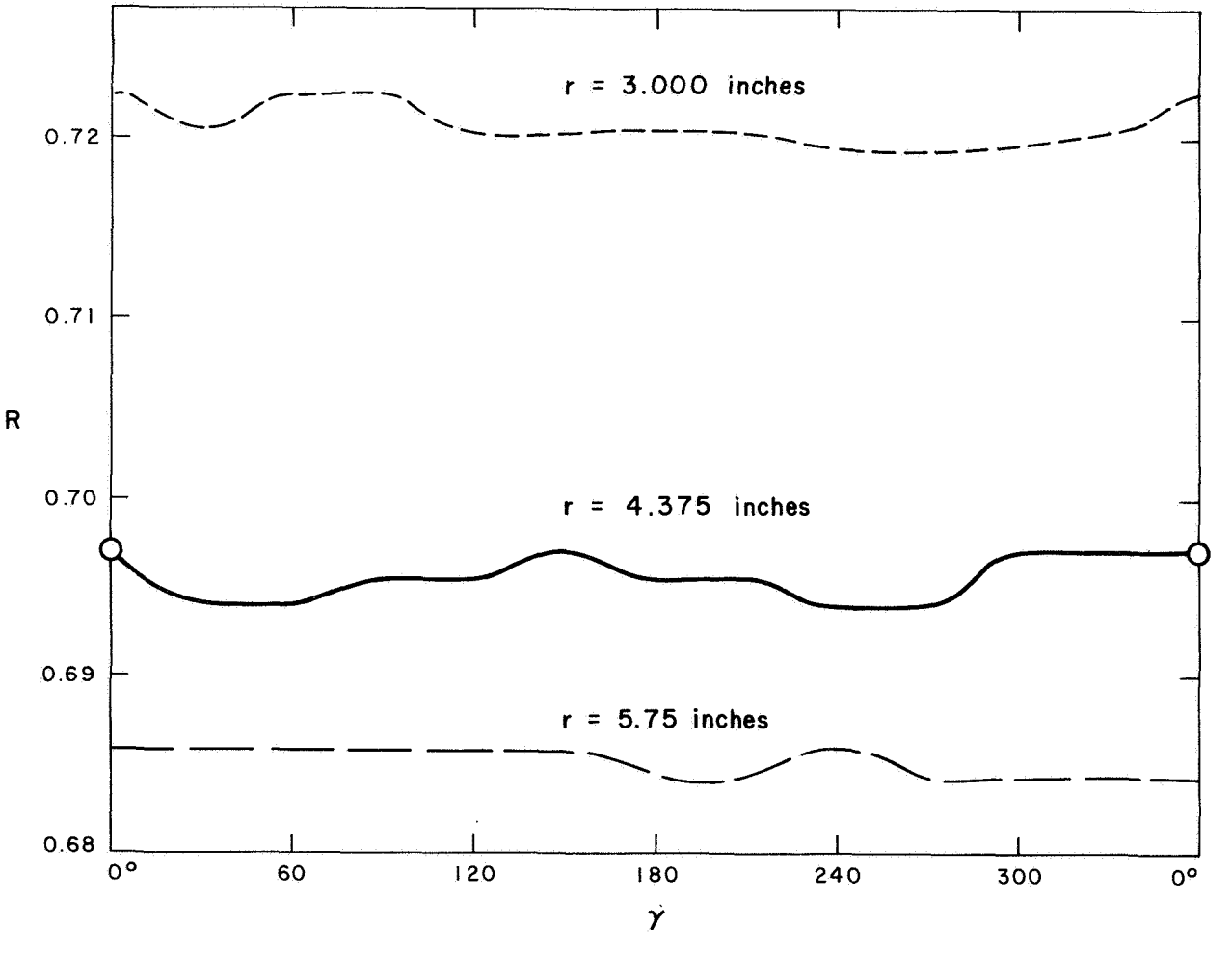

Figure 33. Positional variations of reflectance of mirror 7FP with coating deposited by OCLI in October 1964, measured at 1216 Å, November 11, 1964.

Although sample mirrors could be calibrated in the large reflectometer, it was a somewhat cumbersome procedure; for this reason a smaller reflectometer was constructed specifically for measuring the reflectance of samples. This reflectometer could be mounted on any of the calibration chamber ports. Figure 34 is a schematic view of the essential features of this device. Mirrors are mounted on one end of a shaft that can be rotated and translated along a vertical center line; the center line lies in the plane of the mirror surface. A sodium salicylate detector, mounted adjacent to the mirrors under test, can be independently rotated about the vertical center line to intercept either the reflected or the direct beam. The sample mirror shaft is retracted vertically out of the beam path for direct beam measurements.

Reflectance measurements can be made at angles of incidence varying from 15° to about 75° ; generally, data were obtained at the minimum angle to correspond as closely as possible to data taken in the large reflectometer. The position of mirror and detector relative to the incident beam is adjusted with external control knobs and is indicated by reference scales on these knobs. The detector consists of an RCA 1P28 photomultiplier tube mounted behind a glass screen coated with sodium salicylate.

During the course of this program, we found that for a given sample mirror, measurements made in the sample reflectometer gave reflectances consistently higher than those obtained in the large reflectometer, by a factor independent of wavelength but differing for different runs. Although simple in concept, reflectance measurements on flight mirrors have proved to be rather troublesome in practice. A major cause of the difficulties encountered is the very long beam path necessitated by the large dimensions of the mirrors and the reflectometer design. In addition to creating problems in the optical alignment of the diagonal mirror and detector, the long path plus the natural divergence of the beam result in undesirable beam spread. In practice, if a beam stop of aperture 0.054 in. is placed at the diagonal mirror, the beam incident upon the flight mirror has spread to slightly over 1/4 in. and the reflected beam is about 1/2-in. wide at the detector. Positioning a beam

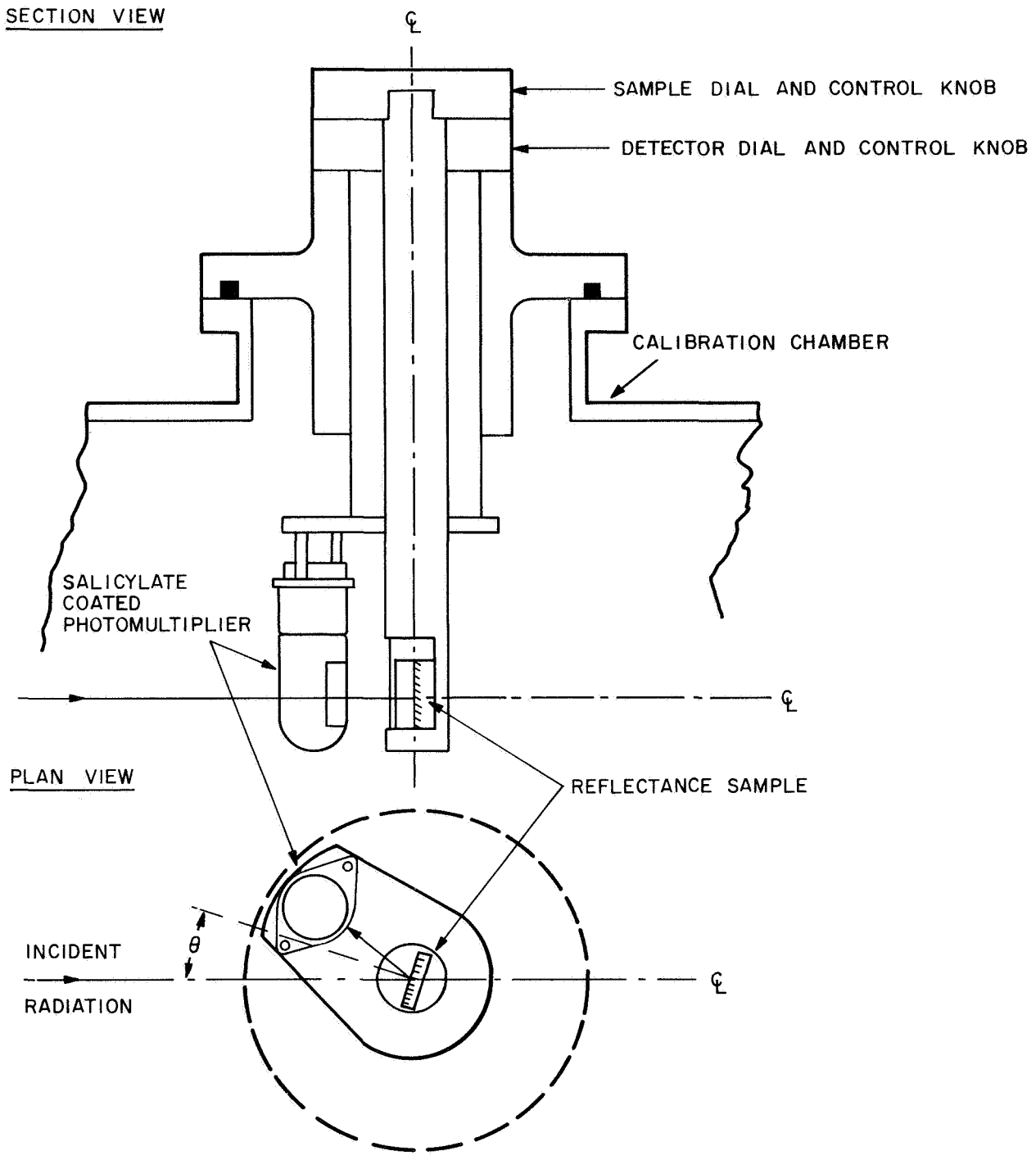

Figure 34. Sample mirror reflectometer.

this large on the salicylate detector was rather critical. An additional problem is that if the detector sensitivity is not uniform over all parts of the detector surface, the difference in reflected and incident beam sizes will yield spurious results.

The sample reflectometer, on the other hand, is small and relatively easy to align. More important, however, is the fact that the beam path to the detector is short and is identical for both incident and reflected paths. One advantage of the short beam path is that the beam diameter can be kept small and its position on the detector surface carefully controlled. For these reasons, the data obtained with the sample reflectometer are considered reliable; this conclusion casts some doubts on the validity of reflectance data obtained in the large reflectometer.

All flight mirrors have been recoated since the last calibration in the large reflectometer chamber. On the basis of those earlier tests, on the basis of the uniformity of measured reflectance for all samples received from OCLI, and a posteriori on the basis of satisfactory agreement between component calibration and subassembly calibration, we have calibrated the reflectances of all flight mirrors on the assumption that the reflectance of a sample mirror is representative of the reflectance of the flight mirror itself. Of the five samples coated in each evaporation, four are retained at SAO under dry-nitrogen storage and one travels with the mirror to which it refers, as a contamination-control sample. Reflectances for the flight-control samples have been remeasured after each vacuum-test exposure to which the payload has been subjected, without any evidence of measurable change in reflectance of any sample. Coatings for all flight mirrors consist of aluminum overcoated with magnesium fluoride of thickness appropriate for maximizing the reflectance at 1216 Å; they were deposited by Optical Coating Labs, Inc., between January and May 1966. The last time control samples were remeasured was July 1968.

In order to speed up reflectance calibration of sample mirrors, remeasurement of contamination-monitor mirrors has been performed by a third technique in which eight samples, including two samples of known reflectance, are intercompared. Figure 35 is a diagram of this comparison reflectometer. It gives results in excellent agreement with those obtained in the direct-measuring reflectometer of Figure 33.

For all points of the field of view within 1°.23 of the optic axis, the entrance aperture is at the primary mirror. Blocking by the secondary mirror and its supports is uniform throughout the field of view. The effective optical collecting area of the system a_E has been determined both by computation from the assembly drawings and optically by use of the F-4 telescope as a collimator to illuminate a diffusing screen; its value is 543.5 cm^2. Beyond a field angle of 1°.23, vignetting occurs from obscuration by the upper end of the outer ion trap, amounting to a maximum of 2% for a field angle of 1°.4 corresponding to the corners of the field of view.

Figure 36 is a schematic diagram of the equipment used for measuring the spectral transmittance of flight filters. The filters are mounted in a V-shaped cradle made of nylon, which is attached directly to a translation table. The cradle is so designed that it can be manually pivoted about a vertical axis lying in the plane of the filter; this allows the angle of incidence of the ultraviolet beam to be varied between approximately 0° and 15°. By means of the elevation and translation controls, the filter can be positioned so that the beam is incident upon any desired portion of the filter surface. A detector is mounted in the beam path behind the filter. With the filter in the position shown in Figure 36, the detector output signal $i_T(\lambda)$ is due to the transmitted beam; to measure the direct beam signal $i_0(\lambda)$, the filter is lowered out of the beam path. The sodium salicylate detector described previously was used as a detector. Filter transmittance is given directly by the equation

$$T_3(\lambda) = \frac{i_T(\lambda)}{i_0(\lambda)} \quad .$$

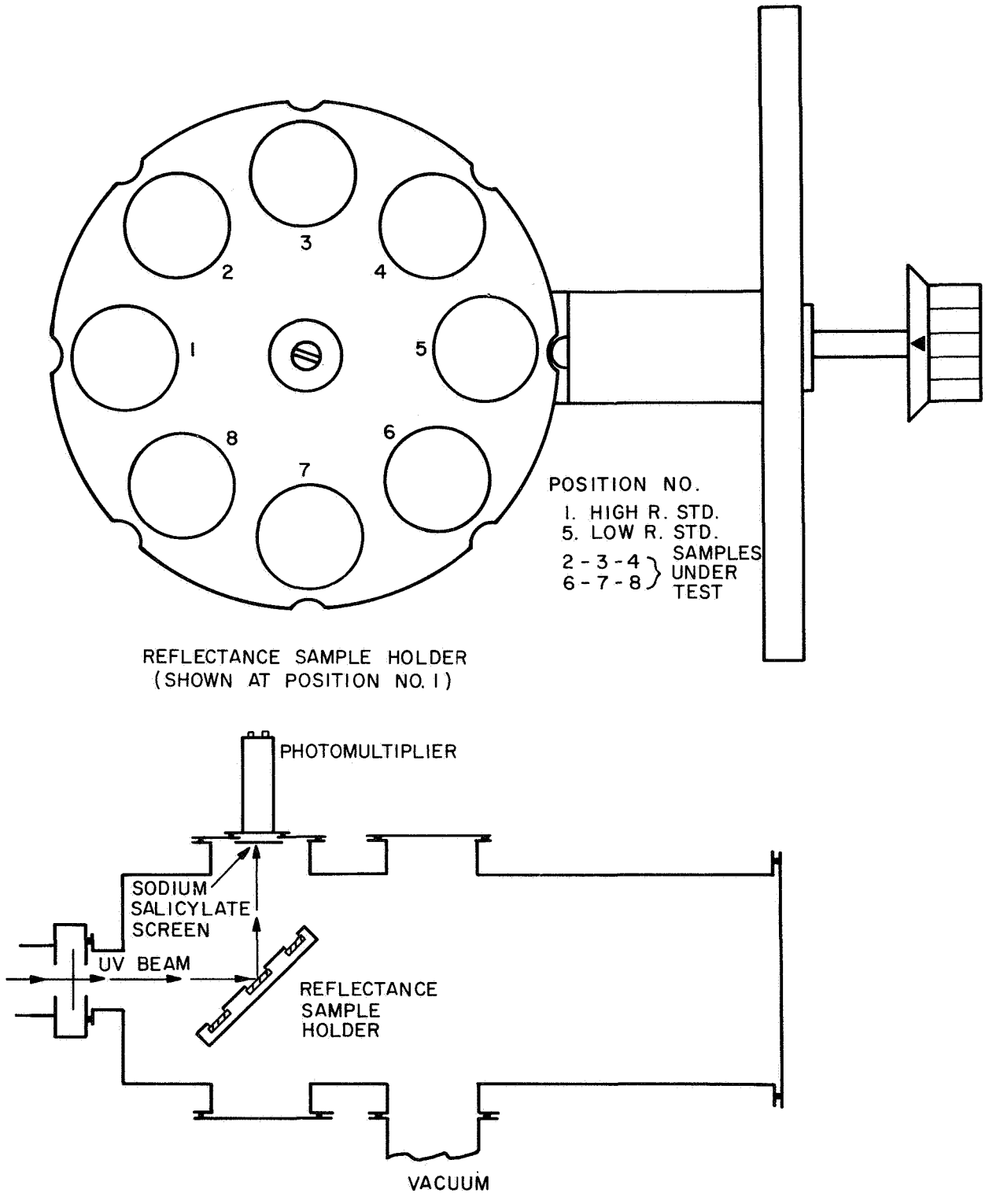

Figure 35. Reflectance comparator.

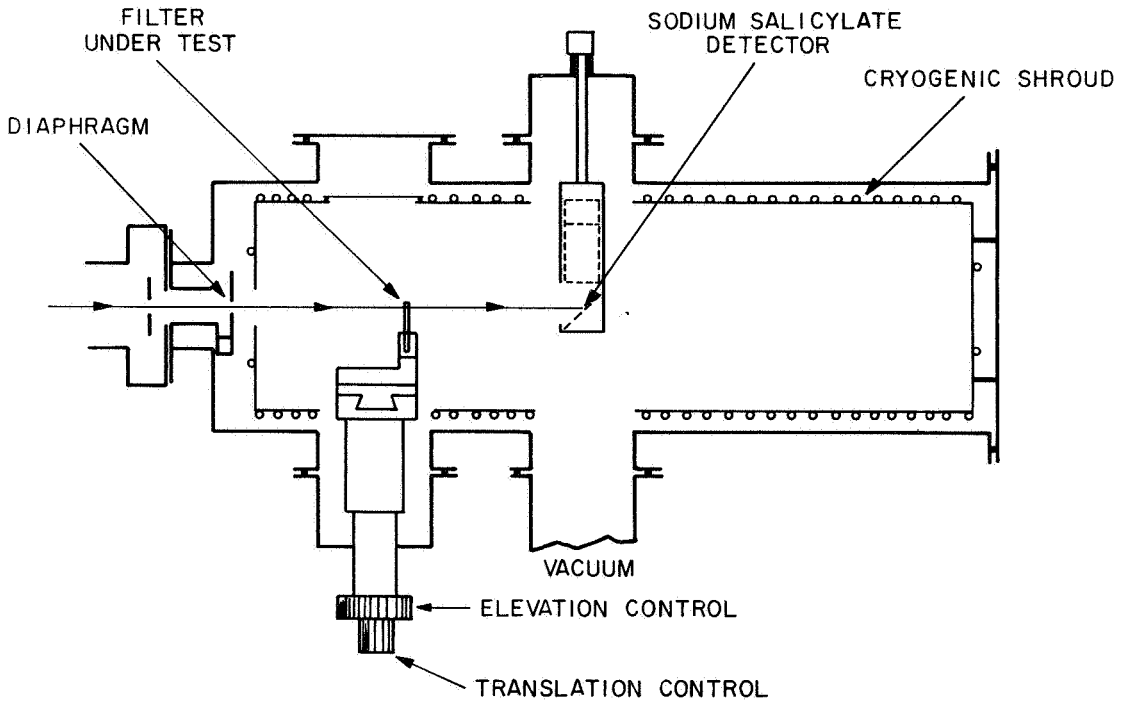

Figure 36. Filter calibration facility.

Also shown in Figure 36 is the cryogenic shroud, which allows the calibration of filters at temperatures as low as -90° C. The shroud consists of a copper cylinder fitted inside the calibration chamber and suspended from the large flange plate at the back end of the tank. Holes cut in the shroud walls match the positions of ports on the calibration chamber to allow access to components inside. Unused access holes are blocked by cover plates of the same composition and finish as the shroud. The shroud is cooled by pumping liquid nitrogen (supplied from self-pressurized dewars) at 10 to 20 psi through coils soldered to the shroud body. Temperature control is achieved by opening or closing a solenoid valve in the discharge end of the cooling coils; the valve is opened and nitrogen flow maintained until a preset temperature is reached, whereupon the valve closes, stopping flow. When the temperature rises slightly, the valve reopens and nitrogen flow resumes. Shroud temperatures are monitored with five thermocouples attached at various points; one of these serves as the sensing element for a regulating device that automatically maintains the temperature constant by controlling

the operation of the solenoid valve. Approximately 5 hours are required for a filter to reach equilibrium at -90° C. Once equilibrium is reached, temperatures remain constant to within less than 5° C.

The inside surface of the shroud body is painted flat black to reduce scattered light and increase thermal emittance. The outside surface is gold plated to minimize radiant heat input from the tank walls. In addition, the translation table is designed to minimize conduction losses through the body of this device.

Filter temperatures are determined by positioning a thermocouple immediately adjacent to the filter under test. Since the shroud interior is not perfectly isothermal, true filter temperatures may differ a few degrees from the measured values. In view of the observed insensitivity of transmittance to temperature, however, this error is considered negligible.

It is necessary to orient each filter with respect to reference scales on the translation table controls. For the purpose of locating the vertical center line, a dummy filter, of the same shape and size of a flight filter and with a vertical center line scribed on its surface, is mounted in the cradle with its flat edge upright. With the aid of a protractor, the dummy is oriented so that the top edge is horizontal and hence the center line is vertical. The dummy filter is then translated until the visible zero-order beam is incident on the scribed line. In this position, the scale reading on the translation control corresponds to the location of the center line. To locate a horizontal reference line, the dummy is replaced with a flight filter to be tested, which is then lowered out of the beam path. The monochromator is adjusted to a wavelength below the short-wave cutoff of the filter and the detector output current i_0 is measured. Next, the filter is elevated until its upper edge begins to enter the beam path and the detector signal begins to decrease. When the signal drops to $1/2\ i_0$, the scale reading on the elevation control corresponds to the location of the top edge of the filter. The final step in orientation is to rotate the filter cradle until the desired angle of beam incidence is obtained.

After angle of incidence and filter temperature are adjusted to their desired values and the filter is positioned so that the beam is incident on one of the predetermined areas, the detector current $i_T(\lambda)$ is recorded while the monochromator scans the spectral region of interest. This procedure is repeated for each of the filter positions to be calibrated, and the direct beam current $i_0(\lambda)$ is periodically recorded. After all necessary data are recorded for a particular choice of temperature and angle of incidence, one or both of these parameters are varied and the transmittance is measured again at as many filter positions as necessary.

The filters selected for installation in the flight payload were found to have variations of transmittance with temperature and position considerably smaller than ±5% total variation at any wavelength within the band of appreciable filter transmittance; these variations need not be taken into account in data reduction. The most significant effects noted were the decrease in cutoff wavelength when the temperature was decreased, amounting to about 0.26 Å per degree Centigrade for lithium fluoride, 0.42 Å per degree for barium fluoride, 0.17 Å per degree for suprasil quartz, and negligible for Corning 7910 glass. These temperature effects are discussed in more detail in Celescope Calibration Report CCR-137 and by Davis (1966b).

Experience gained during our filter calibrations in 1964 indicated that contamination-control samples were necessary for lithium fluoride filters. We found that, below 1600 Å, the transmittance of most samples of lithium fluoride decreased as a function of time, most probably as an effect of exposure to atmospheric humidity. The optical polishing required for fabricating a filter from a cleaved lithium fluoride blank was also found to introduce deterioration similar in magnitude to that encountered after 6-month storage of a cleaved sample at 75% relative humidity or 18-month storage in a plastic box purged with dry nitrogen and sealed. Polished filters do not deteriorate so rapidly in the presence of atmospheric humidity as do cleaved samples.

A typical example of lithium fluoride filter deterioration is shown in Figure 37, where the results of calibration of filter L-6 and its sample (1L1) are compared from 1965 through 1966. Also shown are the results of calibration of sample 1L5, which was stored with 1L1 until November 1966, and was assigned as contamination monitor to filter L1 and the F-4 telescope from November 1966 until May 1967. In Figure 37, solid curves refer to filter L-6, dashed curves to sample 1L1, and dotted curves to sample 1L5. The numbers refer to the time at which the measurement was taken: 1 refers to measurements made on 1L1 in July 1963, at the time 1L1 and 1L5 were received from the supplier; 2 to measurements made on L-6 in January 1964, completion of the first attempt at optical figuring; 3 to measurements made on L-6 and 1L1 in March 1965, L-6 having been refigured and 1L1 having been stored in a chemical desiccator; 4 to measurements made on L-6, 1L1, and 1L5 in April and May 1965, after ultrasonic cleaning in absolute ethyl alcohol; 5 to measurements made on 1L5 and L-6 between March and May 1966, after storage of 1L5 in a chemical desiccator and after recleaning of L-6; 6 to measurements made on 1L1, 1L5, and L-6 in November 1966, after storage of 1L1 and L-6 in EMR's clean room and storage of 1L5 at SAO in a dry-nitrogen purge box; 7 to measurements made on 1L5 in May 1967, after installation of the F-4 telescope holding 1L5 into the flight payload in EMR's clean room, shipment and storage of the flight payload under dry-nitrogen purge, and thermal-vacuum test of the flight payload in GSFC's 12- × 15-foot chamber.

A number of circumstances, all of them connected with the many properties of lithium fluoride that make it undesirable as an optical material, have combined to interfere with our clear understanding of exactly what the relationships are among processing techniques, storage environments, and transmittance for our lithium fluoride optical components. By combining the data from our planned recalibration of contamination-control samples and flight spares, we expect to be able to establish the extent of deterioration for the Uvicons and lithium fluoride filters installed in the flight payload to within about 20%.

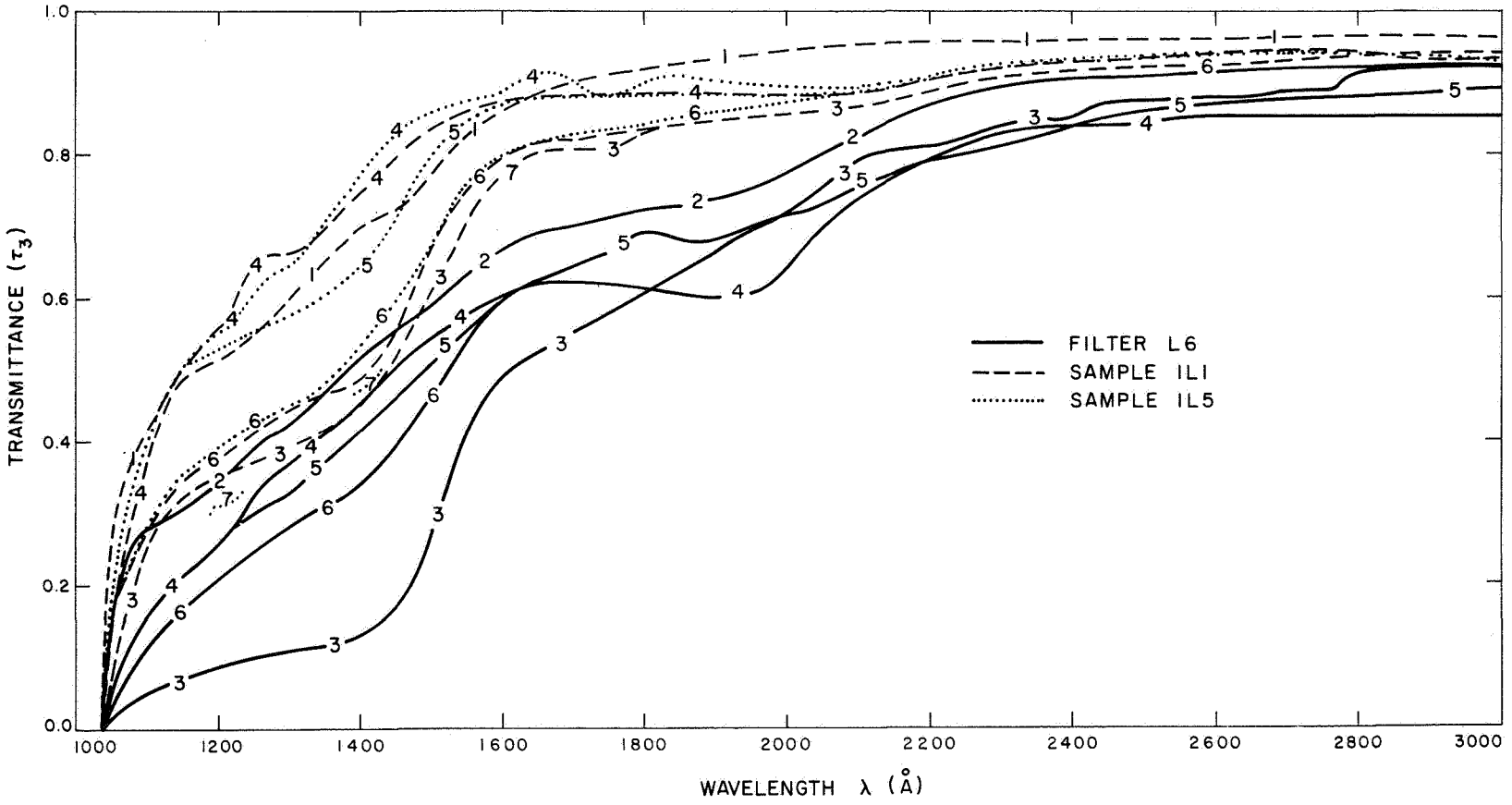

Figure 37. Change in transmittance of L-6 and samples 1L1 and 1L5.

We have also assigned contamination test samples to each barium fluoride filter and recalibrated these samples on the same basis as for lithium fluoride. The only change encountered during the three years since fabrication of the oldest barium fluoride flight filter has been a deepening of the 1450 Å absorption feature, from 35% transmittance in 1964 to 31% in 1966 and 27% in 1967. Our experience with barium fluoride (Davis, 1966b) indicates that this change is a body one, rather than a surface one; that it is irreversible; and that its rate depends primarily upon the storage temperature. We believe that our remeasurement of the test samples will enable us to determine the deterioration of the barium fluoride flight filters to an accuracy of 5%.

We have also studied the effects of the space radiation environment on our filter transmittances (see Celescope Technical Bulletin CTB-14). The degradation in filter transmittance depends only upon the total dose (measured in megarads or equivalent units), and not upon the type of radiation imposed. Our conclusions regarding dose rates for the Celescope experiment, as given in CTB-14, are listed below. These dose rates were computed for an October 1967 launch date; since the largest single contributor to this dose rate (electron irradiation from the Starfish experiment) is decreasing with time, and since all of these values are computed on the basis of pessimistic assumptions concerning the radiation field and the mechanisms for arrival of the radiation at the optical filters, our conclusions regarding total damage to the Celescope experiment represent pessimistic limits.

1. Natural electrons

   a. Penetrating component: None

   b. Scattered component

      Average flux: 2.4×10^{11} MeV cm^{-2} $year^{-1}$

      = 0.02 megarad $year^{-1}$

      Peak flux: 2.2×10^{6} MeV cm^{-2} sec^{-1}

      Flux behind optical filters: None

2. Starfish electrons

a. Penetrating component

Average flux: 1.8×10^{12} MeV cm^{-2} $year^{-1}$

= 0.15 megarad $year^{-1}$

Peak flux: 1.6×10^{7} MeV cm^{-2} sec^{-1}

Flux behing BaF_2 filter: 2.2×10^{11} MeV cm^{-2} $year^{-1}$

= 0.018 megarad $year^{-1}$

Flux behind other filters: 5.8×10^{11} MeV cm^{-2} $year^{-1}$

= 0.03 megarad $year^{-1}$

b. Scattered component

Average flux: 9.6×10^{11} MeV cm^{-2} $year^{-1}$

= 0.07 megarad $year^{-1}$

Peak flux: 8.6×10^{6} MeV cm^{-2} sec^{-1}

Flux behind BaF_2 filter: 1.2×10^{11} MeV cm^{-2} $year^{-1}$

= 0.01 megarad $year^{-1}$

Flux behind other filters: 3.1×10^{11} MeV cm^{-2} $year^{-1}$

= 0.024 megarad $year^{-1}$

3. Protons

a. Penetrating component

Average flux: 1×10^{12} MeV cm^{-2} $year^{-1}$

= 0.08 megarad $year^{-1}$

Peak flux: 1×10^{7} MeV cm^{-2} sec^{-1}

Flux behind BaF_2 filter: 5×10^{10} MeV cm^{-2} $year^{-1}$

= 0.004 megarad $year^{-1}$

Flux behind other filters: 4×10^{11} MeV cm^{-2} $year^{-1}$

= 0.03 megarad $year^{-1}$

b. Scattered component

Average flux: 8×10^{11} MeV cm^{-2} $year^{-1}$

= 0.06 megarad $year^{-1}$

Peak flux: 8×10^{6} MeV cm^{-2} sec^{-1}

Flux behind optical filters: None

4. Gamma rays

Average flux: 9.6×10^{10} MeV cm^{-2} $year^{-1}$
$= 5 \times 10^{-5}$ megarad $year^{-1}$.

Figure 38, based upon the data presented in CTB-14, compares the transmittances of new lithium fluoride filters and Uvicon faceplates with the transmittances to be expected after one year's irradiation at the above levels. On the basis of the findings of Heath and Sacher (1966), we conclude that our calibrations of transmittances of our other filters, and of mirror reflectances, are not affected by irradiation at these levels. Our in-orbit calibration plans include routine remeasurement of calibration star fields that will enable us to establish the changes in lithium fluoride transmittance induced by radiation damage.

Figures 39, 40, and 41 show typical transmittance curves as measured for barium fluoride, quartz, and Corning 7910 filters, respectively.

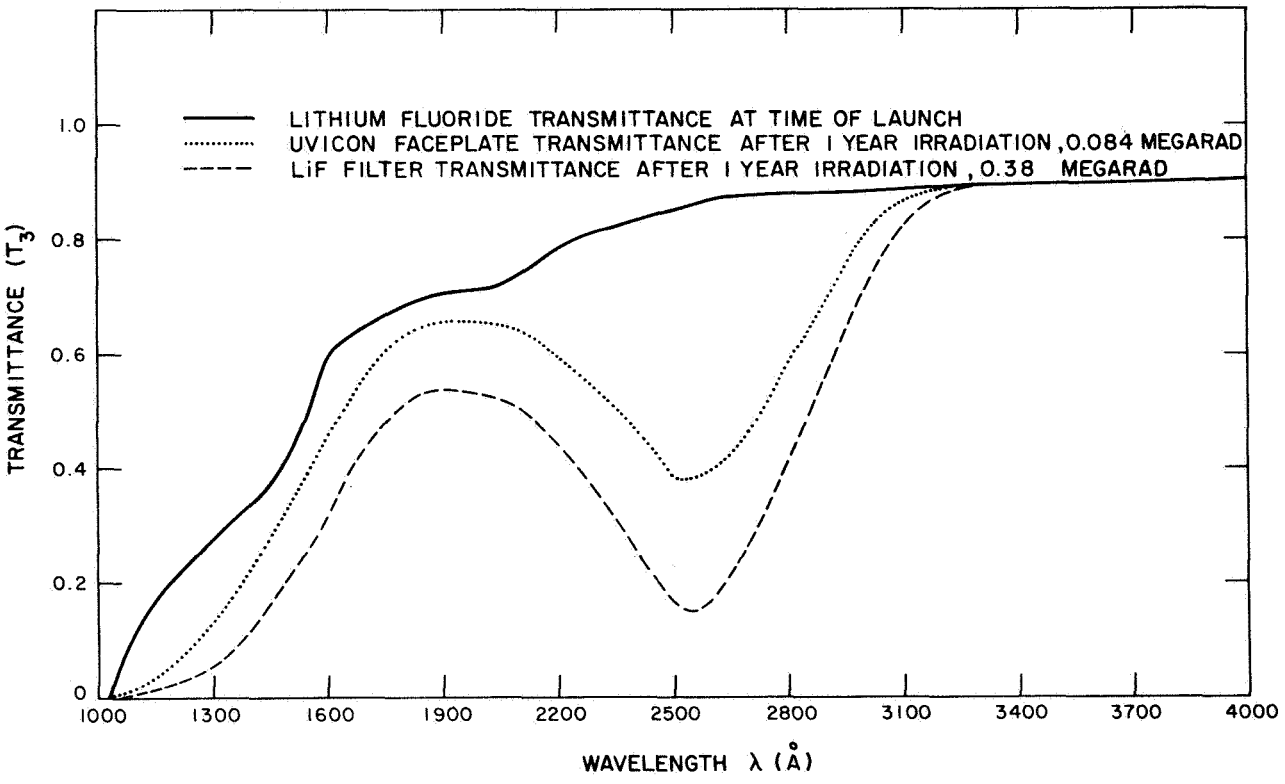

Figure 38. Effects of irradiation on lithium fluoride optical components in the Celescope experiment.

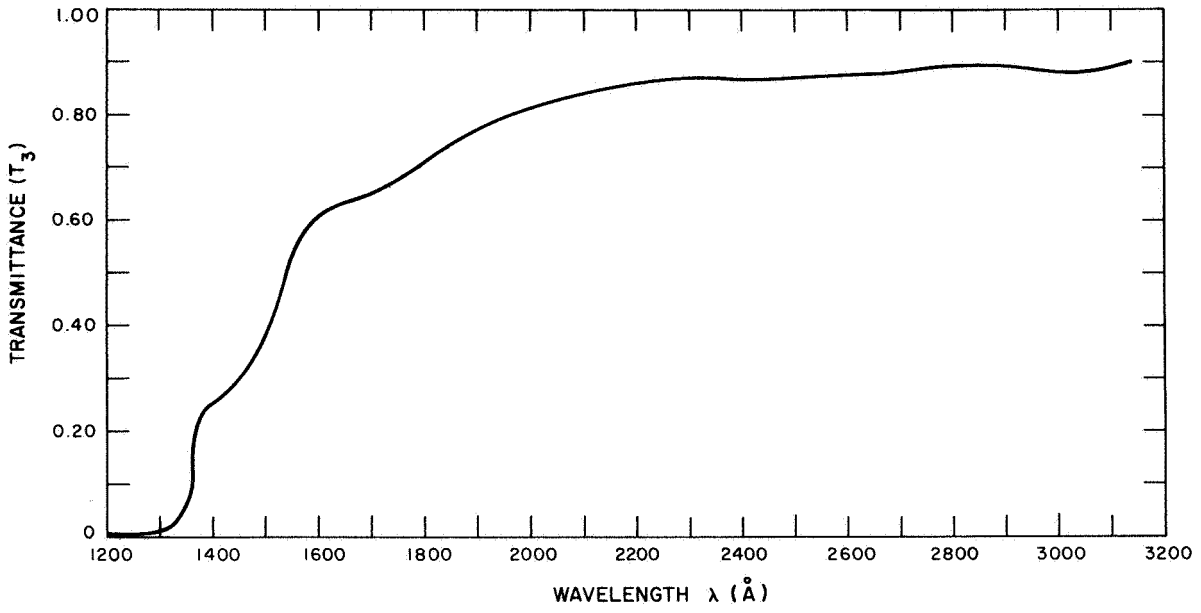

Figure 39. Typical transmittance of barium fluoride flight filter for Celescope.

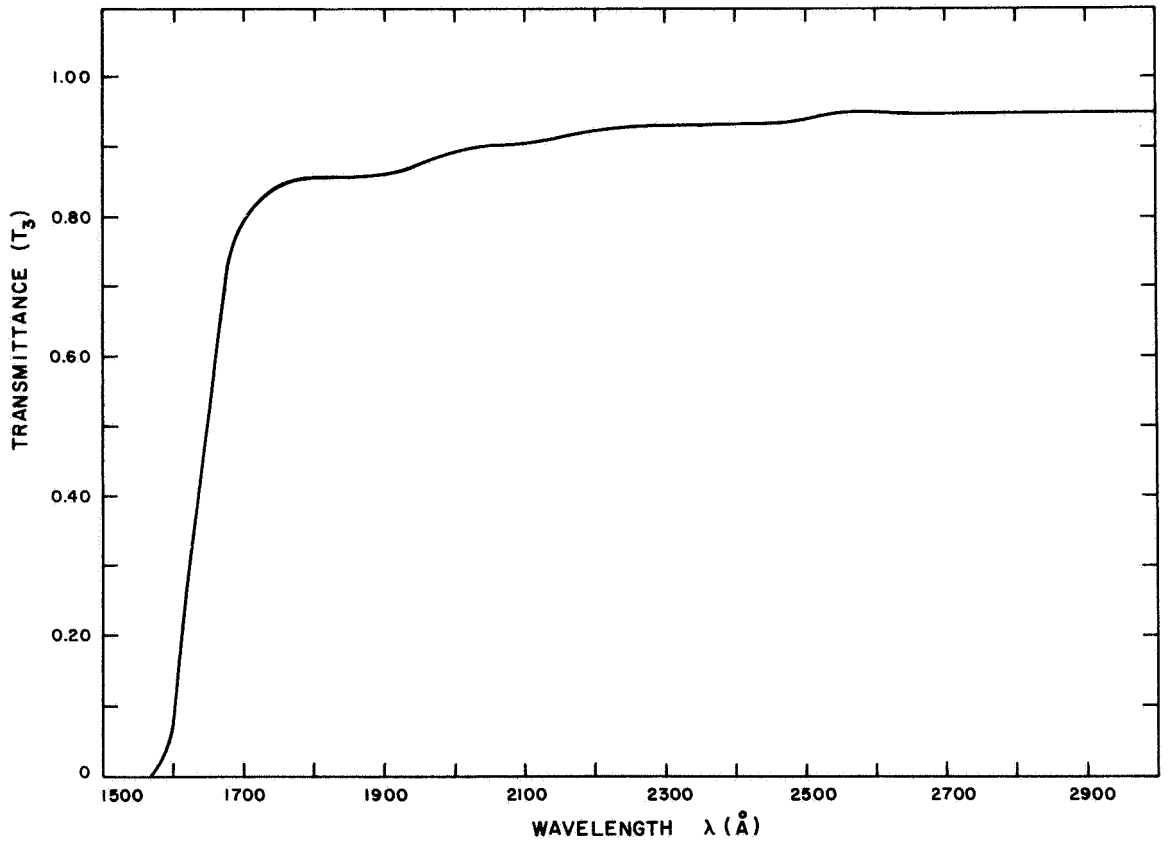

Figure 40. Typical transmittance of quartz filter for Celescope.

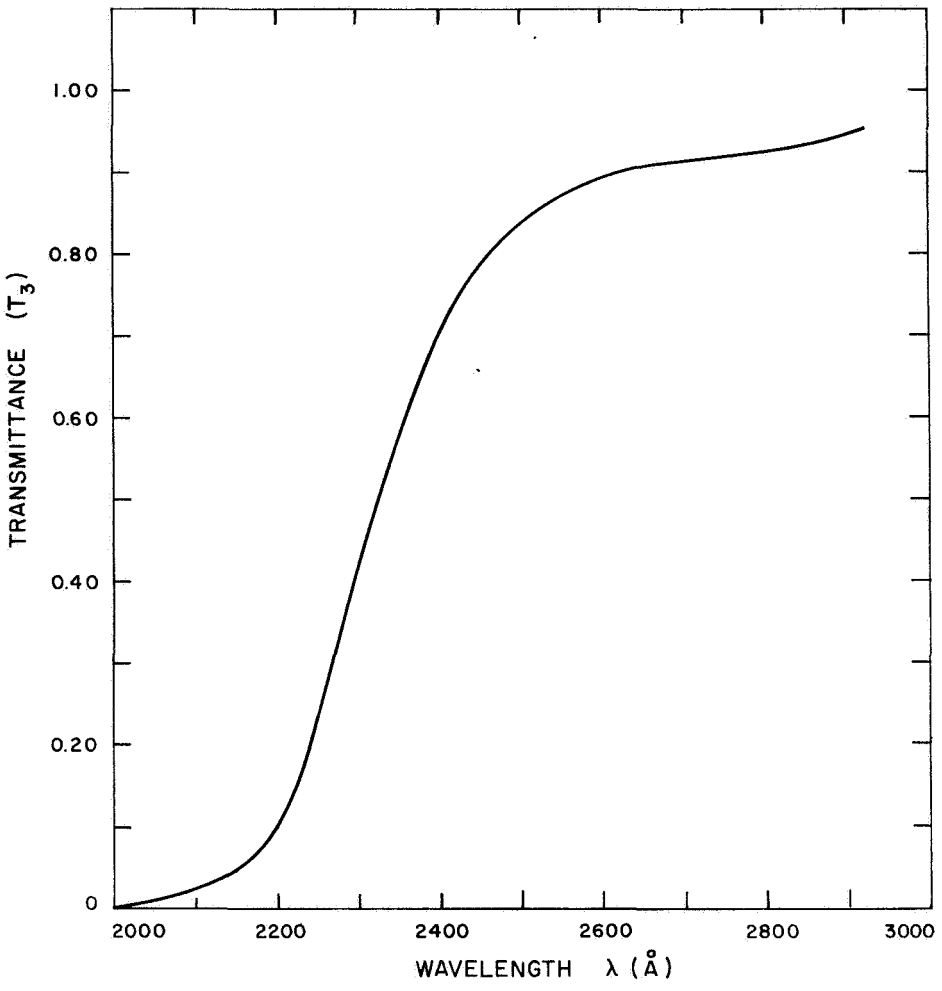

Figure 41. Typical transmittance of Corning 7910 filter for Celescope.

6.2.2 Uvicons

The equation for optical sensitivity given in Section 6.1 includes a term, $Q(\lambda;x,y)$, for the quantum efficiency of the Uvicon as a function of wavelength and position on the photocathode. As for reflectance and transmittance calibrations, the reference device is the sodium salicylate fluorescent detector shown in Figure 30; the Uvicon and reference detector are mounted in the chamber behind the exit slit of the monochromator, as indicated in Figure 29. The primary difference is that now the calibration equation involves the absolute calibration of the reference device,

$$Q_U(\lambda;x, y) = \frac{i_U(\lambda;x, y)}{i_S(\lambda)} \; Q_S(\lambda) \quad ,$$

where the subscript U refers to the Uvicon and the subscript S refers to the reference device. The calibration of the reference device is discussed in Section 6.2.7.

The experimental procedures involved in measuring $Q_U(\lambda)$ can best be discussed by referring to Figure 42 which is a schematic diagram of the calibration chamber and associated components. On the extreme left are shown the exit slits of the monochromator and the flange connecting the tank to the monochromator exit arm. A beam of monochromatic radiation, defined by the exit slits and a diaphragm that can be adjusted in both position and aperture, is incident normally on the Uvicon faceplate. By suitable adjustment of the diaphragm, the beam direction is made coincident with the longitudinal axis of the tank. The tube is shown in normal testing position, mounted on a translation table that permits it to be positioned in two dimensions perpendicular to its optic axis. The beam is approximately 1/10 inch in diameter at the faceplate; its location can be adjusted to any desired position by translating or elevating the Uvicon tube with the external controls shown. Each control is independent of the other and is equipped with a reference scale.

In Figure 42 the calibrated sodium salicylate detector is shown mounted on a top flange of the calibration chamber. By means of a shaft passing through an O-ring vacuum seal, the detector can be lowered into the ultraviolet beam or raised to allow the beam to strike the Uvicon. The detector consists of an RCA 6199 end-window photomultiplier mounted inside and at one end of a blackened brass tube. The opposite end of the tube is capped, and a window approximately 1-in. square is cut in the wall of the tube at that end. Directly inside the window a screen coated with sodium salicylate is mounted at a 45° angle to the axis of the multiplier. Irradiation of the salicylate screen by ultraviolet light causes it to fluoresce strongly in a band

centered around 4200 Å near the peak sensitivity of the photomultiplier tube, which is not in itself sensitive to the ultraviolet radiation. The salicylate detector just described was used to calibrate all Uvicons with the exception of tube R19A. The detector used in that case was modified by placing a salicylate-coated cylindrical glass screen over the window in the brass mounting tube and replacing the diagonal screen with a diffusing plate coated with magnesium oxide. This design was abandoned because of nonuniformity of response over various portions of the salicylate screen.

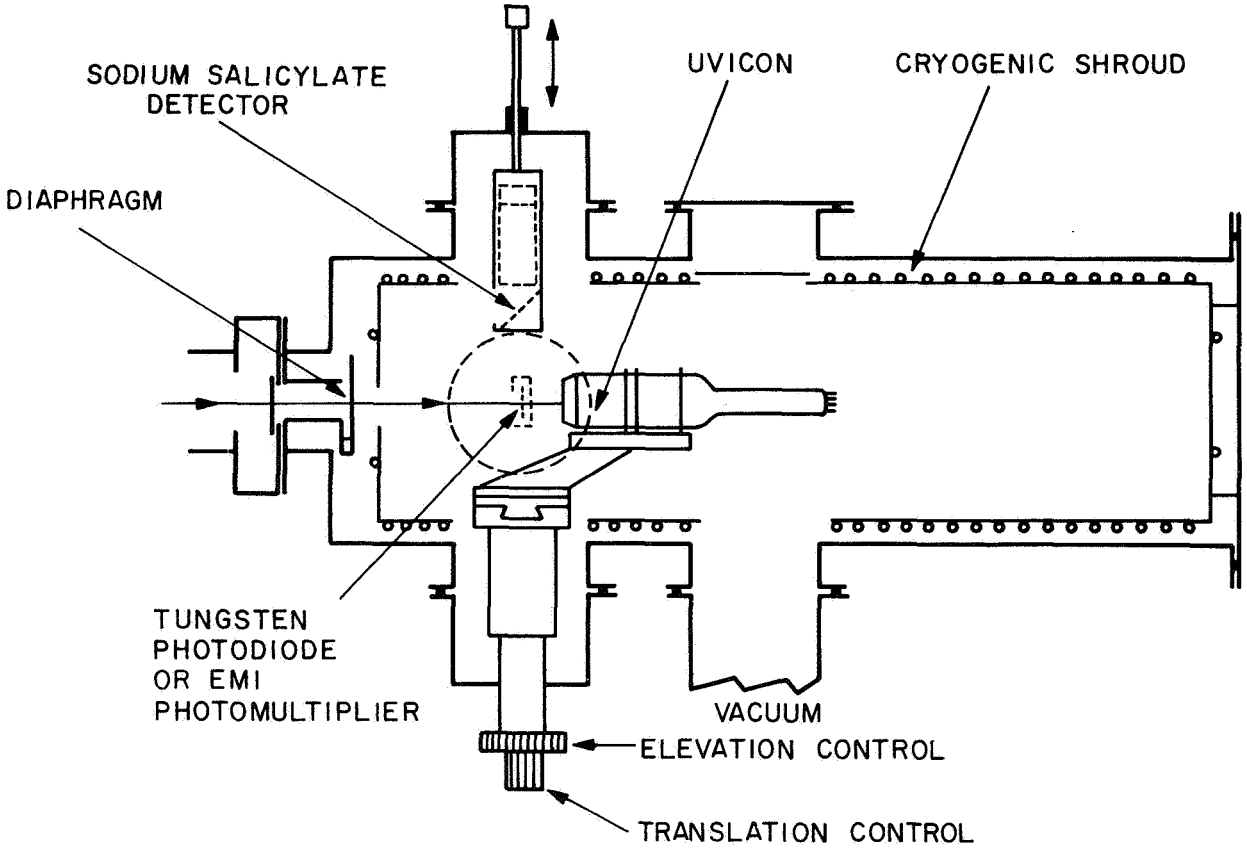

Figure 42. Uvicon calibration facility.

In addition to the salicylate detector, a calibrated photodiode detector was present in the calibration chamber during every Uvicon calibration. Like the salicylate detector, this device could be moved in or out of the

beam by means of a vacuum-seal push rod. For the flight Uvicons, this photodiode consisted of a polished tungsten plate having a response below 1300 Å. In December 1966, we determined that this tungsten photodiode was less stable than the salicylate detector and replaced it with an EMI photomultiplier sensitive at wavelengths above 1600 Å for calibration of the last few spare flight Uvicons.

In order for the parametric dependence of $Q_U(\lambda)$ on position to be measured, it is necessary to set up a two-dimensional coordinate system on the circular Uvicon faceplate. The faceplate itself has a flat rim surrounding the concave central portion. This rim is ground flat and defines a plane normal to the optic axis of the Uvicon; we have used this as our coordinate plane. Conceptually, the faceplate is bisected by two mutually perpendicular diameters, and the intersection of these diameters defines the origin of coordinates. We used a soft lead pencil to mark the ends of two perpendicular diameters on the rim of each Uvicon faceplate before beginning calibration; the reference radius was oriented in the direction of vertical raster advance. The reference radius is marked by the addition of a small circle on the radius mark corresponding to the side of the raster from which scanning proceeds. This mark serves as azimuthal reference for all subsequent calibrations; it is aligned during payload assembly so as to coincide with the $+Y_c$ spacecraft reference direction for telescopes A-1 and D-2, and the $-Y_c$ direction for telescopes A-2 and D-1. For Uvicon R19A, the reference diameters were rotated 15° relative to the raster orientation, a fact explaining the raster tilt of camera C-1 (see Figure 12).

After reference marks are placed on the faceplate rim, the Uvicon is mounted on the translation table cradle inside the Uvicon tank with the diameter H-H in an approximately vertical orientation. The monochromator is adjusted for the zero-order (visible) beam and the Uvicon is translated and elevated on its carriage until the beam is centered exactly on the upper reference mark. With the use of the elevation control only, the tube is raised until the beam falls in the vicinity of the lower reference mark. If the beam is centered laterally on this mark, the tube is properly oriented; if not, the

tube is rotated in its cradle slightly in the appropriate direction and/or translated laterally slightly until the beam is centered on the top and the bottom marks as the tube is alternately raised and lowered with the elevation control. When this occurs, the scale reading (H_O) on the translation control represents the location of the diagonal H-H. The Uvicon is now positioned so that the beam is centered on either the right or the left reference mark. In this position, the elevation-control scale reading V_O gives the location of the diagonal V-V. The optic axis is then located by setting the scales of the translation and elevation controls to H_O and V_O, respectively. To locate any other point on the faceplate, the Uvicon is translated and elevated an appropriate amount, with the calibrated scales on the translation and elevation controls being used.

For calibration purposes, electrical connections with the Uvicons are made to four Kovar flanges on the main body of the tube. The front flange (no. 1) provides a connection with the photocathode surface; the remaining flanges (nos. 2, 3, and 4) are focusing electrodes in the tube. The photocathode current is measured by connecting flange no. 1 to the input of a Keithley Model 417 picoammeter. Flange nos. 2 and 3 are connected together and are biased about +50 volts to provide a collector for electrons emitted from the photocathode. During low-temperature tests, Uvicon temperatures are measured by attaching a thermocouple to flange no. 4. Thermocouple leads are passed unbroken through hermetic seals mounted on the Uvicon-tank cover plates.

Although the cold shroud is designed to provide a nearly isothermal environment for devices under test, some thermal gradients do exist within Uvicon tubes at low temperatures. In particular, the faceplate is slightly warmer than the rest of the tube since it "sees" the diaphragm, which is at approximately room temperature. Because it is not possible to attach thermocouples directly to the faceplate of a flight Uvicon, we have instead measured the temperature of flange no. 4 during actual calibrations. The relationship between flange no. 4 temperature and faceplate temperature was then determined by an experiment on a reject Uvicon. Two thermocouples were attached to the faceplate of this tube, one on the rim and one

in the center. The thermocouples were held firmly in place by small pieces of aluminum-foil-backed adhesive. A third couple was attached to flange no. 4, and the output of each was recorded at various low temperatures. Both the faceplate thermocouples agreed to within less than 1° C; the temperature of the faceplate was 10 to 15° higher than that of flange no. 4, however, at the lowest temperatures imposed.

The first step in the calibration of a Uvicon consists of placing reference marks on the faceplate rim and orienting the tube in the calibration chamber as described above. Electrical connections are made to the Uvicon, and the tank is evacuated to 10^{-5} torr or below. If a thermal test is to be run, the shroud is refrigerated until the desired Uvicon temperature is achieved. The sodium salicylate detector is positioned in the beam, and the output of this device is connected to a Keithley Model 417 picoammeter, which in turn provides an amplified input signal for a Brown high-speed chart recorder or for a Datex digital (punched card) recording system. The output current of the salicylate detector $i_S(\lambda)$ is then recorded as the wavelength of the monochromator output is varied continuously over the spectral region of interest, typically 1000 to 3000 Å. After this scan is finished, the salicylate detector is removed from the beam, the Uvicon under test is positioned so that the beam is incident upon the desired location of the faceplate, and the Uvicon photocathode output $i_U(\lambda)$ is recorded as the spectrum is again scanned. The Uvicon is then repositioned and $i_U(\lambda)$ recorded for another location on the faceplate; this procedure is repeated, rerecording $i_S(\lambda)$ periodically, until all desired locations on the faceplate have been calibrated. An identical sequence of measurements is performed at each temperature required. Assuming that the spectral sensitivity $Q_S(\lambda)$ of the sodium salicylate detector is known, $Q_U(\lambda)$ is determined by the measurement of only two quantities: $i_S(\lambda)$ and $i_U(\lambda)$.

Since $i_U(\lambda)$ and $i_S(\lambda)$ cannot be recorded simultaneously, it is necessary to ensure that the output of the hydrogen discharge source is stable enough to allow a direct comparison of $i_S(\lambda)$ and $i_U(\lambda)$ scans taken 15 min or more apart (approximately 15 min are required to obtain a complete scan). This

stability has been provided by operating the source with a McPherson Model 730 constant-current-regulated power supply. In addition, hydrogen is supplied to the source via a needle valve that permits accurate regulation of the gas pressure in the source. Experience has shown that the source's output generally changes very little during the course of a day after an initial stabilization period. Because of an occasional random variation in output, however, we have made a practice of rerecording $i_S(\lambda)$ after every three measurements of $i_U(\lambda)$.

Calibration of the long-wavelength cutoff characteristics of Uvicons has been performed by a different technique. The Uvicon is mounted on an optic bench, its faceplate covered by a mask containing capped holes in the positions where calibration is desired. The mask is irradiated by ultraviolet illumination from a mercury lamp calibrated for use as a standard by the techniques described in Section 6.2.7. Light of the desired wavelength is selected by means of an interference filter calibrated in the same manner as are the flight filters. The Uvicon is calibrated by removing one cap at a time to expose each position in turn to the known irradiance from the lamp-filter combination. For the A-type Uvicons, this calibration serves as a check on the monochromator calibration at 2537 Å. For the D-type Uvicons, the light level available from the monochromator is insufficient to cause a perceptible signal at 2537 Å, and the bench calibration serves as the only measure of quantum efficiency at that wavelength. For the A-type Uvicons, the bench measurement provides calibration at 3130, 3341, and 3660 Å, in addition to providing a check of the calibration at 2537 Å.

The foregoing discussion outlines in a general manner the procedures used to obtain $Q_U(\lambda; x, y, T_U)$; detailed test plans for Uvicons are provided in Calibration Test Instructions CTI-8 and CTI-8a.

Figures 43 through 46 show typical quantum-efficiency curves for the four flight Uvicons.

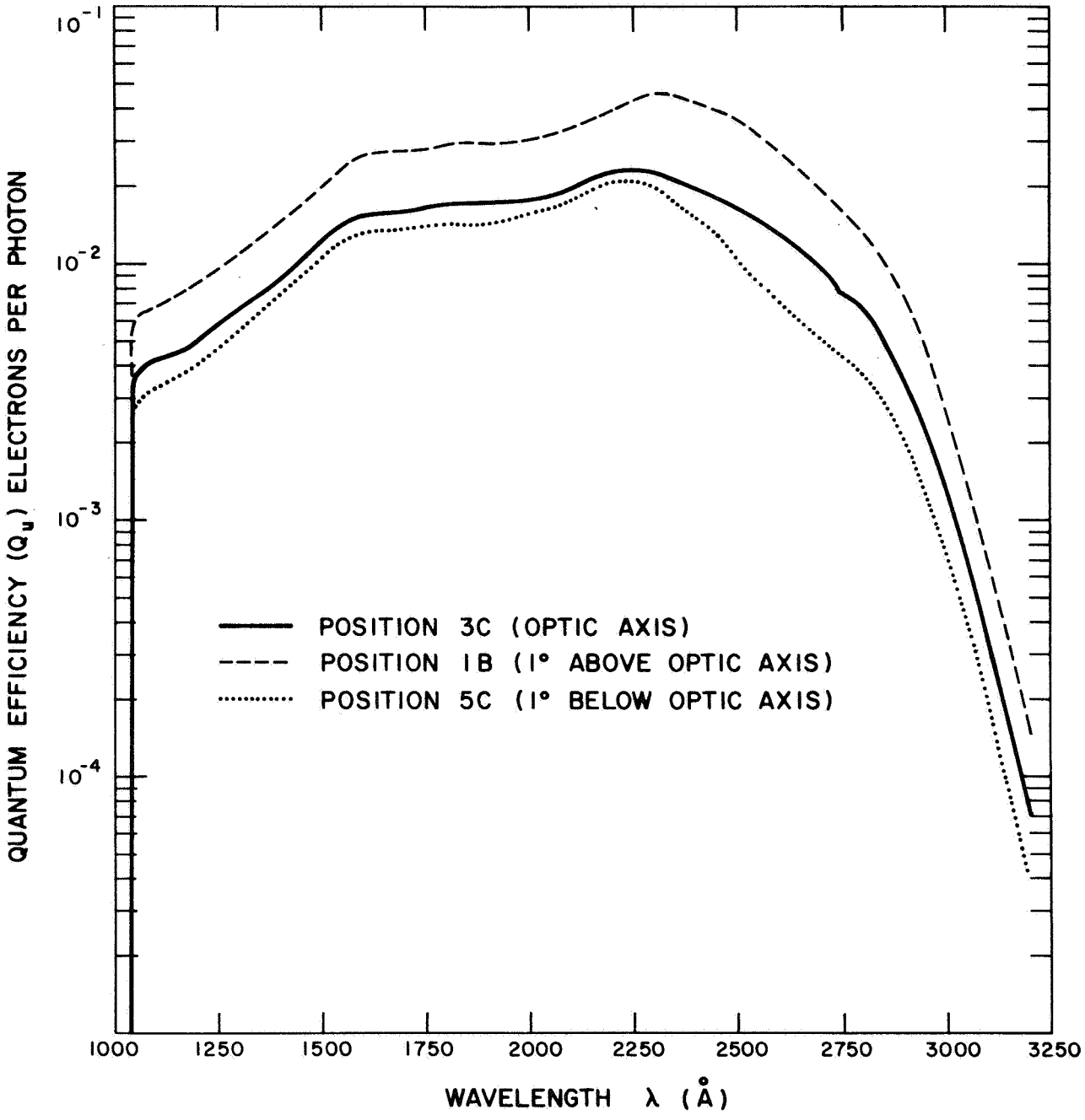

Figure 43. Typical quantum-efficiency curves for Uvicon R19A (F-1 telescope).

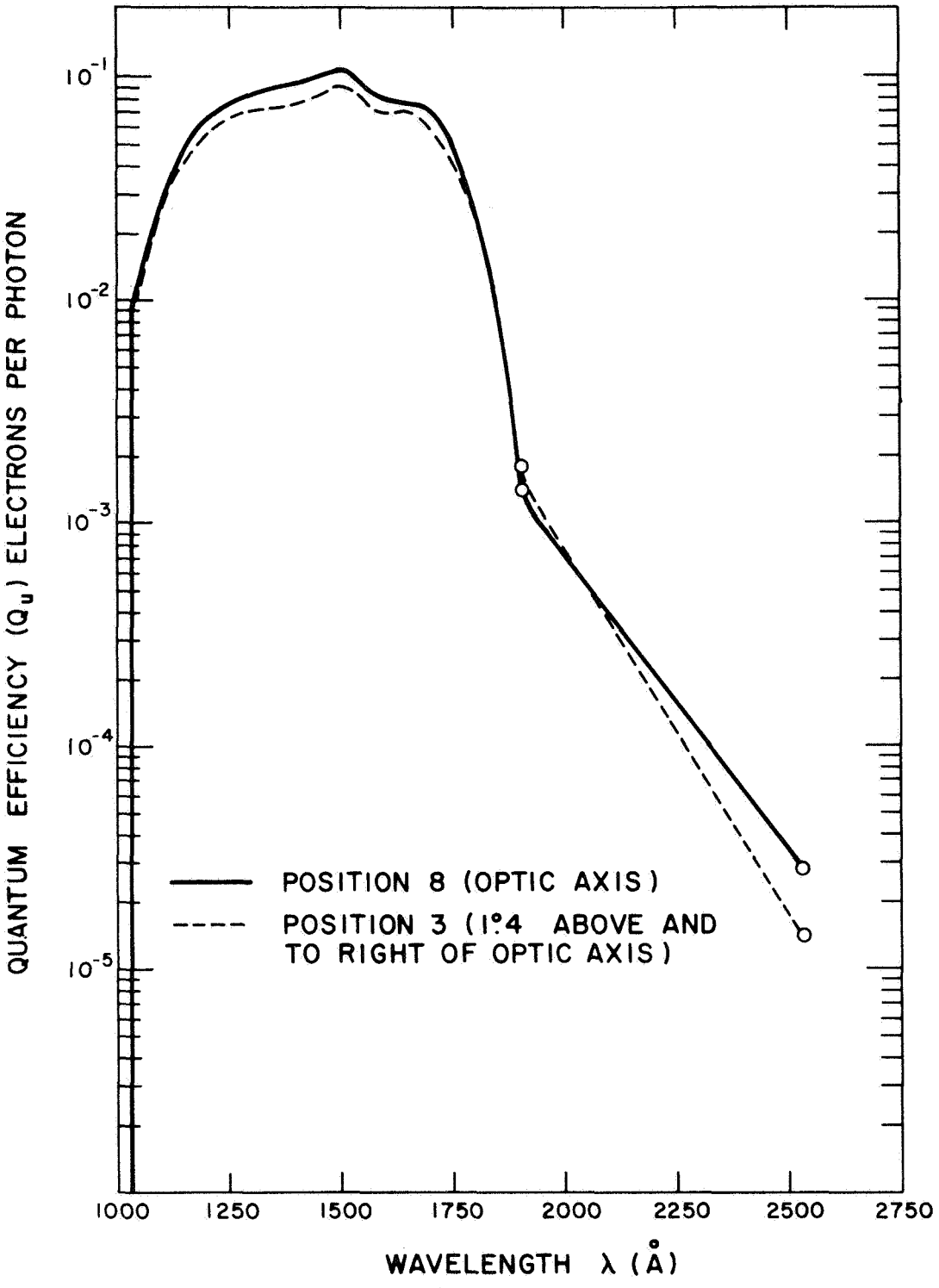

Figure 44. Typical quantum-efficiency curves for Uvicon 65-35-050D (F-2 telescope).

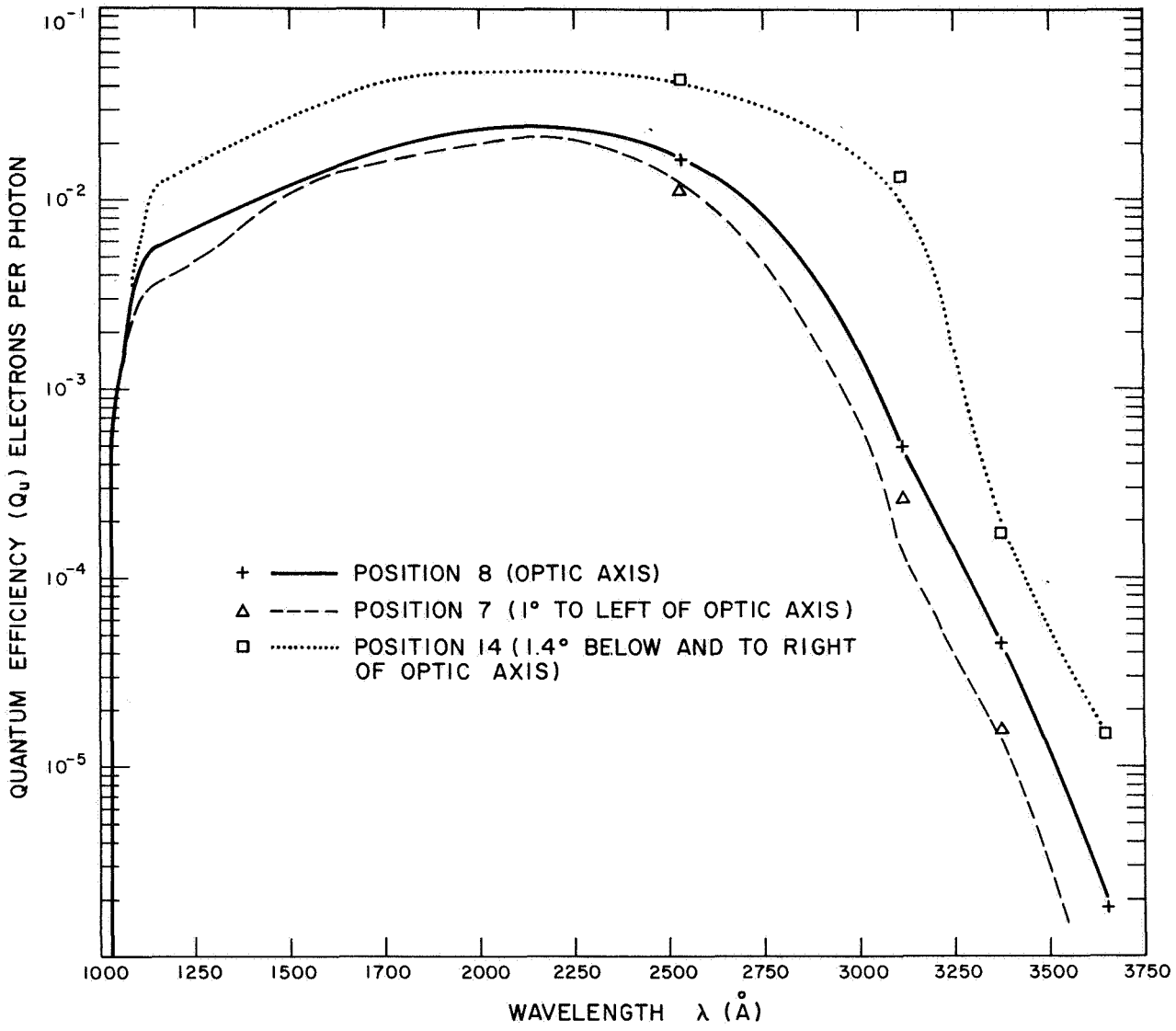

Figure 45. Typical quantum-efficiency curves for Uvicon R29A (F-3 telescope).

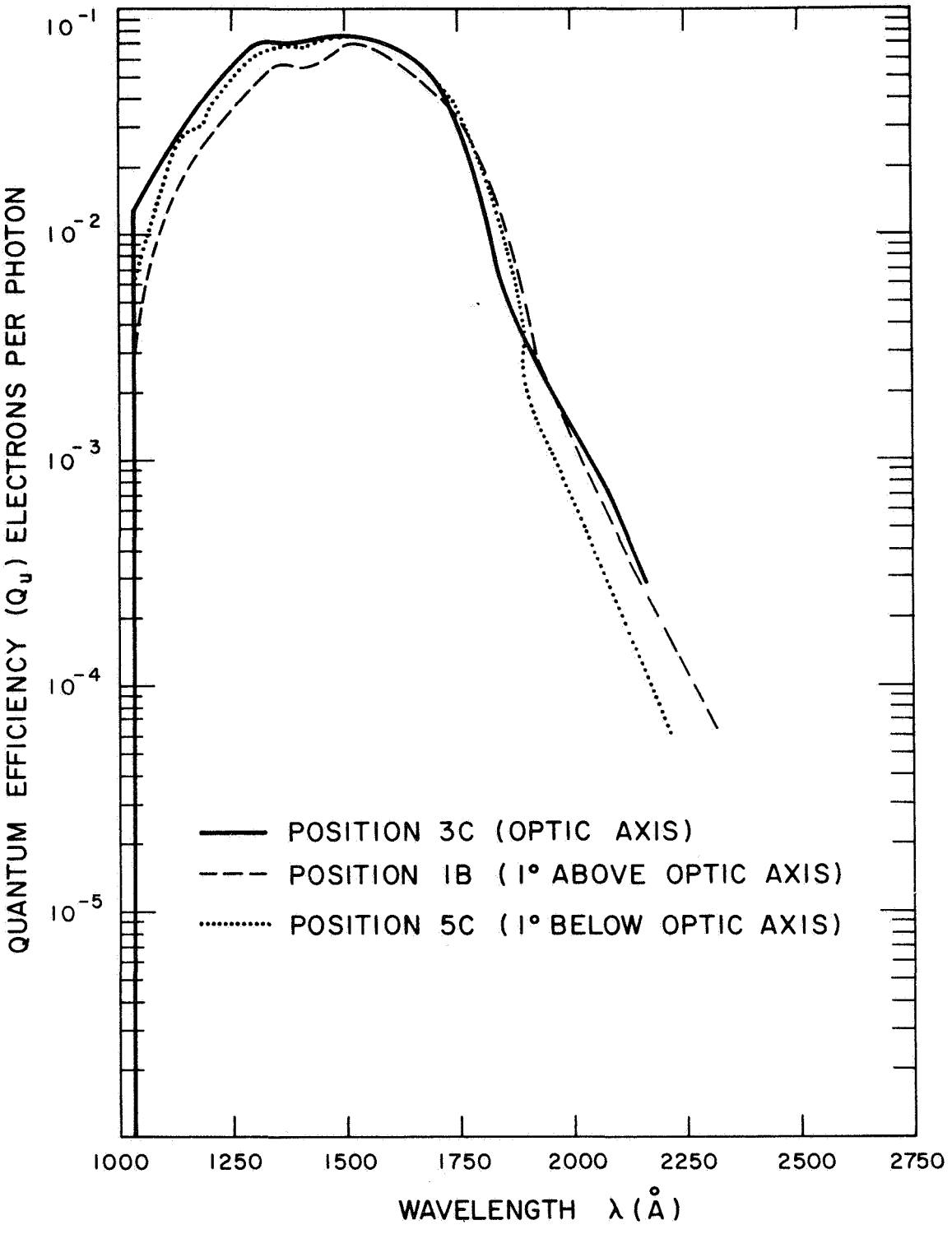

Figure 46. Typical quantum-efficiency curves for Uvicon R42D (F-4 telescope).

Calibration of the electronic transfer function, $N_p(V_\Sigma)$, of the Uvicon requires operation of the tube in a manner identical to that to be used in orbit, under excitation by point sources of known intensity and position. This calibration is performed at EMR in the configuration shown in Figure 47. Light from a mercury calibrator lamp L, masked down to provide a point source, is passed through a filter F of known attenuation. The filters used have been calibrated for transmittance by SAO and found to have essentially constant transmittance between 1800 and 4000 Å. At the faceplate of the Uvicon U the irradiance from this source is independent of position. A reticle R is attached to the Uvicon faceplate to restrict the illumination to the desired configuration on the photocathode. For calibration of the source, the reticle is provided with a hole of 1 cm^2 area and the photoelectric current is measured directly in the same manner as at SAO. For calibration of the Uvicon, the reticle is provided with either 14 or 26 holes evenly distributed throughout the scanned area of the photocathode, with one asymmetrical hole provided as a parity indicator. The area of each hole is approximately 10^{-4} cm^2 and has been calibrated to an accuracy of 1%, geometrically by EMR and optically by SAO. The Uvicon is calibrated as a unit with its high-voltage power supply and camera module, which includes deflection amplifiers and video preamplifier. This unit is controlled, and the video signal is amplified and analyzed by a test set TS equivalent in operation to the Bay E-4 electronic subassembly that will perform these functions in the flight payload. In the digital mode, the signal from the test set is sent to an ASI computer for transcription onto magnetic tape in computer-compatible format. In the analog mode, the signal from the test set is displayed on an oscilloscope and photographed; the signal is also recorded by an Ampex FR-1800 tape recorder. The Uvicon camera module is calibrated throughout its dynamic range at room temperature, and through one decade at the center of its dynamic range at additional temperatures expected to be encountered in orbit. Figures 48 through 51 show typical transfer functions for the four flight Uvicon modules.

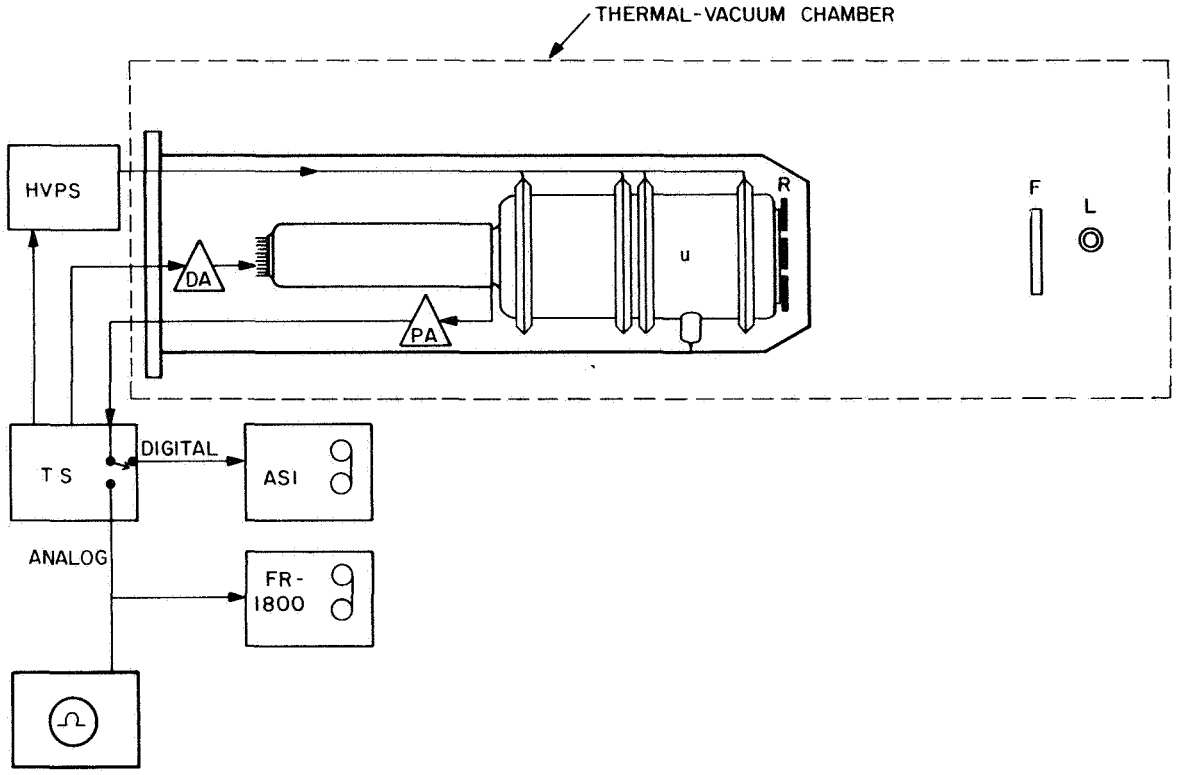

Figure 47. Test configuration for calibration of Uvicon transfer function.

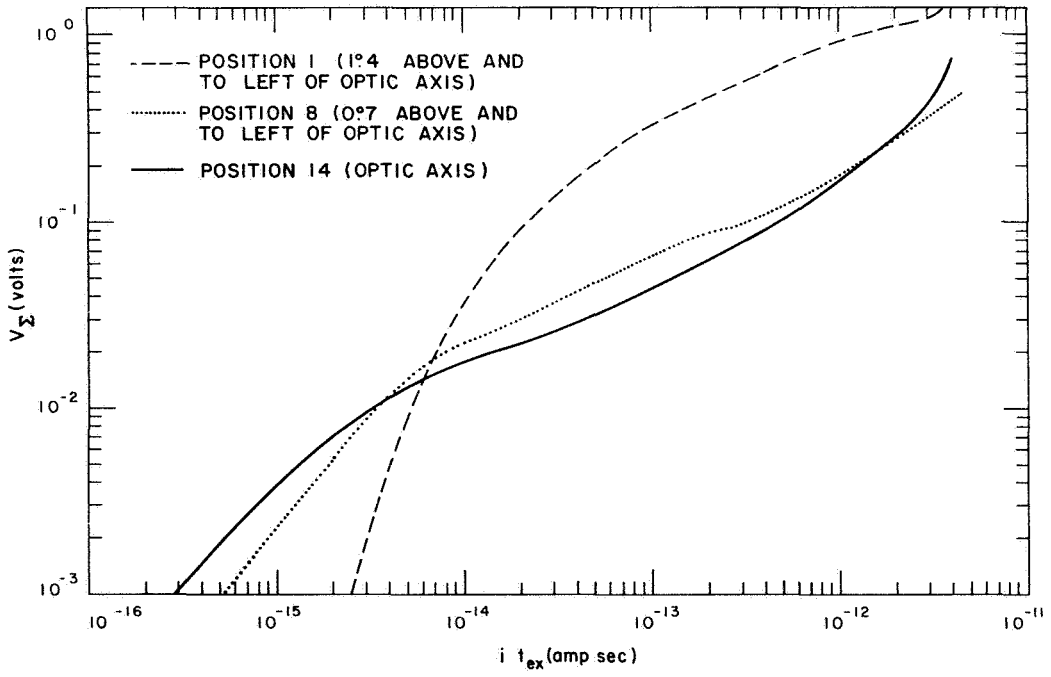

Figure 48. Typical transfer functions for Uvicon R19A (F-1 telescope).

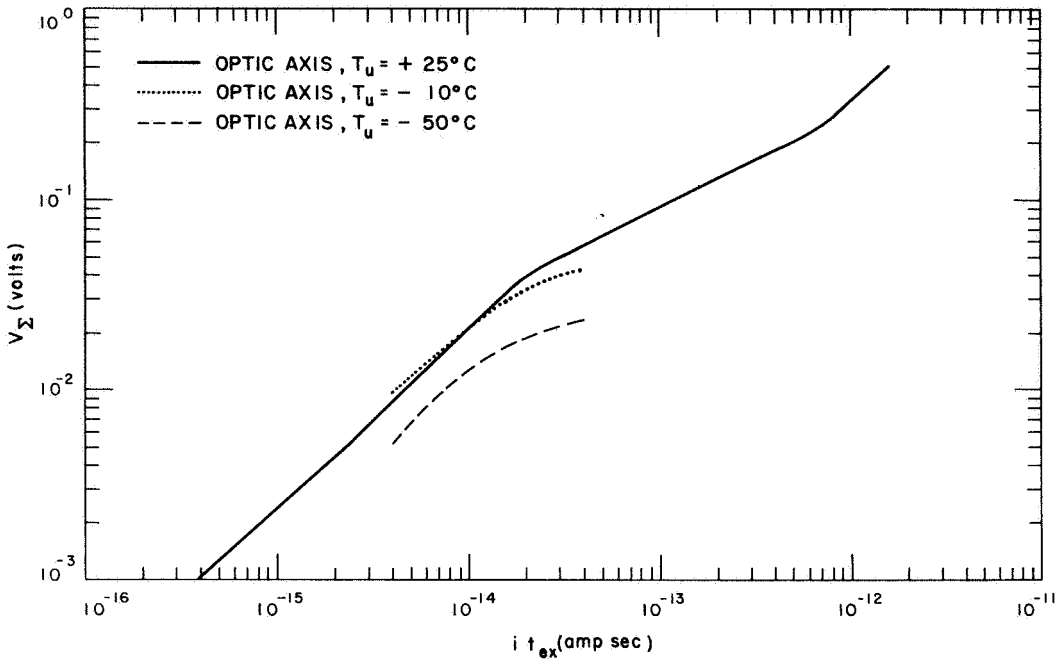

Figure 49. Typical transfer functions for Uvicon 63-35-050D (F-2 telescope).

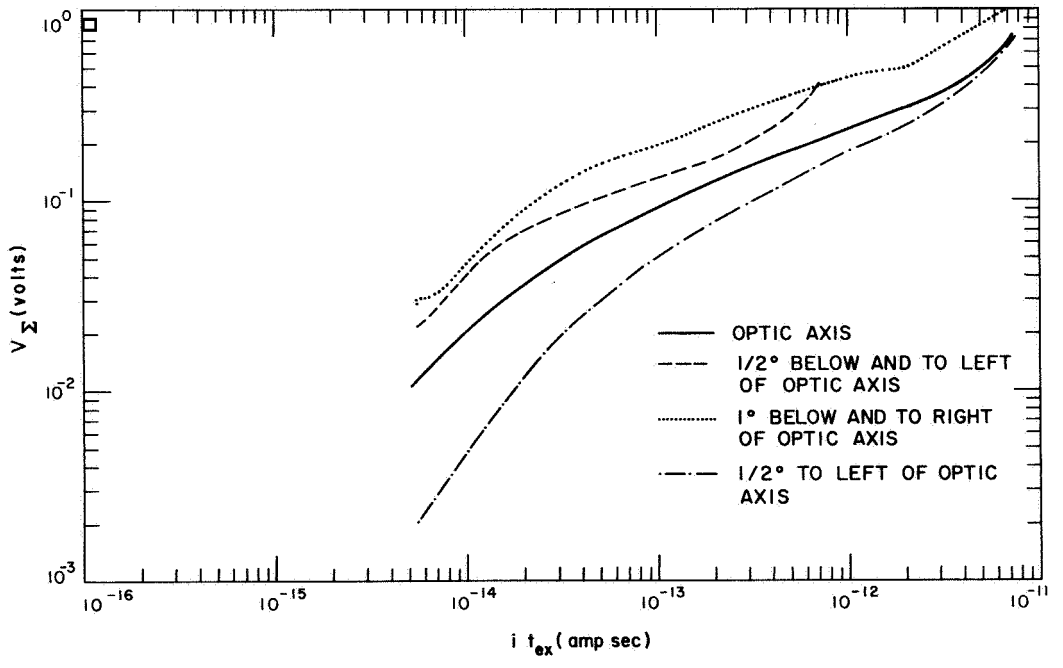

Figure 50. Typical transfer functions for Uvicon R29A (F-3 telescope).

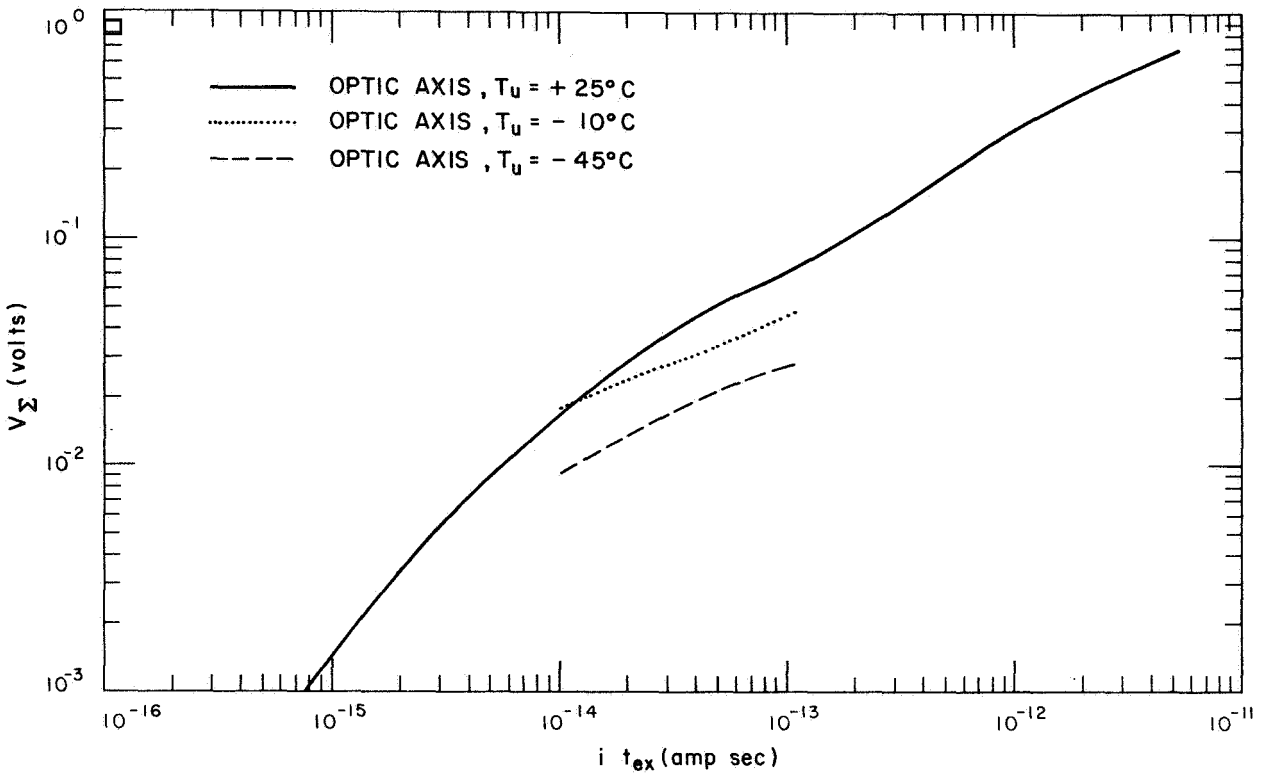

Figure 51. Typical transfer functions for Uvicon R42D (F-4 telescope).

The accuracy with which we can determine the brightness of a source depends in part upon the algorithm used for reducing the output matrix A to a scalar quantity V_Σ. Our present algorithm first performs a statistical analysis of the output signals in a data frame to determine the distribution of values assumed by $a_{k,\ell}$. Figure 52 shows a typical Celescope signal distribution curve. That portion of the picture arising from the noise background produces a characteristic maximum in the distribution in the vicinity of $a_{k,\ell} = 5 \times 10^{-4}$ volts. Any set of adjacent points all of which lie more than three standard deviations above this average noise level is considered to be a signal from a point source; the average noise is subtracted from each of the $a_{k,\ell}$ components of the signal, and $a_{k,\ell}$ for the resulting submatrix is summed over k and ℓ. The number of adjacent points required to form a "set" is usually required to be 4. By retaining the original data tapes, we are able to improve our transfer-function calibration as our algorithm for computing V_Σ is improved.

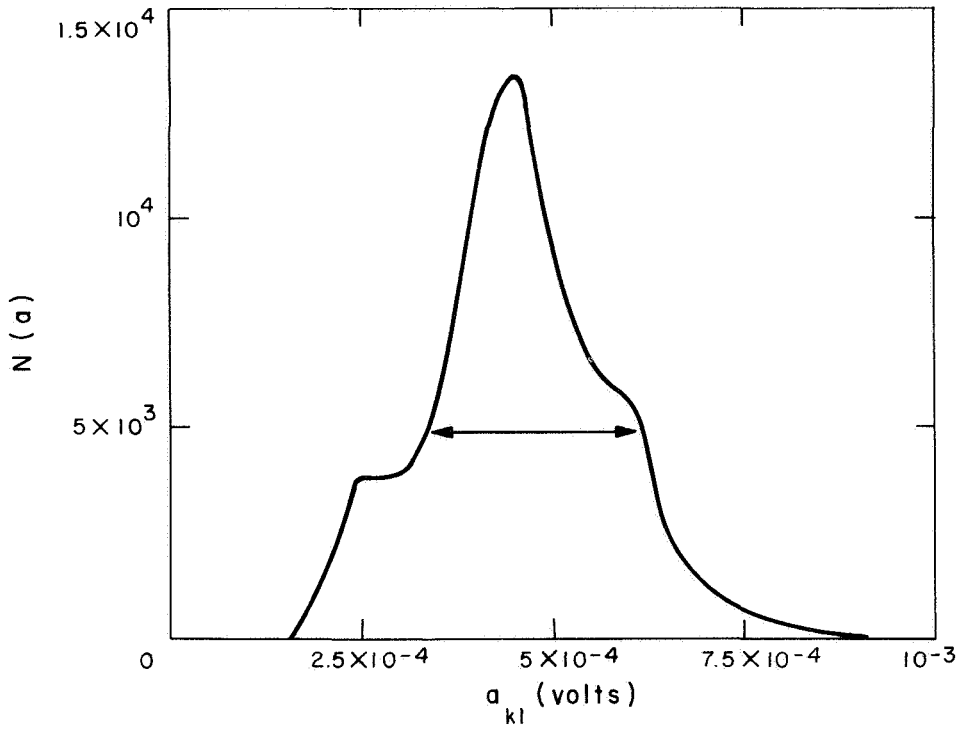

Figure 52. Typical noise-distribution curve.

As can be seen from Figure 47, the positions of the illuminated points (x, y) on the photocathode can be determined from the known positions of the reticle holes and lamp relative to the photocathode by means of a straightforward ray trace. In practice, it turns out to be more convenient to trace these rays backward as if they had arrived via reflection from the telescope mirrors, and thus deduce the equivalent positions (ζ, η) on the celestial sphere. (Refer to Figure 14.) The corresponding raster position (k_0, ℓ_0), is most easily defined as the position for which $a_{k,\ell}$ reaches a local maximum. The electronic calibration of the Uvicon would thus enable us to determine the positional transfer function if the relationship between (k_0, ℓ_0) and (ζ, η) were invariant. It turns out that the position of the raster relative to the optic axis depends upon the direction of the earth's magnetic field relative to the Uvicon, but that the amplitude and direction of the scan relative to the (ζ, η) coordinate system are invariant. The calibration image is invariant in (ζ, η) coordinates and thus serves as a measure of the position of the raster.

The Uvicon transfer functions are most conveniently expressed in terms of camera gain (G_c), deflection sensitivity (J), and raster rotation (θ_0), defined as follows:

$$G_c \equiv \frac{V_\Sigma}{it_{ex}} \quad ,$$

$$J_k \equiv \frac{\eta}{(\ell_0 - \ell_C) \sin \theta_0 + (k_0 - k_C) \cos \theta_0} \quad ,$$

$$J_l \equiv \frac{\zeta}{(\ell_0 - \ell_C) \cos \theta_0 + (k_0 - k_C) \sin \theta_0} \quad ,$$

where (k_C, ℓ_C) is the position of the optic axis in raster coordinates. The raster rotation (θ_0) is defined as the angle between the horizontal sweep direction and the $+Z_c$ spacecraft axis; θ_0 is 15° for telescope F-1, 180° for F-2, 180° for F-3, and 0° for F-4. Typical curves of G_c versus V_Σ can be obtained by a simple transformation of Figures 48 through 51. The deflection sensitivities of all four cameras, along both axes, are very nearly 36 arcsec per television scan line.

6.2.3 Gain calibration of electronic subassemblies

The signal from each Uvicon camera is first amplified by a video amplifier whose gain (G_l) is appropriately tailored for its Uvicon, and then sent to the Bay E-4 subassembly for further processing. In the analog mode of operation, Bay E-4 attenuates the signal slightly and mixes it with synchronization pulses of calibrated amplitude for transmission via the wide-band transmitter. In the PCM mode of digital operation, Bay E-4 encodes the signal $a_{k,\ell}$ into serial words containing 7 bits plus parity for transmission via the wide-band transmitter; the line number (k) is also encoded whenever it changes. In the store mode of digital operation, Bay E-4 encodes the signal ($a_{k,\ell}$) and position (k and ℓ) into parallel 23-bit words; whenever $a_{k,\ell}$ exceeds a threshold specified by ground command, a "Store Digital Word 1" pulse is generated to cause this word to be stored by the Experimenter's Data-Handling Equipment (EDHE).

The gains of the video amplifier (G_1) and of Bay E-4 (G_4) are measured in the standard manner, by comparing the amplitude of an input signal from a proper signal generator with the amplitude of the corresponding output signal. These calibrations are described in detail by Calibration Test Plans CTP-130 and CTP-167.

6.2.4 Calibration of the calibrator-lamp systems

Figure 53 shows, in relationship to the telescope subassembly, the calibrator-lamp system and the fixture used for calibrating it. The calibrator-lamp system consists of a power supply PS current stabilized to provide a stable light output from the lamp; a xenon- or mercury-lamp assembly L mounted on the rim of the telescope tube T; and a diagonal mirror M and focusing lens F, mounted on the back of the secondary mirror assembly. In normal operation, light passing through a pinhole aperture in the lamp assembly is focused through the optical filter O onto the Uvicon photocathode U. The mercury lamp is used for the A-type Uvicons. It is temperature stabilized to maintain constant light output. Its output is essentially monochromatic at 2537 Å. The xenon lamp is used for the D-type Uvicons. The xenon-lamp assembly includes a temperature probe to provide data for determining its output, which varies as a function of temperature. Its output is essentially monochromatic at 1470 Å. The mercury-lamp output is focused by a quartz lens through the Corning 7910 optical filter; the xenon-lamp output is focused by a lithium fluoride lens through the lithium fluoride optical filter.

Calibration of the calibrator system is performed as one step in thermal-vacuum calibration of the telescope subassembly, described in Section 6.2.5. The calibration fixture C is bolted to the telescope tube T so that mirror R causes the calibrator output image to be focussed onto the center of the photocathode of a solar-blind photomultiplier PMT. During mercury-lamp calibrations, an auxiliary Corning 7910 filter A is mounted in the calibration fixture. The calibration fixture is calibrated by SAO against the laboratory standards described more fully in Section 6.2.7; the details of this

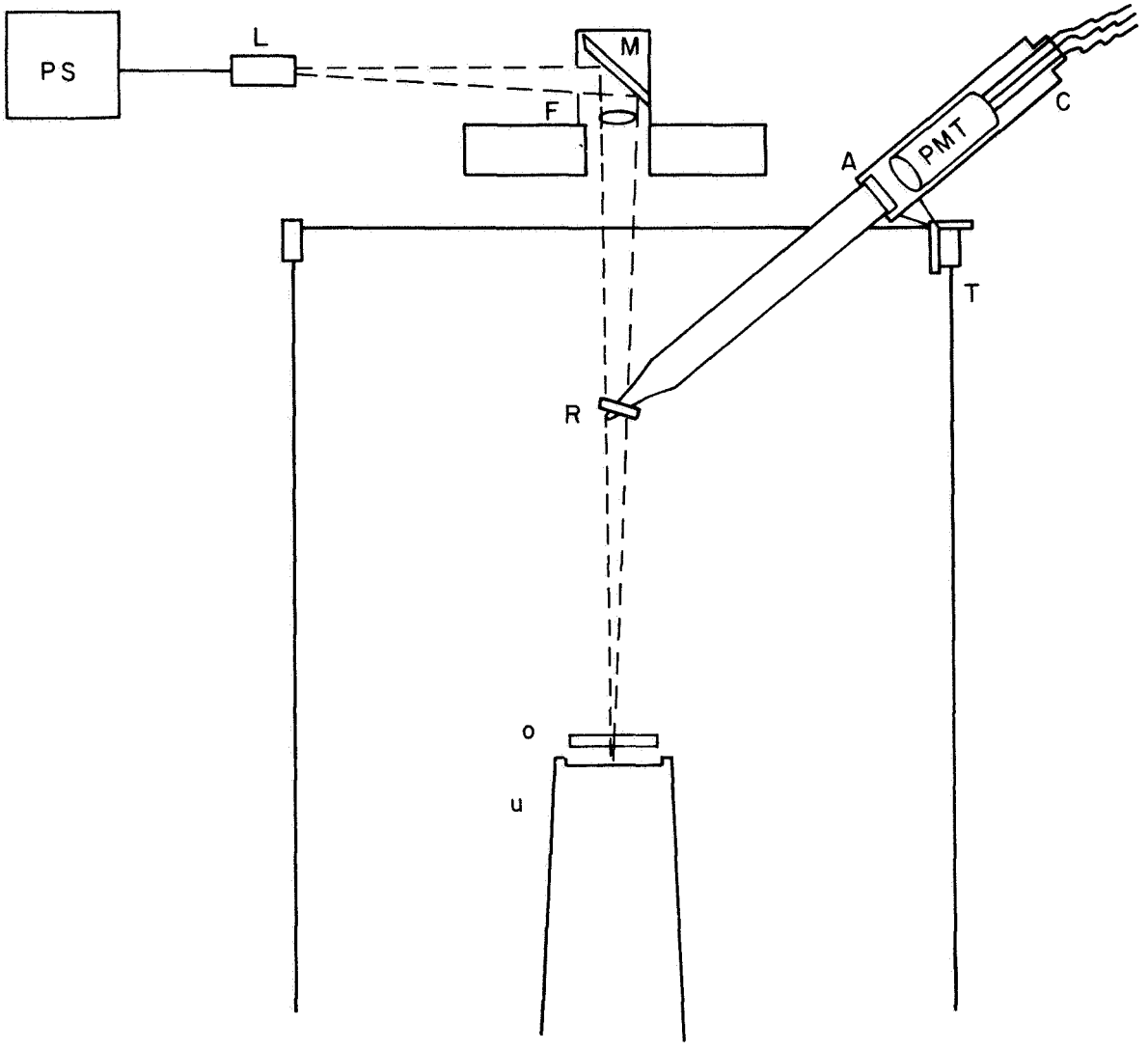

Figure 53. Arrangement for calibrating the calibrator-lamp system.

calibration are specified in Calibration Test Instruction CTI-3B. The procedures for using this device in the calibration of the calibrator system are given in Celescope Test Plan CTP-158. These procedures yield the monochromatic flux output from the calibrator system at room temperature, $\Phi_{CAL}(T_0)$. The temperature dependence of the xenon-calibrator system is determined during thermal-vacuum testing of the xenon-calibrator-lamp assembly (Celescope Test Plan CTP-124). For the F-2 telescope, this dependence is found to be

$$\Phi_{CAL}(T) = \left(\frac{T}{T_0}\right)^{-0.63} \Phi_{CAL}(T_0) \quad .$$

For the F-4 telescope, this dependence is found to be

$$\Phi_{CAL}(T) = \left(\frac{T}{T_0}\right)^{-0.39} \Phi_{CAL}(T_0) \quad ,$$

where temperatures are expressed in degrees Kelvin.

6.2.5 Calibration of telescope subassemblies

In order to provide a direct comparison between the "component" calibrations described above and the subassembly calibration that they imply, we calibrate every telescope subassembly in EMR's Thermal-Vacuum Optical Bench (TVOB) in a collimated beam of monochromatic light. This calibration uses the same test equipment to generate and analyze the television signal as was used during Uvicon transfer-function calibration. The brightness of the collimated beam is established by using the photomultiplier from the calibrator-system calibration fixture as a beam probe. It is an incomplete calibration, in that it is made at only one wavelength, at only one position, and over only a limited range of intensity. Its primary purpose is to provide an indication of any systematic deviations between observed and computed subassembly calibrations and to provide a firm indication of the integrity of the subassembly before it is mounted in the structural assembly and connected

to the Bay E-4 electronics. Telescope calibration is described fully in Celescope Test Plan CTP-171.

TVOB calibration establishes only the correctness of the intensity transfer function; it includes no tight requirement concerning the alignment of the collimated beam relative to the optic axis. Positional calibration accuracy is confirmed by a set of measurements performed in the ambient clean-room environment at EMR, in which the position of the signal in the raster is compared with the direction of the input beam relative to the optic axis for a number of positions throughout the field of view. During this test, the telescope is rotated 90° between calibrations of deflection sensitivities in the Y_c and Z_c directions. The resulting change in the configuration of the telescope relative to the earth's magnetic field induces a shift in the position of the raster relative to the optic axis, so that this test cannot be used for "locating" the optic axis in raster coordinates. The procedure for locating the optic axis is described in Section 6.2.6. The procedure for positional calibration of the telescope subassembly is described in Celescope Test Plan CTP-178.

During vibration testing, telescope F-3 changed its characteristics in such a manner that the calibration performed earlier on its Uvicon module (R29A) was compromised. It was therefore necessary to expand the subassembly calibration of this telescope so as to supply full calibration data. Except for the addition of a large number of extra calibration points and the requirement for accurate calibration and control of beam intensity, this test was similar to normal positional calibration as described by CTP-178.

6.2.6 System calibration

System calibration is performed in the Vacuum Optical Bench (VOB) at GSFC. It, too, is a partial calibration, in which each input parameter (except temperature) is varied over a small number of steps, for comparison of the observed output with an output computed from the results of component and subassembly tests. VOB calibration was performed at four

wavelengths, four positions, three operating modes, three exposure times, and three beam intensities. The wavelengths selected were 1216, 1608, 1849, and 2537 Å. Exposure times were 5, 15, and 60 sec. Intensity and exposure time together covered the range from 10 to 1000 times threshold for the most sensitive camera. Of course, not all wavelengths are above threshold for any one camera, even at the most intense settings. Beam intensity was determined by mechanical scanning of the beam with a probe holding two photomultipliers: one furnished and calibrated by SAO, the other furnished by GSFC and calibrated by ASCOP.

One of the positions for VOB calibration is with the beam parallel to the optic axis, as defined by the optical alignment cube attached to the COP structure. With the beam in this orientation, the raster position of the optic axis can be directly compared with the raster position of the calibrator lamp image at the same time. The difference between these two positions in raster coordinates remains constant, thus enabling us to determine the position of the raster relative to the optic axis during orbital operation.

6.2.7 Calibration of SAO's laboratory standards

The calibration of Uvicons and photomultipliers, required for certain of the measurements described above, involves the comparison of the unknown device against a laboratory standard whose sensitivity or irradiance is presumed to be known. At SAO, we have developed two types of "presumably known" laboratory standards: the sodium salicylate fluorescent detector shown in Figure 30, of presumably known sensitivity; and the mercury-lamp assembly shown in Figure 54a, of presumably known irradiance when the temperature and current are controlled by the electronic control unit shown in Figure 54b.

Our most accurately established calibration point is the 2537 Å irradiance of our mercury-lamp assemblies. This calibration is performed by direct comparison at the National Bureau of Standards (NBS) against their 2537 Å irradiance standard; as a detector, one of SAO's ASCOP solar-blind photomultipliers is operated as a photodiode, in combination with one of

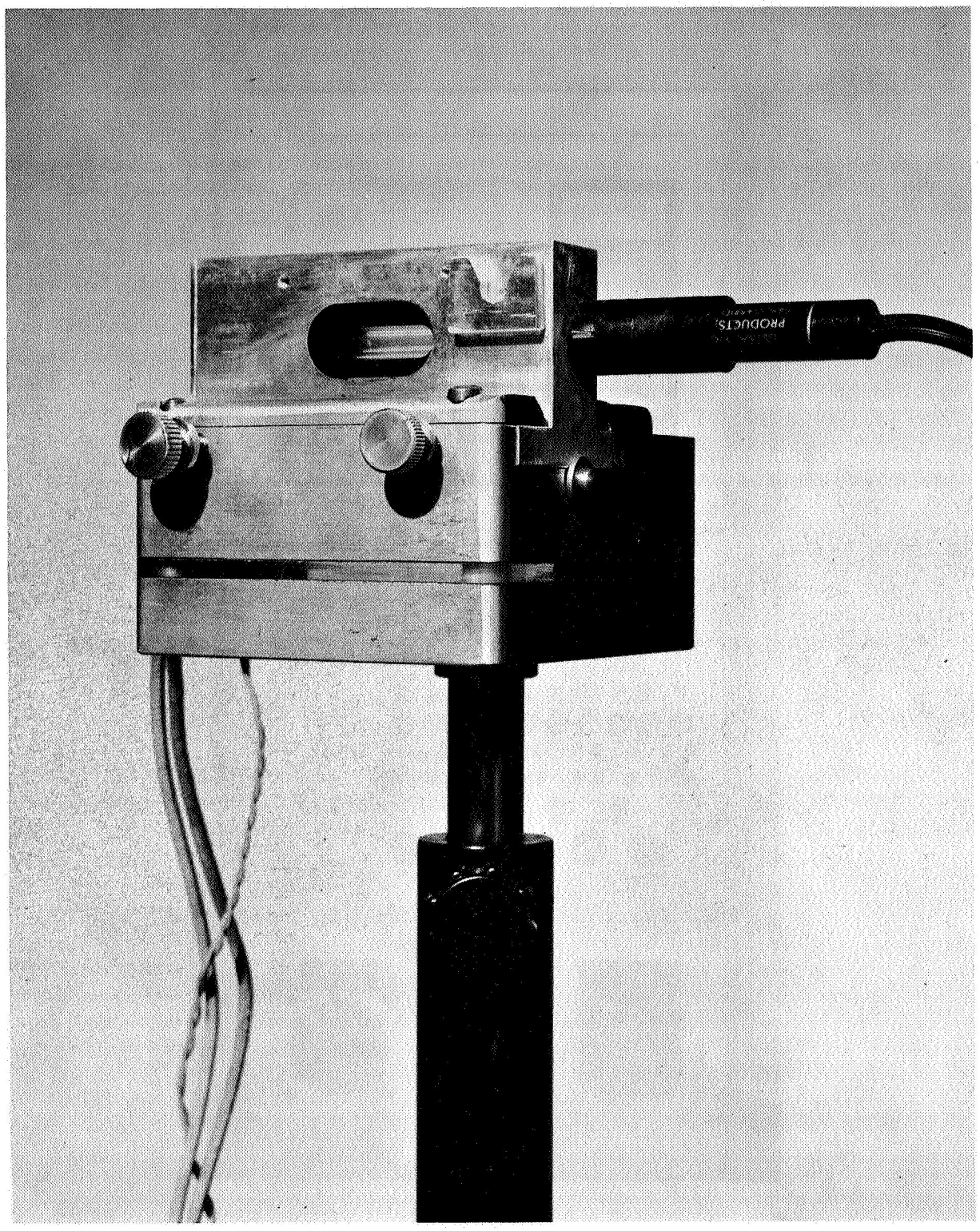

Figure 54a. SAO mercury-lamp ultraviolet-irradiance standard.

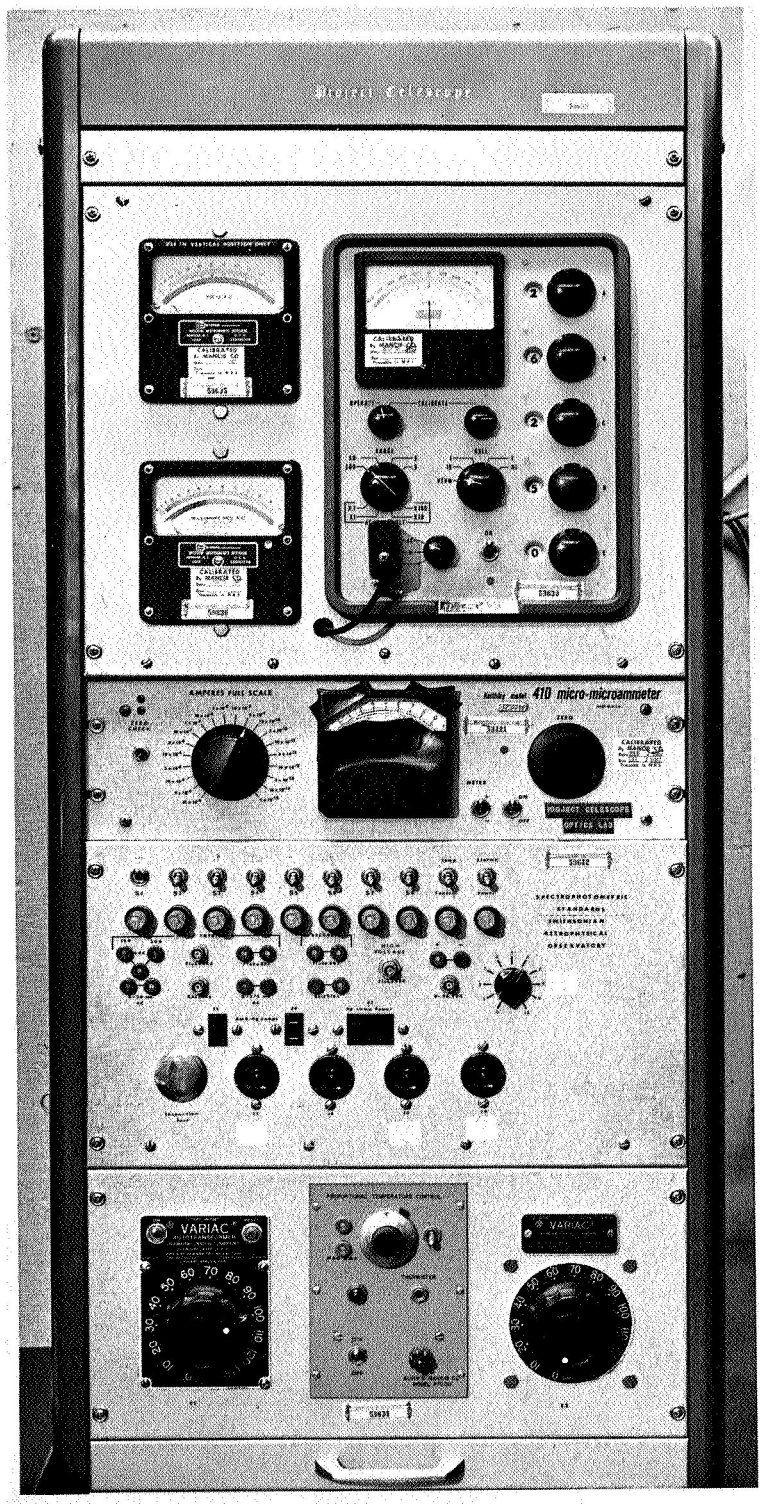

Figure 54b. Electronic control unit for SAO mercury-lamp ultra irradiance standard.

SAO's 2537 Å interference filters and an aperture stop whose area has been calibrated. The distance of the SAO standard lamp from the aperture stop is adjusted until the signals from the SAO lamp and the NBS lamp are equal. The results of such calibrations during the past four years are summarized in Celescope Calibration Report CCR-112; SAO lamp No. Hg-2 has maintained constant irradiance during this period to a precision of ±2%. The accuracy of calibration of the NBS standard is stated by NBS to be ±5%. This is a bright source; its irradiance is 0.322 w/m^2.

The spectral sensitivity of our sodium salicylate detector is first determined by comparison against the spectral sensitivities of a set of sodium salicylate screens as observed by an RCA 6199 photomultiplier in a different configuration from that of the laboratory standard, as shown in Figure 55. Also visible in Figure 55 is an ASCOP photomultiplier, normally the same one as is used for the 2537 Å calibration with mercury lamps. The laboratory standard is visible above the screens, in its retracted position. Since the mercury-lamp calibration serves to determine the sensitivity of the photomultiplier at 2537 Å, the sensitivities of the five salicylate detectors at that wavelength can be determined by comparison against it. The relative sensitivities of the six detectors are normally determined as a function of wavelength between about 900 and 3000 Å, since calibration outside this range requires a change in the working gas for our discharge lamp. Our results during the 3-1/2 years since screens SS-1, SS-3, and SSR-1 were produced are most simply interpreted under the assumption that screens SS-1 and SS-3 and the procedure for producing screens have provided invariant spectral-sensitivity responses over this time interval. The most stable ASCOP photomultiplier has, during this time, slowly decreased in absolute photodiode sensitivity without appreciably changing in regard to the shape of the spectral-response curve between 1000 and 3000 Å. The working standard changed its spectral response at an accelerating rate, beginning from near identity with the sodium salicylate reference standards in July 1964 and terminating with a rapid deterioration of its response below 1600 Å in April 1967; in June 1967 it was replaced with a new working standard of the same type. Figure 56 shows how its spectral response changed with time. Figure 57 compares the rate of this deterioration at 1216 Å against environmental exposure for this device.

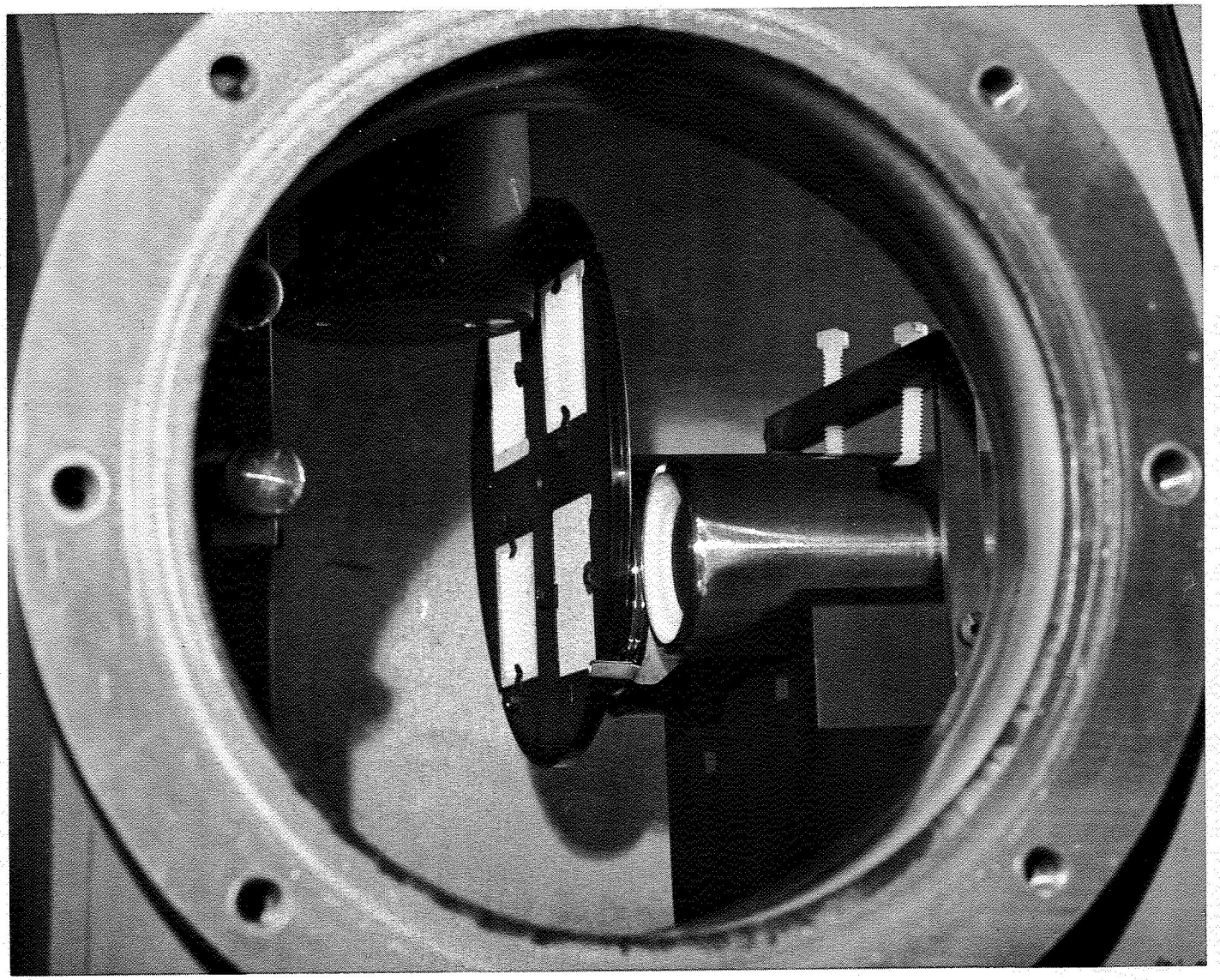

Figure 55. Arrangement for intercomparing spectral responses of standard sodium salicylate screens, ASCOP photomultiplier, and laboratory standard detector.

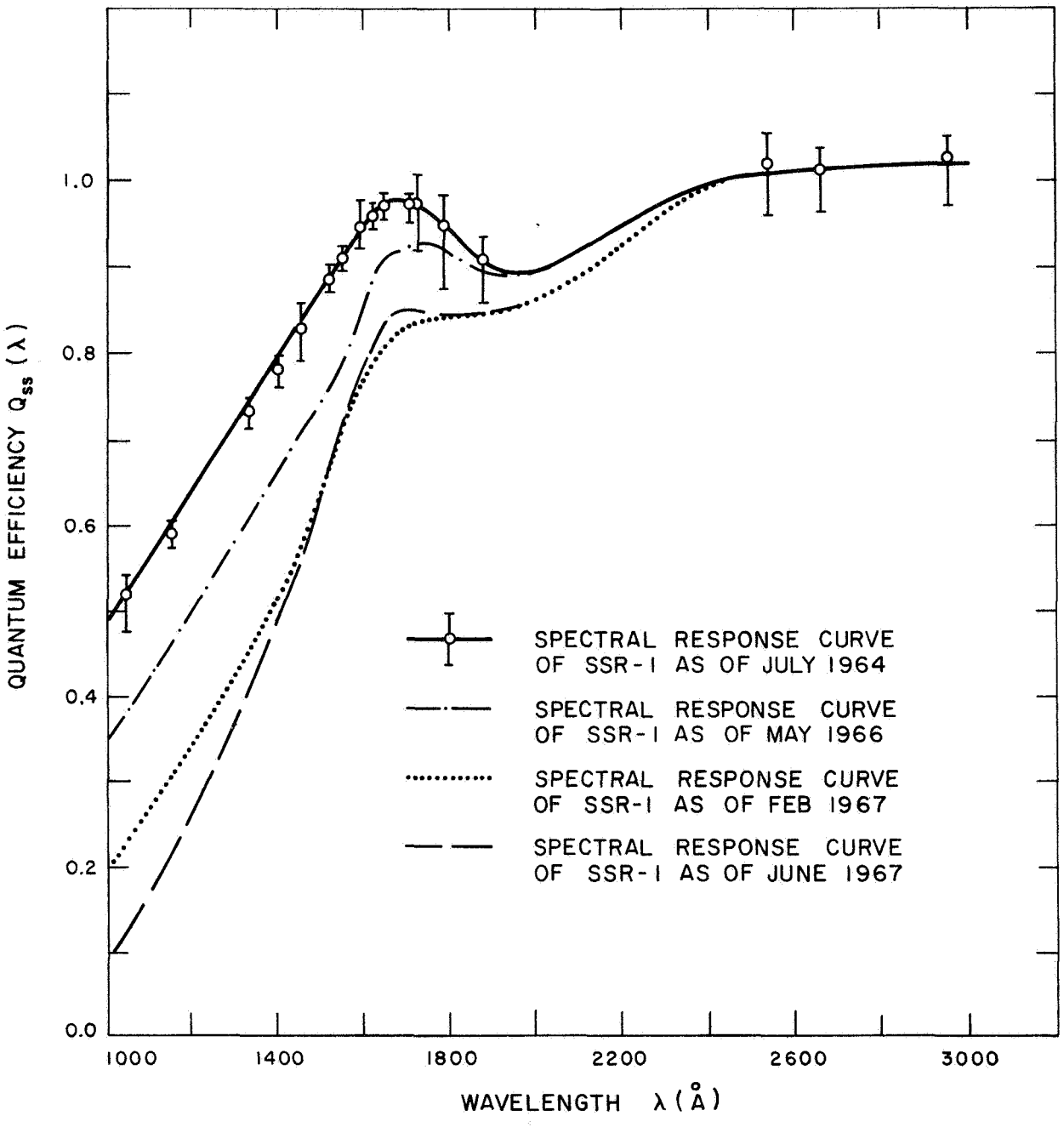

Figure 56. Spectral response of sodium salicylate laboratory standard detector as a function of time.

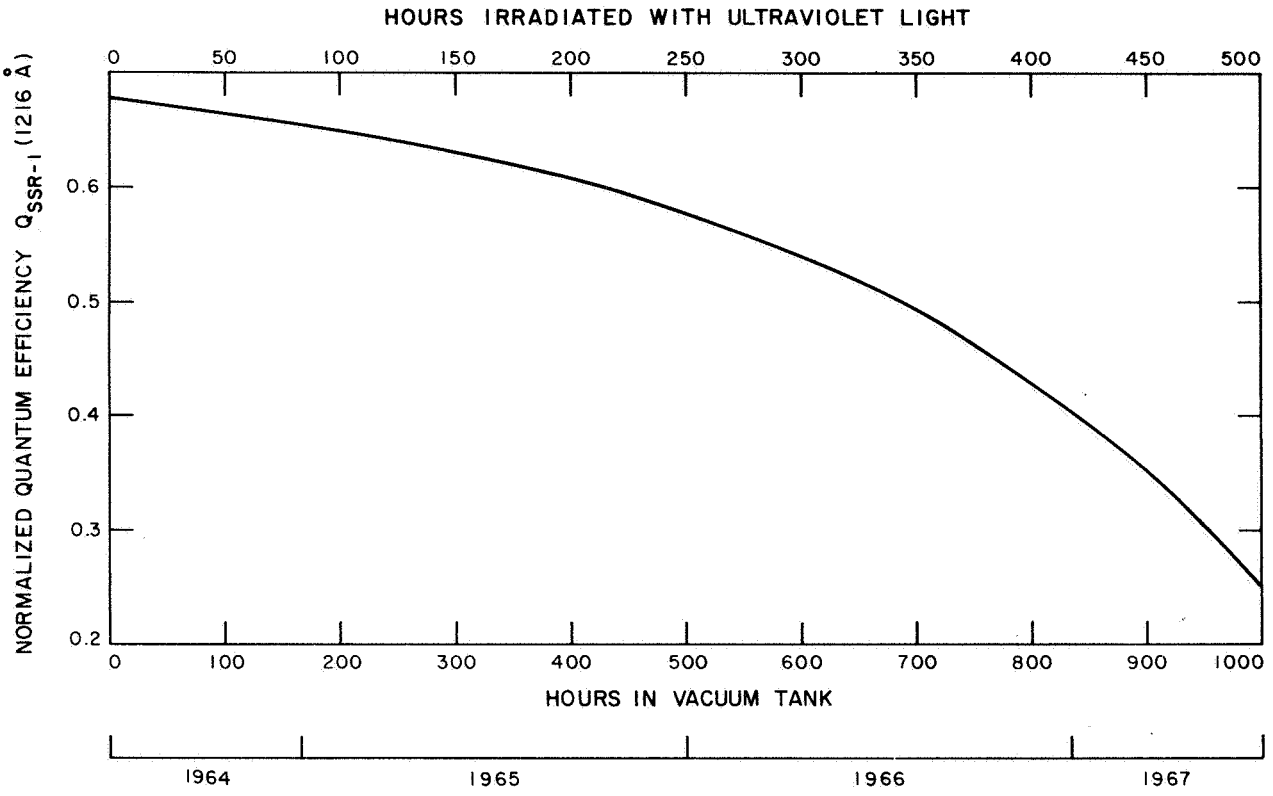

Figure 57. Deterioration of fluorescent detector SSR-1 at 1216 Å as a function of environmental exposure.

Choice of sodium salicylate as our fluorescent agent was based on the hope that we could determine its spectral-response characteristics either by reference to the considerable scientific literature on that subject or by calibration against a better standard in some other laboratory. The results of our literature search are summarized by the statement that the only assurance a worker in this field has that he has reproduced the results described in the literature is to calibrate his fluorescent screens against a better standard. In 1965, after preliminary calibrations of our working standard against nitric oxide ionization chambers in our own laboratory and elsewhere led us to believe our sodium salicylate did not behave as we had expected it to, we decided to study the usefulness of thermocouples as our most basic standard of spectral sensitivity at wavelengths other than 2537 Å. The problems of using thermocouples in this application are discussed by Canfield,

Johnson, Codling, and Madder (1967). Our study, conducted for us by the consulting firm of A. D. Little, Inc., is described in their final report to us (report ADL-66). Since, as shown above, we have in essence calibrated our laboratory standards at 2537 Å against a standard lamp at NBS, we can complete our calibration by comparing these standards against our thermocouple and establishing the spectral-response curve for the thermocouple. We considered the following departures of our thermocouple calibration techniques from the ideal case for which a uniformly sensitive, perfectly black thermocouple is compared against the unknown device in a constant beam of perfectly monochromatic light: (a) We assumed that the only nonthermal losses from the thermocouple were photoelectric emission, and that the photoelectric quantum efficiency was that found by Johnston and Madden (1965). This correction is less than 2% for even the shortest wavelengths we use. (b) We assumed that no correction is required for nonuniformities of illumination or thermocouple response. This assumption is now being tested in a manner similar to that used by Canfield et al. (1967). (c) We determined, by experiments with an infrared-transparent chopper of KRS-5 glass, that the infrared background signal was the expected signal arising from a difference in temperature between monochromator and calibration chambers amounting to less than 2°. This signal was more easily and accurately measured as a background level for monochromator wavelength settings known to produce no ultraviolet signal. (d) We found, as an unexpected source of departure from the ideal case, that significant thermal energy was carried through the monochromator by the flow of hydrogen gas from our windowless light source. This background and the infrared background were measured together, in the manner indicated above; the total background signal is about 10% of the ultraviolet signal at 1216 and 1608 Å, where the ultraviolet signal is most intense.

The absolute sensitivity of the thermocouple to radiant energy was determined both by calibration against our mercury-lamp 2537 Å irradiance standard and by calibration against a carbon-filament total-irradiance standard sold and calibrated by the NBS. These two calibrations agreed to better than 1%.

Our calibration techniques, described above, can thus be summarized by the following equations:

1. Calibration of SAO mercury lamp against NBS mercury lamp at 2537 Å:

$$F_S(D) = F_N(1\ m) \quad ,$$

where F_S is the 2537 Å irradiance of the SAO lamp at distance D, and F_N is the 2537 Å irradiance of the NBS lamp at 1 m.

2. Calibration of SAO thermocouple against SAO mercury lamp at 2537 Å:

$$P = \frac{V_T}{F_S T_C a_C} \quad ,$$

where P is the sensitivity of the thermocouple, V_T is the signal voltage from the thermocouple, T_C is the combined transmittance of the filters used between the lamp and the thermocouple, and a_C is the area of the aperture stop used.

3. Calibration of SAO thermocouple against NBS carbon-filament total-irradiance standard at SAO:

$$P = \frac{V_T}{F_C T_W a_C} \quad ,$$

where F_C is the total irradiance of the carbon-filament lamp, and T_W is the effective transmittance of the quartz window of the vacuum chamber.

4. Calibration of ASCOP photodiode against SAO mercury lamp at 2537 Å:

$$Q_S(2537) = \frac{i_S}{F_S T_C a_C} \frac{hc}{e\lambda} \quad ,$$

where Q_S is the quantum efficiency of the ASCOP photodiode, i_S is the signal current, e is the charge on the electron, λ is the wavelength (2537 Å), h is Planck's constant, and c is the velocity of light.

5. Calibration of working standard against ASCOP photodiode at 2537 Å:

$$Q_{SSR}(2537) = Q_S(2537) \frac{i_{SSR}}{i_S} \quad ,$$

where $Q_{SSR}(2537)$ is the quantum efficiency of the working standard at 2537 Å, and i_{SSR}/i_S is the ratio of photocurrents between the working standard and the ASCOP photodiode at 2537 Å.

6. Calibration of working standard against thermocouple:

$$Q_{SSR}(\lambda) = P \frac{i_{SSR}}{V_T} \frac{hc}{e\lambda} \quad ,$$

where i_{SSR}/V_T is the ratio of the photocurrent from the working standard to thermoelectric voltage from the thermocouple as a function of wavelength.

6.3 Data Reduction

The input information supplied to the experimenter consists of two parts: the video signal and the telemetry record. The first step in data reduction is conversion of the video-signal tape into a standard format. For the PCM mode of operation, this conversion is a trivial format conversion, the basic form of the data being preserved. For the store mode of operation, this conversion is accomplished by adding zeroes in the locations that were suppressed by the thresholding function. For the analog mode of operation, this conversion is accomplished by analog-to-digital conversion on the Celescope data-handling equipment at the rate of one sample every 2 μsec; the resulting matrix of approximately 300 × 800 element is converted to the necessary 256 × 251 element matrix by interpolation.

Figures 58 and 59 show two portions of the video-signal matrix from a 5-sec exposure taken during testing of the F-1 telescope, using the digital test set to perform the functions of the Bay E-4 equipment. The telemetry record for this exposure gives N = 1, M = PCM (Digital Test Set), T_U = +25° C, T_4 = +25° C, T_1 = +25° C, and t_{ex} = 5.0 sec.

k \ ℓ	115	116	117	118	119	120	121	122	123	124	125	126	127	128	129
133	10	9	10	12	11	11	9	11	11	9	14	12	11	12	10
134	13	9	12	8	11	9	9	11	10	9	12	8	12	14	10
135	9	9	7	7	9	11	8	8	9	13	12	9	7	8	12
136	9	12	11	11	12	11	9	9	15	10	7	8	7	10	8
137	13	10	9	9	12	12	8	8	10	11	10	10	9	8	10
138	8	13	13	13	9	9	11	12	8	10	10	10	12	11	13
139	16	11	10	17	10	12	25	48	32	15	14	11	9	8	9
140	9	9	11	8	13	17	48	102*	76	9	7	8	9	13	13
141	8	10	8	9	9	10	43	60	30	7	10	11	7	10	8
142	8	12	11	12	9	9	12	16	13	12	11	10	12	10	11
143	13	13	8	7	9	8	8	12	10	10	14	12	13	10	11
144	10	11	10	12	14	12	13	12	11	10	8	12	13	10	10
145	11	7	12	11	14	9	7	12	9	7	8	13	10	11	12
146	12	12	13	9	8	12	12	12	10	11	11	10	12	13	8
147	9	11	10	8	9	12	10	7	10	10	14	11	6	9	11

Figure 58. Values of $a_{k,\ell}$ in vicinity of collimated beam image during tests of F-1 telescope.

X = 129 Y = 161

k \ ℓ	122	123	124	125	126	127	128	129	130	131	132	133	134	135	136
154	12	11	13	9	9	10	7	9	12	12	10	12	10	11	6
155	7	12	10	10	11	13	10	9	8	8	12	9	9	10	10
156	9	7	12	11	11	7	7	7	12	10	9	8	9	8	8
157	7	9	9	12	11	13	10	12	10	11	9	13	11	10	15
158	12	9	11	12	11	12	14	13	14	12	13	8	11	12	9
159	11	12	9	9	12	8	12	28	22	11	12	13	9	12	11
160	11	8	10	8	8	11	36	108	95	47	10	10	7	10	7
161	13	10	8	9	9	19	61	114*	108	36	11	10	11	10	9
162	9	10	11	12	10	12	34	84	62	14	11	10	8	12	13
163	9	6	7	8	6	12	7	8	10	8	9	5	6	6	10
164	11	7	13	11	12	9	12	14	13	12	9	12	14	10	12
165	9	12	11	9	11	10	13	12	9	6	10	9	8	10	7
166	10	12	13	11	6	11	9	12	10	9	9	9	9	6	10
167	12	12	13	10	9	13	11	10	11	10	11	9	12	11	11
168	10	10	11	12	12	12	13	12	10	12	8	9	8	11	7

Figure 59. Values of $a_{k,\ell}$ in vicinity of calibration-lamp image during tests of F-1 telescope.

The second step in data reduction is to locate the stars in the output matrix and determine the raster position (k_0, ℓ_0) and integrated amplitude (Σ) for each star in accordance with the algorithms described briefly in Section 6.2.6. Applying these algorithms to Figures 58 and 59, we obtain $\ell_0 = 122$, $k_0 = 140$, $\Sigma = 381$, $\ell_{CAL} = 129$, $k_{CAL} = 161$, $\Sigma_{CAL} = 714$.

The third step in data reduction extracts the following information from the telemetry record: operating mode (M), camera number (N), exposure time (t_{ex}), subsystem selection (B), relevant temperatures (T_U, T_1, T_4), and spacecraft orientation $(\alpha_0, \delta_0, \rho)$. These telemetry data, insofar as they apply to this particular test, are listed above. For operation with the digital test set, there is no subsystem selection nor spacecraft orientation.

Data reduction then proceeds in accordance with the following equations, which essentially represent a reversal of the calibration process. The calibration data required for this analysis are available in CCR-182 in tabular, graphical, and punched-card formats.

A. To find the position of the raster relative to the optic axis:

1. The quantities θ_0, $V_{HC} - V_{HCAL}$, $V_{VC} - V_{VCAL}$, and Γ_4 depend only on N and can be determined directly from the calibration tables listing those quantities as functions of N. For the F-1 telescope, $\theta_0 = 16.^\circ 8$, $V_{HC} - V_{HCAL} = -0.02$ volt, $V_{VC} - V_{CAL} = -0.71$ volt, and $\Gamma_4 = 0.^\circ 0$.

2. The high- and low-deflection voltages, H_H, H_V, L_H, and L_V depend only on M, N, and T_4; they can be determined by interpolation in the corresponding calibration tables. For the digital test set, $H_H = +3.05$ volts, $H_V = +3.09$ volts, $L_H = -2.83$ volts, and $L_V = -2.91$ volts.

3. The deflection voltages corresponding to the raster position of each star are determined from the equations

$$V_H = L_H + \frac{\ell_0}{256}(H_H - L_H) \quad ;$$

$$V_V = L_V + \frac{k_0}{256}(H_V - L_V) \quad .$$

For the calibration-lamp image, these equations give the deflection voltages for the calibration position (V_{HCAL}, V_{VCAL}). From these equations we find, for our F-1 test example, $V_H = -0.03$ volt, $V_V = +0.37$ volt, $V_{HCAL} = +0.13$ volt, and $V_{VCAL} = +0.86$ volt.

4. The position of the optic axis (V_{HC}, V_{VC}) and the rotation of the vertical reference direction relative to the $+Y_c$ direction, $(\theta_0 + \Gamma_4)$ can then be determined from the above information: $V_{HC} = +0.11$ volt, $V_{VC} = +0.15$ volt, $\theta_0 + \Gamma_4 = 16.^\circ 8$.

B. To find the position of each star:

1. The position transfer functions, f_Y and f_Z, depend upon V_H, V_V, M, and N. They can be determined by interpolation in the corresponding calibration tables. For our example, $f_Y = 0.532$ degree volt^{-1}, $f_Z = 0.501$ degree volt^{-1}, $f_{YCAL} = 0.530$ degree volt^{-1}, and $f_{ZCAL} = 0.498$ degree volt^{-1}.

2. The position of each star on the celestial sphere, relative to the OAO coordinate system, is then determined from the equations

$$\zeta = f_Z[(V_H - V_{HC}) \cos(\theta_0 + \Gamma_4) + (V_V - V_{VC}) \sin(\theta_0 + \Gamma_4)] \quad ,$$

$$\eta = f_Y[(V_H - V_{HC}) \sin(\theta_0 + \Gamma_4) + (V_V - V_{VC}) \cos(\theta_0 + \Gamma_4)] \quad .$$

For our example, $\zeta = -0.^\circ 04$, $\eta = 0.^\circ 09$, $\zeta_{CAL} = 0.^\circ 11$, and $\eta_{CAL} = 0.^\circ 36$.

3. Conversion from spacecraft coordinates to equatorial coordinates for epoch 1950.0 is effected through the following equations:

$$\phi'' = \sqrt{\eta^2 + \zeta^2} \quad ;$$

$$\theta'' = \tan^{-1}\left(\frac{\zeta}{\eta}\right) \quad .$$

If ζ is positive, θ'' is in the first or second quadrant; if ζ is negative, θ'' is in the third or fourth quadrant.

The declination δ of the star is found from the law of cosines for spherical triangles:

$$\sin \delta = \sin \delta_0 \cos \phi'' + \cos \delta_0 \sin \phi'' \cos (\theta'' - \rho) \quad .$$

By definition, δ lies between $+90°$ and $-90°$.

The right ascension α of the star is found from the law of sines for spherical triangles:

$$\sin (\alpha - \alpha_0) = \frac{\sin (\theta'' - \rho) \sin \phi''}{\cos \delta} \quad .$$

Unless δ_0 is within $1.^{\circ}5$ of the pole, $\alpha - \alpha_0$ will lie in the first or fourth quadrant. If it is necessary to ascertain the quadrant of $(\alpha - \alpha_0)$, we compute

$$\cos (\alpha - \alpha_0) = \frac{\cos \phi'' - \sin \delta \sin \delta_0}{\cos \delta \cos \delta_0} \quad .$$

Finally,

$$\alpha = \alpha_0 + (\alpha - \alpha_0) \quad .$$

For our example, taken in the test chamber this computation is not performed.

C. To find the brightness for each star:

1. The gain of the video amplifier G_1 depends only upon N and T_1 and can be obtained by interpolation in the calibration tables.

2. The gain of the Bay E-4 electronics G_4 depends upon M, N, B, and T_4, and can be obtained by interpolation in the calibration tables. For the digital test set, $G_1 G_4 = 2 \times 10^4$ volt^{-1}.

3. The Uvicon camera output summation V_Σ is obtained from the equation

$$V_\Sigma = \frac{\Sigma}{G_1 G_4} \quad .$$

For our example, $V_\Sigma = 1.90 \times 10^{-2}$ volt and $V_{\Sigma CAL} = 3.57 \times 10^{-2}$ volt.

4. The integrated optical sensitivity U as defined in Section 6.1, depends upon N, ζ, and η, and can be found by interpolation in the calibration tables. The calibration tables for U have been assembled for each telescope from the calibration data for mirror reflectances, filter transmittances, and Uvicon quantum efficiencies, and are listed separately for each position where Uvicon quantum-efficiency calibration was performed. For our example, $U = 5.82 \times 10^{-12}$ m^3 amp sec joule^{-1} and $U_{CAL} = 4.55 \times 10^{-12}$ m^3 amp sec joule^{-1}.

5. The camera gain G_c depends upon N, M, T_U, V_H, V_V, and V_Σ. It can be determined by interpolation in the G_c calibration tables. For our example, $G_c = 1.73 \times 10^{12}$ volt amp^{-1} sec^{-1} and $G_c(CAL) = 1.00 \times 10^{12}$ volt amp^{-1} sec^{-1}.

6. The brightness of each star $I(\Lambda)$ is then determined from the equation

$$I(\Lambda) = \frac{V_\Sigma}{UG_c t_{ex}} \quad ,$$

where the effective wavelength Λ is known to lie within the passband of the color system defined by the camera number N and the position of the star relative to the filter split line. This equation, as explained above, is based on the mean-value theorem, and is valid only for a continuous spectrum. If we apply this equation to our example, we obtain $I(\Lambda) = 8.19 \times 10^{-4}$ watt m^{-3} $= 8.19 \times 10^{-11}$ erg cm^{-2} sec^{-1} Å^{-1}, $I_{CAL}(\Lambda_{CAL}) = 1.54 \times 10^{-3}$ watt m^{-3} $= 1.54 \times 10^{-10}$ erg cm^{-2} sec^{-1} Å^{-1}, with Λ lying between 1550 and 3200 Å, and Λ_{CAL} lying between 2100 and 3200 Å. Since, however, we know that one of the images was formed from collimated monochromatic light of 2537 Å wavelength, and the other by means of the calibration-lamp and calibrator optics system, it is more appropriate to determine the quantities

$$F^*(\lambda) = \frac{V_\Sigma W}{UG_c t_{ex}} = I(\Lambda)W(\lambda) \quad ,$$

where $\lambda = 2.537 \times 10^{-7}$ m is the known wavelength for the collimated beam and $W(\lambda) = S(\lambda)/U$, with $S(\lambda)$ being the sensitivity of the optical system for conversion of collimated monochromatic light to photoelectric current, and

$$\Phi^*_{CAL} = \frac{V_\Sigma \, CW_{CAL}}{UG_c t_{ex}} = I_{CAL}(\Lambda_{CAL}) CW_{CAL} \quad ,$$

where C is the optical collection efficiency of the telescope and $W_{CAL} = S_{CAL}/U_{CAL}$, with S_{CAL} being the sensitivity of the optical system for for photoelectric conversion at the position of the calibration image. For our example, $W(\lambda) = 1.07 \times 10^{-7}$ m, $C = 0.0448$ m^2, and $W_{CAL} = 1.07 \times 10^{-7}$ m, giving $F^*(\lambda) = 8.75 \times 10^{-12}$ watt m^{-2} and $\Phi^*_{CAL} = 7.40 \times 10^{-12}$ watt.

D. The calibration image is observed once per orbit, and we will attempt to repeatedly observe a number of objects. We will use these recalibration data to keep our calibration tables up to date as the instrumentation ages during orbital operations.

E. At this point, the information can be sorted for output as a partial catalog containing calculated position and brightness for each star observed. These partial catalogs can then be merged with each other and with the identification catalog in whatever manner is most appropriate for final astrophysical analysis. For the basic Celescope catalog, we plan to publish our ultraviolet observations merged with entries from the identification catalog, by right ascension in 1° declination zones. For guest investigators, we can furnish the data in whatever form is agreed upon as most appropriate.

REFERENCES

BEYER, R. R. and GOETZE, G. W.

1966. An optically scanned SEC camera tube. Adv. Electron. Electron Phys., vol. 22, pp. 241-250.

BEYER, R. R., GREEN, M. and GOETZE, G. W.

1966. Point-source imaging with the SEC target. Adv. Electron. Electron Phys., vol. 22, pp. 251-260.

BLESS, R. C., CODE, A. D. and HOUCK, T. E.

1968. Astronomical radiation measurements. III. An analysis of far ultraviolet filter observations of stars. Astrophys. Journ., in press.

BOERIO, A. H., BEYER, R. R. and GOETZE, G. W.

1966. The SEC target. Adv. Electron. Electron Phys., vol. 22, pp. 229-239.

BOGGESS, A., III and BORGMAN, J.

1964. Interstellar extinction in the middle ultraviolet. Astrophys. Journ., vol. 140, pp. 1636-1639.

BYRAM, E. T., CHUBB, T. A. and FRIEDMAN, H.

1961. Ultraviolet light from celestial sources. Mem. Soc. Roy. Soc. Liège, Ser. 5, vol. 4, pp. 469-475.

BYRAM, E. T., CHUBB, T. A. and WERNER, M. W.

1965. 1115 Å far ultraviolet stellar photometry. Ann. d'Astrophys., vol. 28, pp. 594-597.

CANAVAGGIA, R. and PECKER, J.-C.

1953. Les géantes jaunes. II. Spectres continus. Ann. d'Astrophys., vol. 16, pp. 47-59.

CANFIELD, L. R., JOHNSON, R. G., CODLING, K. and MADDEN, R. P.

1967. Comparison of an ionization chamber and a thermopile as absolute detectors in the extreme ultraviolet. Appl. Opt., vol. 6, pp. 1886-1888.

CHUBB, T. A. and BYRAM, E. T.

1963. Stellar brightness measurements at 1314 and 1427 Å. Observation of O I twilight glow. Astrophys. Journ., vol. 138, pp. 617-630.

DAVIS, R. J.

1966a. The use of the Uvicon-Celescope television system for ultraviolet astronomical photometry. Adv. Electron. Electron Phys., vol. 22, pp. 875-884.

1966b. Factors affecting the transmittance of lithium fluoride and barium fluoride in the vacuum ultraviolet. Journ. Opt. Soc. Amer. vol. 56, pp. 837-839.

DOUGHTY, D. D.

1966. Ultra-violet sensitive camera tubes incorporating the SEC principle. Adv. Electron. Electron Phys., vol. 22, pp. 261-271.

GOETZE, G. W.

1966. Secondary electron conduction (SEC) and its application to photo-electronic image devices. Adv. Electron. Electron Phys., vol. 22, pp. 219-227.

GRIGGS, M.

1966. Atmospheric Ozone. In The Middle Ultraviolet — its Science and Technology, ed. by A. E. S. Green, John Wiley & Sons, Inc., pp. 83-117.

HEATH, D. F. and SACHER, P. A.

1966. Effects of a simulated high-energy space environment on the ultraviolet transmittance of optical materials between 1050 Å and 3000 Å. Appl. Opt., vol. 5, pp. 937-944.

HEDDLE, D. W. O.

1964. Southern hemisphere observations of ultra-violet radiation from celestial objects. III. Stellar photon fluxes at wavelengths near 2000 Å. Proc. Roy. Soc., A, vol. 279, pp. 533-543.

HENIZE, K. G. and WACKERLING, L. R.

1966. Stellar ultraviolet spectra from Gemini 10. Sky and Telescope, vol. 32, pp. 204-205.

HENIZE, K. G., WACKERLING, L. R., and O'CALLAGHAN, F. G.

1967. Ultraviolet stellar spectroscopy on Gemini 11. Science, vol. 155, pp. 1407-1408.

HUNGER, K.

1955. Die atmosphäre des A0-sternes Alpha Lyrae. Zeitschr. f. Astrophys., vol. 36, pp. 42-97.

JOHNSTON, R. G. and MADDEN, R. P.

1965. On the use of thermopiles for absolute radiometry in the far ultraviolet. Appl. Opt., vol. 4, pp. 1574-1580.

KAMIYAMA, H.

1959. Vertical distribution of molecular oxygen. Sci. Rep. Tohoku Univ., ser. 5, vol. 11, pp. 84-97.

KRISHNA SWAMY, K. S. and O'DELL, C. R.

1967. Distinction between models of interstellar grains. Astrophys. Journ., vol. 147, pp. 937-942.

MARSHALL, F. B. and ROANE, G. D.

1966. Performance comparison of the SEC camera tube and the image orthicon. Adv. Electron. Electron Phys., vol. 22, pp. 291-304.

MIHALAS, D.

1965. Model atmospheres and line profiles for early-type stars. Astrophys. Journ. Suppl., vol. 9, pp. 321-438.

MORTON, D. C.

1965. Theoretical line profiles in the ultraviolet spectra of early-type stars. Astrophys. Journ., vol. 141, pp. 73-82.

1967. The far-ultraviolet spectra of six stars in Orion. Astrophys. Journ., vol. 147, pp. 1017-1024.

MORTON, D. C. and SPITZER, L., Jr.

1966. Line spectra of Delta and Pi Scorpii in the far-ultraviolet. Astrophys. Journ., vol. 144, pp. 1-12.

NOZAWA, Y.

1966. A digital television system for satellite-borne ultra-violet photometer. Adv. Electron. Electron Phys., vol. 22, pp. 865-874.

PATTERSON, D. A. and VAUGHAN, W. H.

1963. Influence of crystal surface on the optical transmission of lithium fluoride in the vacuum-ultraviolet spectrum. Journ. Opt. Soc. Amer., vol. 53, pp. 851-855.

ROGERSON, J. B., Jr.

1963. The orbiting astronomical observatories. Space Sci. Rev., vol. 2, pp. 621-652.

SMITH, A. M.

1967. Stellar photometry from a satellite vehicle. Astrophys. Journ., vol. 147, pp. 158-171.

STECHER, T. P.

1965. Interstellar extinction in the ultraviolet. Astrophys. Journ., vol. 142, pp. 1683-1684.

1967. Stellar spectrophotometry from a pointed rocket. Astron. Journ., vol. 72, p. 831.

STECHER, T. P. and MILLIGAN, J. E.

1962. Stellar spectrophotometry from above the atmosphere. Astrophys. Journ., vol. 136, pp. 1-13.

TOUSEY, R.

1961. Ultraviolet spectroscopy of the Sun. In Space Astrophysics, ed. by W. Liller, McGraw-Hill Book Co., New York, pp. 1-16.

TRAVING, G.

1955. Die atmosphäre des B0-sternes τ Scorpii. Zeitschr. f. Astrophys., vol. 36, pp. 1-41.

UNDERHILL, A. B.

1951. A model atmosphere for an early O-type star. Publ. Dominion Astrophys. Obs. Victoria, vol. 8, pp. 357-384.

VAN DE HULST, H. C.

1949. The solid particles in interstellar space. Rech. Obs. Astron. Utrecht, vol. 11, part 2, pp. 1-50.

VITENSE, E.

1951. Der aufbau der sternatmospharen. IV. Kontinuierliche absorption und streuung als funktion von Druck und temperatur. Zeitschr. f. Astrophys., vol. 28, pp. 81-112.

WHITEOAK, J. B.

1966. The wavelength dependence of interstellar extinction. Astrophys. Journ., vol. 144, pp. 305-317.

ZIEMER, R. R.

1961. Orbiting astronomical observatories. Astronautics, vol. 6, no. 5, pp. 36-37 and 58-62.

APPENDIX A

SUPPORTING DOCUMENTS

In this Special Report, we have referred to a number of the supporting documents listed in this Appendix. These documents contain detailed information concerning the Celescope experiment. Copies can be obtained upon request to Project Celescope, Smithsonian Astrophysical Observatory, 60 Garden Street, Cambridge, Massachusetts 02138.

1. ADL Reports (final reports by A. D. Little, Inc., on the techniques developed for SAO for spectrophotometric calibration):

ADL-65: "Final Report on Calibration of Celescope Components," describing the techniques for calibration of mirror reflectance, filter transmittance, and Uvicon quantum efficiency.

ADL-66: "A Thermocouple System as a Standard of Intensity in the Vacuum Ultraviolet," describing the techniques and results for calibration of laboratory standards against a thermocouple and for calibration of the thermocouple against standard lamps.

2. CCR (Celescope Calibration Reports) (SAO reports giving detailed results of spectrophotometric calibrations of individual components). Celescope Technical Bulletin CTB-15 lists the CCR's that present calibration results for individual flight components. In addition, the following CCR's describe more general results that are relevant to the calibration of the Celescope experiment:

CCR-111: "Spectral Sensitivity of Sodium Salicylate Fluorescent Detectors."

CCR-112: "Calibration of Photodiode Sensitivity of ASCOP Photomultiplier, Type 541F, Serial No. 3030."

CCR-113: "Calibration of Monochromatic Irradiance from SAO Standard Mercury-Lamp Assemblies at 2537 Å."

CCR-136: "Reflectance of Mirror Samples 6FP-4-OCL-2 (High Reflectance Standard), 2DP2F2 (Low Reflectance Standard) and X-110-GSFC (GSFC Comparison Mirror)."

CCR-137: "Effect of Temperature on the Transmittance of Celescope Filters."

CCR-148: "Calibration of Uvicon S31A."

CCR-177: "Comparison of Spectrophotometric Response Calibrations Performed by SAO's Spectrophotometric Standards Laboratory with Those Performed by Westinghouse Research Laboratory and by Westinghouse Tube Division."

CCR-179: "Thermal effects on the Quantum Efficiencies of Uvicons."

CCR-182: "Celescope System Calibration."

3. CER (Celescope Engineering Reports) (EMR reports giving detailed results of engineering tests, analyses, and calibrations performed by EMR). Celescope Technical Bulletin CTB-15 lists the CER's that present calibration results for individual flight components. In addition, the following CER describes more general results that are relevant to the calibration of the Celescope experiment:

CER-126: "Uvicon Parametric Response Study."

4. COM (Celescope Operations Manual) (EMR document listing the command and telemetry functions of the Celescope experiment, standard command sequences, and operating rules and limitations).

5. CTB (Celescope Technical Bulletins) (SAO reports giving detailed information concerning special studies). The following CTB's give information relevant to the performance of the Celescope experiment:

CTB-14: "The Radiation Environment for the Orbit of the OAO A-2 Satellite, and its Effects on the Celescope Optical System."

CTB-15: "Status Report on Celescope Calibration."

6. CTI (Celescope Test Instruction) (SAO test instructions giving detailed procedures for calibrations performed in SAO's Spectrophotometric Standards Laboratory). Those CTI's relevant to the calibration of the Celescope experiment are listed in CTB-15.

7. CTP (Celescope Test Plan) (EMR test instructions giving detailed procedures for calibrations, acceptance tests, qualification tests, etc., performed on Celescope instrumentation). Those CTP's relevant to the calibration of the Celescope experiment are listed in CTB-15.

8. CTR (Celescope Test Report) (EMR test report giving detailed results of tests performed on Celescope instrumentation). Those CTR's relevant to the calibration of the Celescope experiment are listed in CTB-15.

9. LR (Laboratory Reports) (SAO reports giving detailed results of individual calibration tests performed in the Spectrophotometric Standards Laboratory).

10. Technical Manuals (EMR manuals giving detailed descriptions of the design and operation of the Celescope experiment and associated ground-support equipment).

APPENDIX B

SYMBOLS AND ABBREVIATIONS USED IN THIS SPECIAL REPORT

A: (1) Indicates operation in analog mode.
(2) May also be used as symbolic representation of system output matrix.

A_c: Output matrix during calibration with digital test set.

a: (1) This symbol, without subscript, should be reserved for short-wavelength cutoff.
(2) This symbol, with one subscript, should be reserved for area.
(3) With two subscripts, this symbol should be reserved for system matrix element.

a_C: Area of SAO calibration reticle hole (m^2).

a_E: Effective area of telescope (m^2).

a_T: Area of SAO thermocouple aperture stop (m^2).

a_n: Area of nth hole in EMR calibration reticle (m^2).

ASCOP: A division of Electromechanical Research, Inc., Princeton, N. J.

B: E-4 subsystem selection.

BTL: Bit time line.

b: (1) This symbol, without subscript, should be reserved for long-wavelength cutoff.
(2) This symbol, with two subscripts, should be reserved for Uvicon module matrix element.

C: Collecting power of telescope (m^2) at calibration wavelength; $C = a_E R_1(\lambda_{CAL}) R_2(\lambda_{CAL})$.

COP: Celescope Optical Package.

c: (1) Velocity of light in vacuum (2.997925×10^{8} m sec^{-1}).
(2) With the subscripts, this symbol should be reserved for element of matrix A_c.

CAL: Subscript referring to calibration.

D: (1) Operation in digital mode.
(2) Distance between mirror vertices (m).

d: With no subscript, this letter should be used solely as a symbol for differentiation.

E: Photoelectron input (amp sec).

e: Charge on the electron (1.60210×10^{-19} amp sec).

EMR: Electromechanical Research, Inc., Sarasota, Fla.

ETCU: Experiment Test Checkout Unit.

F: Monochromatic irradiance (joule m^{-2} sec^{-1}).

F_L: Monochromatic irradiance of SAO standard mercury lamp (joule m^{-2} sec^{-1}).

f_H: Horizontal-position transfer function (degrees $volt^{-1}$).

f_V: Vertical-position transfer function (degrees $volt^{-1}$).

f_Y: Position transfer function parallel to Y_c axis (degrees $volt^{-1}$).

f_Z: Position transfer function parallel to Z_c axis (degrees $volt^{-1}$).

FSTE: Fixed System Test Equipment.

f_p: Arbitrary transfer function.

f_D: Digital intensity transfer function (volt m^3 $joule^{-1}$).

f_A: Analog intensity transfer function (volt m^3 $joule^{-1}$).

f_M: Intensity transfer function in arbitrary mode (volt m^3 $joule^{-1}$).

f_{CALX}: Intensity transfer function as determined from calibration star (volt m^3 $joule^{-1}$).

G_1: Voltage gain of video amplifier.

G_A: Voltage gain of Bay E-4 analog chain.

G_D: Voltage gain of Bay E-4 digital chain ($volt^{-1}$).

G_4: Voltage gain of Bay E-4 analog or digital chain ($volt^{-1}$).

G_c: Camera-module transfer function ($volt\ amp^{-1}\ sec^{-1}$).

G_{PM}: Gain of photomultiplier.

G_{TS}: Gain of digital test set (volts).

G_X: Relative xenon calibrator-lamp flux normalized to unity at V_{XR}.

g_{PM}: Relative gain of photomultiplier.

GSE: Ground-Support Equipment.

GSFC: Goddard Space Flight Center, Greenbelt, Md.

H: Subscript referring to mercury calibrator lamp.

H_{AA}: Peak-to-peak amplitude of analog horizontal sweep (volt).

H_{AO}: Analog horizontal sweep, direct current offset (volt).

H_{DA}: Peak-to-peak amplitude of digital horizontal sweep (volt).

H_{DO}: Digital horizontal sweep, direct current offset (volt).

H_H: High horizontal voltage (volts).

H_V: High vertical voltage (volts).

h: Planck's constant (6.6256×10^{-34} joule sec).

I: Spectral irradiance ($joule\ m^{-3}\ sec^{-1}$).

i: Matrix row number.

i_U: Photoelectric current from Uvicon (amps).

i_s: Photoelectric current from SAO laboratory standard (amp).

i_{SS}: Photoelectric current from sodium salicylate detector (amp).

i_{SSR}: Photoelectric current from sodium salicylate reflector detector (amp).

i_W: Photoelectric current from tungsten (amp).

i_{NO}: Photoelectric current from nitric oxide (amp).

i_{PM}: Photomultiplier signal current (amp).

J: Deflection sensitivity of Celescope system (degrees $volt^{-1}$).

j: Matrix column number.

K: Analog Group II counts.

k: Raster line number.

k_{cal}: Centroid of calibration-image matrix in k.

k_0: Centroid of point-source matrix in k.

L: Distance from vertex of secondary mirror to Uvicon reference plane (m).

L_H: Low horizontal voltage (volts).

L_V: Low vertical voltage (volts).

ℓ: Raster element number.

ℓ_{cal}: Centroid of calibration-image matrix in ℓ.

ℓ_0: Centroid of image in l.

M: System operating mode.

MSCE: Mobile System Checkout Equipment.

m: Number of holes in calibration reticle.

N: Number of camera.

n: (1) Serial number of EMR calibration position.
(2) May also be used for index of refraction.

OAO: Orbiting Astronomical Observatory.

OCL: Operation Code Line.

P: Sensitivity of Thermocouple (joule $volt^{-1}$ sec^{-1}).

p: Any arbitrary parameter.

Q_U: Effective quantum efficiency of Uvicon (electrons photon^{-1}).

Q_{NO}: Quantum efficiency of nitric oxide (electrons photon^{-1}).

Q_s: Quantum efficiency of SAO laboratory standard (electrons photon^{-1}).

$\bar{Q}_{SS}$: Quantum efficiency of sodium salicylate detector normalized to unity at $\lambda = 2537$ Å.

Q_W Quantum efficiency of tungsten.

Q_{PM}: Quantum efficiency of photomultiplier.

q_U: Quantum efficiency of Uvicon relative to sodium salicylate detector.

q_{PM}: Quantum efficiency of photomultiplier relative to sodium salicylate detector.

q_{SS}: Quantum efficiency of sodium salicylate detector relative to standard detector.

R_1: Reflectivity of primary mirror.

R_2: Reflectivity of secondary mirror.

RMS: Root Mean Square.

S: Spectral sensitivity of photo-optical system (m^2 amp sec joule^{-1}).

s: Spectral sensitivity of photo-optical system (amp sec joule^{-1}).

SAO: Smithsonian Astrophysical Observatory, Cambridge, Mass.

T_C: Transmittance of SAO calibration filter.

T_U: Uvicon case temperature (°C).

T_1: Temperature of video amplifier (°C).

T_3: Transmittance of optical filter.

T_4: Temperature of Bay E-4 (° C).

TVOB: Thermal-vacuum optical bench.

t: Time.

t_{ex}: Exposure time (sec).

t_H: Time measured from start of horizontal sweep (sec).

t_V: Time measured from start of vertical sweep.

t_{AH}: Horizontal sweep time duration (sec).

t_{AV}: Vertical sweep time duration (sec).

U: Optical passband integrated sensitivity (m^3 amp sec $joule^{-1}$).

V_{AA}: Peak-to-peak amplitude of analog vertical sweep (volt).

V_{AO}: Analog vertical sweep, direct current offset (volt).

V_{CALA}: Amplitude of analog calibration pulse at output of analog chain in Bay E-4 (volt).

V^*_{CALA}: Amplitude of analog calibration pulse associated with video signal after leaving Bay E-4 (volt).

V_{DA}: Peak-to-peak amplitude of digital vertical sweep (volt).

V_{DO}: Digital vertical sweep, direct current offset (volt).

V_T: Signal voltage from thermocouple (volt).

V_{TT}: Uvicon target temperature probe voltage (volt).

V_X: Xenon lamp temperature probe voltage (volt).

V_{XR}: Probe voltage associated with calibrator calibration test (volt).

V_1: Probe voltage associated with video amplifier (volt).

V_4: Bay E-4 temperature probe voltage (volt).

v_H: Horizontal sweep voltage (volt).

V_{HC}: Horizontal sweep voltage for center of photocathode (volt).

v_V: Vertical sweep voltage (volt).

V_{VC}: Vertical sweep voltage for center of photocathode (volt).

V_Σ: Uvicon camera intensity output summation (volts).

VOB: Vacuum Optical Bench.

W: Effective spectral bandwidth (m).

X: Subscript referring to xenon calibrator lamp.

x, y, z: Distance (m) parallel to the (X'_c, Y'_c, Z'_c) axis. (Y'_c, Z'_c plane is defined by outer flat surface of Uvicon faceplate; X'_c axis is optical axis of telescope. $+Y'_c$ and $+Z'_c$ are in approximately the same direction as $+Y_c$ and $+Z_c$ spacecraft axes. The SAO reference mark (ϕ) defines the $+Y'_c$ axis. $+X'_c$ is in approximately the same direction a $-X_c$ spacecraft axis.)

Y1: Raster line number at which signal first appears.

Y2: Raster line number at which signal disappears.

X1: Raster element number at which signal first appears.

X2: Raster element number at which signal disappears.

α: Right ascension (1950.0 coordinates) (degrees) (see Figure B-1).

α_0: Right ascension (1950.0 coordinates) of spacecraft $-X_c$ axis (see Figure B-1).

Γ_3: Angle between spacecraft X_cZ_c plane and plane through optic axis and filter split line (degrees) (see Figure B-2).

Γ_4: Angle between spacecraft X_cY_c plane and telescope $X'_cY'_c$ plane (degrees) (see Figure B-2).

δ: Declination (1950.0 coordinates) (degrees) (see Figure B-1).

δ_0: Declination (1950.0 coordinates) of spacecraft $-X_c$ axis (degrees) (see Figure B-1).

Δ: An operator signifying differences.

ζ: Distance from projection of $X_c - Y_c$ plane on celestial sphere (degrees) (see Figures B-1 and B-2).

η: Distance from projection of $X_c - Z_c$ plane on celestial sphere (degrees) (see Figures B-1 and B-2).

Θ: Threshold setting.

θ: Azimuth in object space of telescope (degrees) (see Figure B-2).

θ_0: Rotation of raster relative to Uvicon reference mark (degrees) (see Figure B-2).

θ_3: Rotation of filter split line relative to Uvicon reference mark (degrees) (see Figure B-2).

θ'': Azimuth in object-space of spacecraft (degrees) (see Figures B-1 and B-2).

Λ: Effective wavelength (m).

λ: Wavelength (m).

λ_{CALX}: UV wavelength from xenon calibrator (m).

π: Ratio of circumference to diameter of the circle, 3.1415926536.

ρ: Roll angle of spacecraft, measured from Y_c axis to north direction (see Figure B-1).

ρ_c: Angle from $+Y_c$ axis of spacecraft to direction of telescope optic axis (degrees) (see Figure B-1).

Σ_A: System Analog intensity output summation (volt).

Σ_D: System Digital intensity output summation (dimensionless).

Φ_{CAL}: Calibrator flux (joule sec^{-1}).

ϕ: Polar angle (measured from optic axis) in object-space of telescope (degrees) (see Figure B-2).

ϕ_x: Angle between optic axis of telescope and $-X_c$ axis of spacecraft (degrees) (see Figure B-2).

ϕ'': Polar angle (measured from $-X_c$ axis) in object-space of spacecraft (degrees) (see Figures B-1 and B-2).

Ω: Store-mode transfer matrix.

ω_{ij}: Element of store-mode transfer matrix.

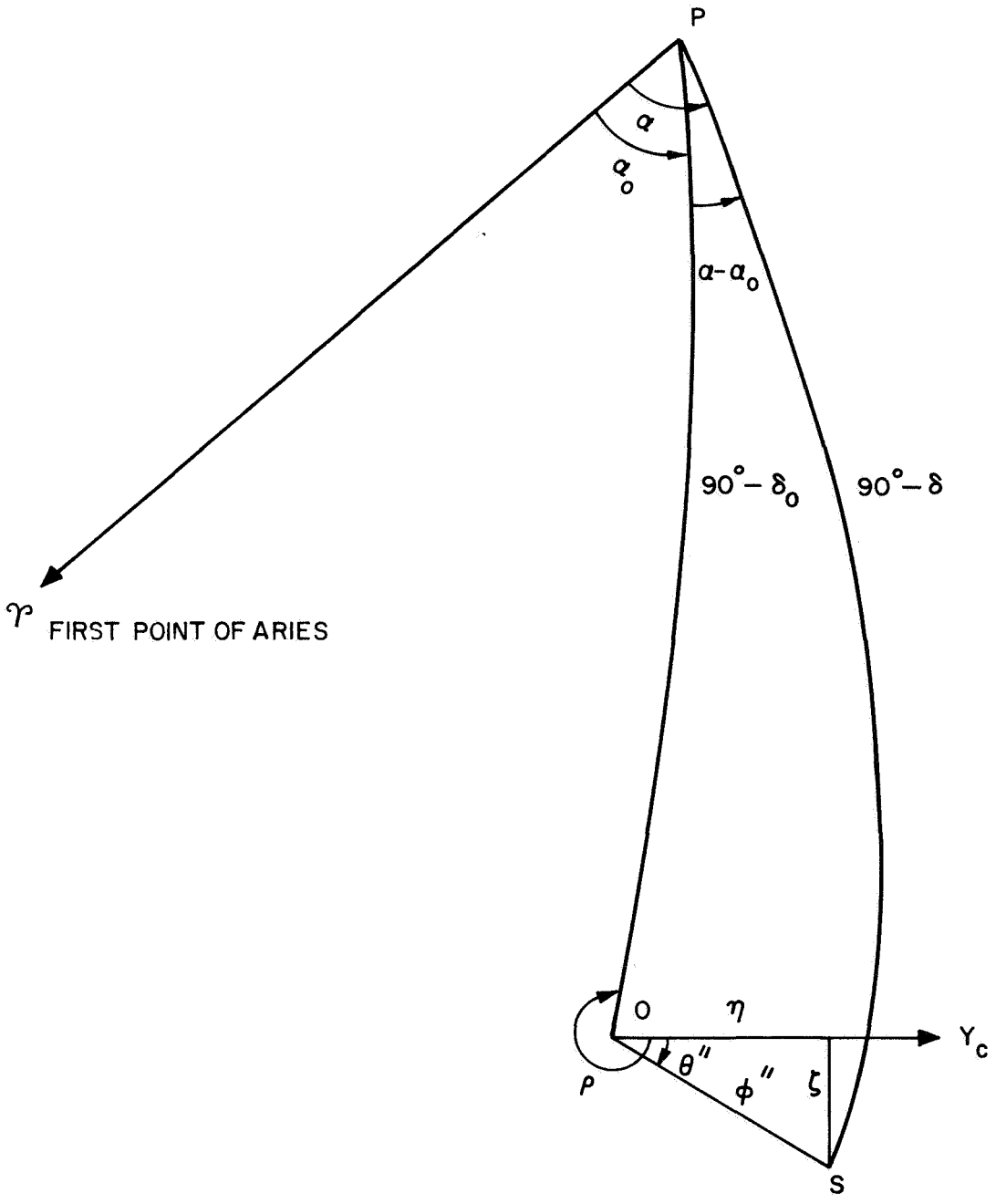

Figure B-1. Star position and OAO coordinate system as seen looking into the celestial sphere from outside.

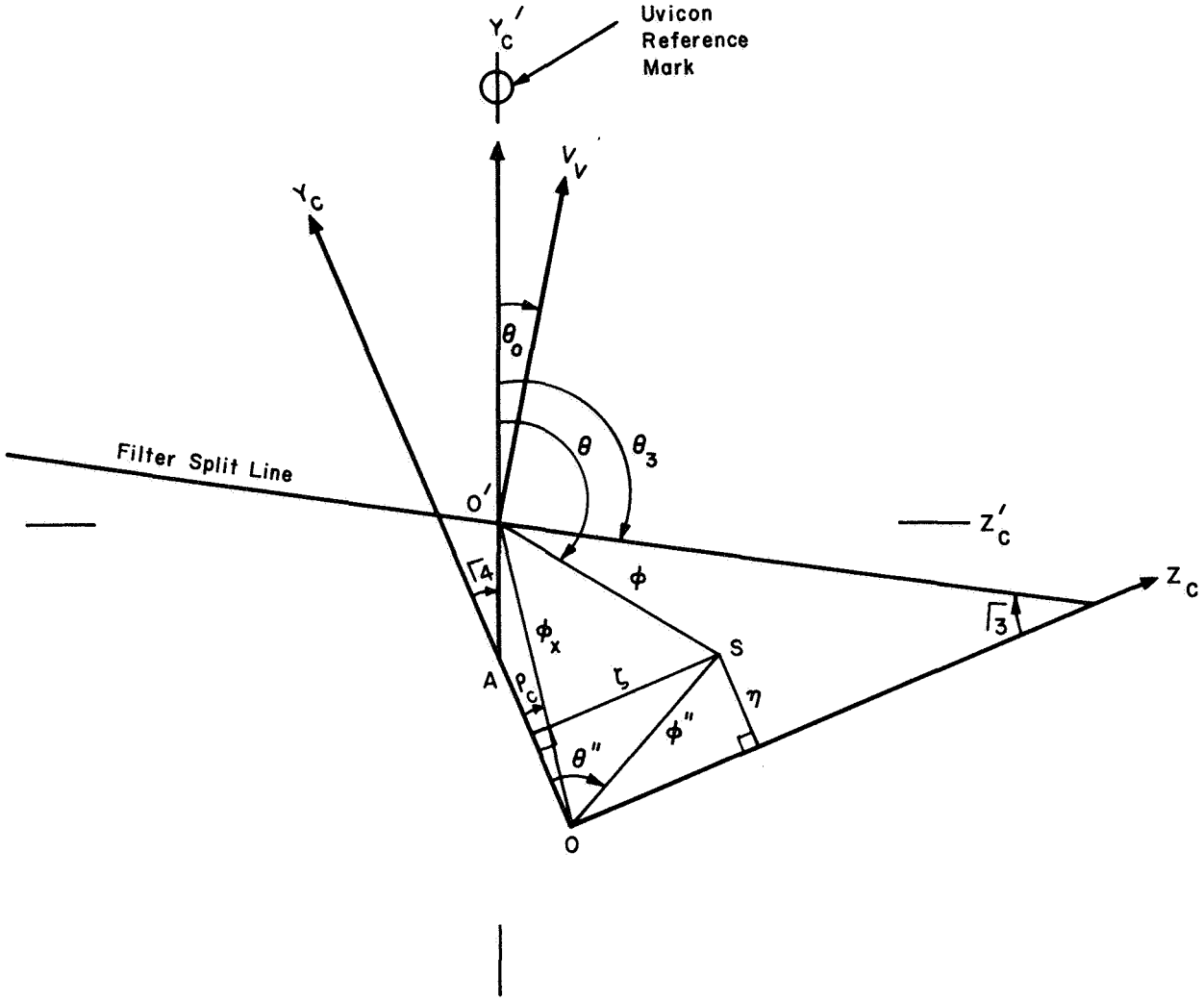

Figure B-2. Celescope and OAO coordinate systems as seen looking in toward the Uvicon faceplate.

BIOGRAPHICAL NOTE

ROBERT J. DAVIS received the A. B., A. M., and Ph. D. degrees in astronomy from Harvard University in 1951, 1956, and 1960, respectively.

Before joining the staff at Smithsonian Astrophysical Observatory in 1956, Dr. Davis was an astrophysicist at Varo Manufacturing Company, Garland, Texas. He also held a teaching fellowship at Harvard College Observatory from 1955 to 1958.

His general field of investigation is ultraviolet photometry. Dr. Davis has been scientist in charge of Project Celescope since its inception.

NOTICE

This series of Special Reports was instituted under the supervision of Dr. F. L. Whipple, Director of the Astrophysical Observatory of the Smithsonian Institution, shortly after the launching of the first artificial earth satellite on October 4, 1957. Contributions come from the Staff of the Observatory.

First issued to ensure the immediate dissemination of data for satellite tracking, the reports have continued to provide a rapid distribution of catalogs of satellite observations, orbital information, and preliminary results of data analyses prior to formal publication in the appropriate journals. The Reports are also used extensively for the rapid publication of preliminary or special results in other fields of astrophysics.

The Reports are regularly distributed to all institutions participating in the U. S. space research program and to individual scientists who request them from the Publications Division, Distribution Section, Smithsonian Astrophysical Observatory, Cambridge, Massachusetts 02138.